TU WIEN
DEPARTMENT OF GEODESY
AND GEOINFORMATION
RESEARCH DIVISIONS
PHOTOGRAMMETRY & REMOTE SENSING

DISSERTATION

Towards the European-Wide Forest Mapping and Classification Using the Sentinel-1 C-Band Synthetic Aperture Radar Data

Ausgeführt zum Zwecke der Erlangung des akademischen Grades eines
Doktors der technischen Wissenschaften (Dr.techn.)

Unter der Leitung von
Univ.Prof. Dipl.-Ing. Dr.techn. Wolfgang Wagner

E120.1
Department für Geodäsie und Geoinformation
Forschungsgruppe Fernerkundung

Eingereicht an der Technischen Universität Wien
Fakultät für Mathematik und Geoinformation

von

Dipl. Ing. Alena Dostálová
Matrikelnummer: 01028873
[redacted]

Wien, Österreich,

Alena Dostálová

TU WIEN
DEPARTMENT OF GEODESY
AND GEOINFORMATION
RESEARCH DIVISIONS
PHOTOGRAMMETRY & REMOTE SENSING

DISSERTATION

Towards the European-Wide Forest Mapping and Classification Using the Sentinel-1 C-Band Synthetic Aperture Radar Data

A thesis submitted in fulfilment of the academic degree of

Doktors der technischen Wissenschaften (Dr.techn.)

Under the supervision of

Univ.Prof. Dipl.-Ing. Dr.techn. Wolfgang Wagner

E120.1
Department of Geodesy and Geoinformation
Research Group Remote Sensing

Research conducted at TU Wien
Faculty of Mathematics and Geoinformation

by

Dipl. Ing. Alena Dostálová

Matriculation number: 01028873

[redacted]

Wien, Österreich,

Alena Dostálová

Supervisor: Prof. Dr. Wolfgang Wagner

Technische Universität Wien

Department of Geodesy and Geoinformation

Research Group Remote Sensing

Wiedner Hauptstraße 8/E120.1, A-1040 Vienna, Austria

E-Mail: wolfgang.wagner@geo.tuwien.ac.at

Referees: Prof. Dr. Heiko Balzter

University of Leicester

School of Geography, Geology and the Environment

E-Mail: hb91@le.ac.uk

Mait Lang, PhD

Tartu Observatory

Department of Remote Sensing

E-Mail: mait.lang@to.ee

Alena Dostálová

Towards the European-Wide Forest Mapping and Classification Using the Sentinel-1 C-Band Synthetic Aperture Radar Data

Dissertation, 7th December 2021

Technische Universität Wien

Department of Geodesy and Geoinformation

Research Group Remote Sensing

Wiedner Hauptstraße 8/E120.1, A-1040 Vienna, Austria

Erklärung zur Verfassung der Arbeit – Author's Statement

Hiermit erkläre ich, dass ich diese Arbeit selbstständig verfasst habe, dass ich die verwendeten Quellen und Hilfsmittel vollständig angegeben habe und dass ich die Stellen der Arbeit - einschließlich Tabellen, Karten und Abbildungen - die anderen Werken oder dem Internet im Wortlaut oder dem Sinn nach entnommen sind, auf jeden Fall unter Angabe der Quelle als Entlehnung kenntlich gemacht habe.

I hereby declare that I independently drafted this manuscript, that all sources and references are correctly cited, and that the respective parts of this manuscript - including tables, maps, and figures - which were included from other manuscripts or the internet either semantically or syntactically are made clearly evident in the text and all respective sources are correctly cited.

Vienna, Austria, 20 January 2022

Alena Dostálová

Kurzfassung

Wälder bedecken rund 38% der europäischen Landfläche und sind von großer ökonomischer und ökologischer Bedeutung. Zur Aufrechterhaltung der Funktionsfähigkeit der Waldökosysteme sind zuverlässige und häufig aktualisierte Informationen über Waldressourcen erforderlich. Heutzutage werden terrestrische in-situ-Beobachtungen durch Fernerkundungsmethoden ergänzt. Die Fernerkundungsdaten liefern großräumiges überblick von vielen forstwirtschaftlichen Parametern wie Waldbedeckung, Typ und Struktur des Waldes, oder Biomasse. Flugzeuggestützte Kampagnen liefern einen hohen Detailgrad, können jedoch nur begrenzte räumliche Abdeckung und zeitliche Auflösung erreichen. Im Vergleich dazu bietet die satellitengestützte Fernerkundung regelmäßige Aufnahmen, die dazu beitragen die Lücke in der räumlichen und zeitlichen Abdeckung zu schließen.

In den letzten Jahren sind satellitengestützte Waldprodukte für Länder, Kontinente oder die gesamte Landoberfläche verfügbar geworden. Zurzeit nutzt die Mehrheit dieser großräumiger Walddatensätze optische Daten als Input. Die zeitliche Abdeckung optischer Datensätze ist jedoch aufgrund häufiger Wolkenbedeckung oder eingeschränkter Sonneneinstrahlung in vielen Gebieten begrenzt. Aus diesem Grund rückt die Synergie von Synthetic Aperture Radar (SAR) und optischen Sensoren zunehmend in den Fokus der Forschung.

Der Start der Sentinel-1-Satelliten in 2014 und 2016 (Sentinel-1A bzw. -1B) sicherte eine regelmäßige globale Abdeckung von hochauflösenden C-Band-SAR-Daten. Im Großteil des europäischen Kontinents werden 4 bis 8 Dual-Polarisation-Aufnahmen alle 12 Tage bereitgestellt, was zu sehr dichten Zeitreihen führt. Der hochqualitative multitemporale Datensatz kann dazu beitragen, einige der bekannten Einschränkungen von C-Band SAR in forstwirtschaftlichen Anwendungen zu überwinden. Dazu gehören zum Beispiel die fehlende Sensitivität von C-Band Backscatter für hohe Biomasswerte oder die Empfindlichkeit des Signals gegenüber Umweltbedingungen wie Feuchtigkeit oder Frost / Tauwetter.

Die Verfügbarkeit konsistenter Zeitreihen aus den Sentinel-1-Daten motivierte die Entwicklung eines neuen Wald -kartierungs und -klassifizierungsalgorithmus, der die Unterschiede zwischen den zeitlichen Signaturen verschiedener Vegetationstypen ausnutzt. Die Eignung dieses Algorithmus für die kontinentale Waldklassifizierung wurde getestet, indem er für den gesamten europäischen Kontinent angewendet und evaluiert wurde. Diese Validierung ergab eine hohe Übereinstimmung, zu einem mit den europaweiten Copernicus High Resolution Layers Wald-Datensätzen (Gesamtgenauigkeiten von 86,1% bzw. 73,2% für die Wald-/Nichtwald- bzw. Waldtypkarten und Pearson-Korrelationskoeffizient von 0,83 für die Walddichtekarten), als auch mit nationalen Waldkarten (durchschnittliche Gesamtgenauigkeit von 88,2 % bzw. 82,7 % für Wald-/Nichtwald- bzw. Waldtypkarten). Diese Ergebnisse zeigen, dass die Sentinel-1 SAR-Sensoren für die

Waldkartierung und Waldtypklassifizierung auf einem Großteil der Flächen in Europa gut geeignet sind. Die Ergebnisse sind besonders vielversprechend und relevant, da diese Karten mit einem hohen Automatisierungsgrad erstellt werden können und nur ein Jahr an Sentinel-1-Daten als Input benötigen. Als Ausblick können in Gebirgsregionen weitere Verbesserungen erzielt werden, indem ein zusätzlicher radiometrischer Terrain-Abflachungsschritt in die SAR-Datenverarbeitung einbezogen wird.

Abstract

Forests cover around 38% of the European land surface and are of great economic and ecological importance. Reliable and frequently updated information on forest resources is needed to maintain the functioning of forest ecosystems. Nowadays, terrestrial in-situ observations are complemented by remote sensing techniques that provide area-wide spatial data of many forestry parameters such as forest cover, forest type and composition or biomass. While airborne campaigns can provide high level of details with limited coverage and temporal resolution, the spaceborne remote sensing provides regular acquisitions that help to bridge the gap in the spatial and temporal coverage.

In recent years, satellite-based forest maps became available for whole countries, continents, or the entire world. Currently, the majority of these global or continental forest datasets exploit optical data. However, the temporal coverage of optical datasets is limited due to frequent cloud coverage or limited sun illumination of the surface in some areas. For this reason, the synergy of Synthetic Aperture Radar (SAR) and optical sensors or SAR-only based products are also increasingly addressed by research.

Launch of the Sentinel-1 constellation in 2014 and 2016 for Sentinel-1 A and B respectively secured a regular global coverage of high-resolution C-Band SAR data. Over the majority of the European continent, 4 to 8 dual polarisation acquisitions are provided every 12 days resulting in very dense time series. Such dense multi-temporal dataset can help to overcome some of the known limitations of C-Band SAR in forestry applications, such as the backscatter saturation at moderate growing stocks or the sensitivity of the signal to the environmental conditions such as moisture or freeze/thaw events.

The availability of dense time-series of Sentinel-1 data motivated the development of new forest mapping and classification algorithm that exploits the differences between the temporal signatures of various vegetation types. The suitability of this algorithm for continental-scale forest classification was tested by applying and validating it for the entire European continent. This validation revealed high correspondence with the European-wide Copernicus High Resolution Layers forest datasets (overall accuracies of 86.1% and 73.2% for the forest/non-forest and forest type maps respectively and Pearson correlation coefficient of 0.83 for tree cover density map) as well as with national forest maps (average overall accuracy of 88.2% and 82.7% for forest/non-forest and forest type maps respectively). These results show, that the Sentinel-1 SAR sensors are well suited for the forest mapping and forest type classification over majority of the European Continent. This is especially promising due to the fact, that these maps can be produced with a high degree of automation and that only a single year of Sentinel-1 data is required. Also, further improvements can be achieved in undulated regions by including an additional radiometric terrain flattening step in the SAR data pre-processing.

Table of Contents

Acknowledgements

I would like to express my sincerest gratitude to everybody who supported me during this dissertation. First of all, I would like to thank my supervisor, Wolfgang Wagner. Due to the circumstances, I spent large part of my PhD working only remotely, so I would like thank you for always finding a way and supporting me during this time. It enabled me to be very flexible and combine both the PhD and family life however I needed at each time.

I would like to thank all other colleagues at GEO department for support, scientific discussions and very nice working atmosphere. In particular I would like to thank Markus Hollaus for his help with collecting forestry datasets, Senmao Cao and Vahid Freeman for their help whenever I had some problem with Sentinel-1 data processing and our IT group for the great support with remote working environment.

At the beginning of my work, I struggled with the lack of reference data. I would like to thank all people and institutions, who helped me to overcome this and provided me the forestry datasets. Especially my thanks goes to Mait Lang, Lars T. Waser and Sebastian Schnell for their help with the datasets and valuable comments.

However, completing this dissertation, would not be possible without the great support of my family. Special thanks go out to my parents and parents-in-law who spent many hours with our small sons, providing me with enough time for scientific work. I am very grateful to have such a supportive environment. I would also like to thank my friends who gave me energy and helped me to relax whenever I needed it.

Last but not least, I would like to thank my husband, Petr, and our two sons, Michal and Tomáš. Combining motherhood, work and PhD can be sometimes very hard and chaotic, but thanks to you, there is always safe and calm place at our home. Thank you for always being there for me.

Relevant Publications

In the following, I list the publications, datasets and conference proceedings that are related to this doctoral thesis.

The following articles have been published in peer review journals and conference proceedings and are included in this thesis:

Dostálová, Alena, Markus Hollaus, Milutin Milenković, and Wolfgang Wagner. "Forest area derivation from Sentinel-1 data." ISPRS Annals of the Photogrammetry, Remote Sensing and Spatial Information Sciences 3 (2016): 227.

Dostálová, Alena, Wolfgang Wagner, Milutin Milenković, and Markus Hollaus. "Annual seasonality in Sentinel-1 signal for forest mapping and forest type classification." International Journal of Remote Sensing 39, no. 21 (2018): 7738-7760.

Dostálová, Alena, Mait Lang, Janis Ivanovs, Lars T. Waser, and Wolfgang Wagner. "European Wide Forest Classification Based on Sentinel-1 Data." Remote Sensing 13, no. 3 (2021): 337.

Dostálová, Alena, Claudio Navacchi, Isabella Pfeil, David Small, and Wolfgang Wagner. "Influence of the Radiometric Terrain Flattening on the SAR-based Forest Mapping and Classification." In review.

During the doctoral studies I contributed to the following studies which have been published in peer review journals and conference proceedings and are not included in this thesis:

Naeimi, Vahid, Stefano Elefante, Senmao Cao, Wolfgang Wagner, Alena Dostalova, and Bernhard Bauer-Marschallinger. "Geophysical parameters retrieval from sentinel-1 SAR data: a case study for high performance computing at EODC." In Proceedings of the 24th High Performance Computing Symposium, pp. 1-8. 2016.

Dostálová, Alena, M. Milenkovic, M. Hollaus, and W. Wagner. "Influence of Forest Structure on the Sentinel-1 Backscatter Variation-Analysis with Full-Waveform LiDAR Data." In *Living Planet Symposium*, vol. 740, p. 202. 2016.

Dostálová, Alena, Vahid Naeimi, Wolfgang Wagner, Stefano Elefante, Senmao Cao, and Henrik Persson. "Geocoding uncertainty analysis for the automated processing of Sentinel-1 data using

Sentinel-1 Toolbox software." In *Image and Signal Processing for Remote Sensing XXII*, vol. 10004, p. 1000402. International Society for Optics and Photonics, 2016.

Bruggisser, Moritz, Wouter Dorigo, Alena Dostálová, Markus Hollaus, Claudio Navacchi, Stefan Schlaffer, and Norbert Pfeifer. "Potential of Sentinel-1 C-Band Time Series to Derive Structural Parameters of Temperate Deciduous Forests." *Remote Sensing* 13, no. 4 (2021): 798.

Iglseder, Anna, Moritz Bruggisser, Alena Dostálová, Norbert Pfeifer, Stefan Schlaffer, W. Wagner, and M. Hollaus. "The potential of sentinel-1 data to supplement high resolution earth observation data for monitoring green areas in cities." *International Archives of the Photogrammetry, Remote Sensing and Spatial Information Sciences-ISPRS Archives* 43, no. B3-2021 (2021): 567-574.

The following dataset has been prepared and published within the scope of my doctoral study:

Dostálová, Alena, Senmao Cao and Wolfgang Wagner. European Sentinel-1 Forest Type and Tree Cover Density Maps (1.0) [Data set]. TU Wien. 2021. DOI: 10.48436/tkkfs-11b75

List of Figures

List of Tables

List of Abbreviations and Symbols

β	Backscatter-local incidence angle linear regression slope parameter
β^0	Beta nought
γ_{rtf}	Radiometrically terrain flattened gamma
γ^0	Gamma nought
θ	Projected local incidence angle
κ	Cohen's Kappa coefficient
σ^0	Sigma nought
R^2	Coefficient of determination
r	Pearson correlation coefficient
ACube	Austrian Data Cube
ALOS-PALSAR	Advanced Land Observing Satellite Phased Arrayed L-band SAR
ALS	Airborne Laser Scanning
BFW	Austrian Research Centre for Forests
CC	Crown Coverage
CLC	Corine Land Cover
dB	Decibel
DEM	Digital Elevation Model
EEA	European Environment Agency
EnviSAT-ASAR	Environmental Satellite - Advanced Synthetic Aperture Radar
ERS	European Remote Sensing Satellite
ESA	European Space Agency
EW	Extra Wide swath
FAO	Food and Agriculture Organisation
FFG	Austrian Research Promotion Agency
FMI	Czech Forest Management Institute
FOEN	Fderal Office of the Environment (CH)
FTY	Forest Type
GRD	Ground Range Detected
HAND	Height Above Nearest Drainage
HH	Horizontal transmit, horizontal receive polarisation
HV	Horizontal transmit, vertical receive polarisation
HRL	High Resolution Layers
IGN	Institut National de L'Information Geographique et Forestriere
IRS-RS2	Indian Remote Sensing-ResourceSat 2
IW	Interferometric Wide swath
JAXA	Japan Aerospace Exploration Agency
JERS	Japan Earth Resources Satellite
JPRL	Register Jednotiek Priestoroveho Rozdelenia Lesa (SVK)
LIA	Local Incidence Angle
LiDAR	Light Detection and Ranging
MMU	Minimum Mapping Unit
MMW	Minimum Mapping Width
nDSM	Normalized Digital Surface Model
NFI	National Forest Inventory
NFK	Nemzeti Földügyi Központ (HU)
NRMSD	Normalized Root Mean Square Difference
NRSC	Normalized Radar Cross Section

PA	Producer's Accuracy
RADARSAT	Radar Satellite
RTC	Radiometric Terrain Correction
RTF	Radiometric Terrain Flattening
SAR	Synthetic Aperture Radar
SGRT	SAR Geophysical Retrieval Toolbox
SIR-C/X SAR	Spaceborne Imaging Radar-C/X-band Syntheric Aperture Radar
SLU	Swedish University of Agricultural Sciences
SNAP	Sentinel Application Platform
SPOT	Satellite Pour l'Observation de la Terre
SRTM	Shuttle Radar Topography Mission
SYKE	Finish Environment Institute
RGB	Red-Green-Blue
RMSD	Root Mean Square Difference
TCD	Tree Cover Density
TU Wien	Technische Universität Wien (AT)
UA	User's Accuracy
VH	Vertical transmit, horizontal receive polarisation
VV	Vertical transmit, vertical receive polarisation
WSL	Swiss Federal Institute for Forest, Snow and Landscape Research

1 Introduction

1.1 Rationale

Being vital to many of the Earth's ecosystems, forests provide a variety of functions, such as providing habitat for animals and plants, protecting watersheds (Ernst, Gullick et al. 2004, Calder, Hofer et al. 2008) and preventing soil erosion (Pimentel and Kounang 1998). Reliable information on forest resources and condition from the local to global scale is needed for analysis, sustainable forest management as well as for large number of other applications. This information can either be derived from in-situ observations or by remote sensing. Terrestrial in-situ measurements offer high level of details and are still the standard in most of Europe (Barrett, McRoberts et al. 2016). However, in-situ measurements are costly, and the forest inventories based on the terrestrial measurements are commonly based on sample plots with limited spatial and temporal distribution. Such inventories provide a precise statistical estimation of the forest composition, however, certain forest parameters such as forest cover, forest type or composition etc. may be better described using area-wide spatial data (Barrett, McRoberts et al. 2016, Ginzler, Price et al. 2019).

Remote sensing offers an alternative, allowing area-wise acquisition of a number of forest parameters (Vidal, Alberdi et al. 2016, White, Coops et al. 2016, Kangas, Astrup et al. 2018). Nowadays, airborne campaigns with multispectral cameras or Light Detection and Ranging (LiDAR) are carried out and the derived forest parameters complement the forest inventories. High cost of these campaigns cause, that the temporal resolution is still in range of 3-10 years or that the regular updates are not secured at all. Spaceborne remote sensing data help to bridge the gap in the temporal resolution and spatial coverage. In recent years, satellite-based forest maps became available for whole countries, continents or the entire world (Hansen, Potapov et al. 2013, Langanke, Büttner et al. 2013, Shimada, Itoh et al. 2014, Lang, Kaha et al. 2018, Martone, Rizzoli et al. 2018, Waser, Rüetschi et al. 2021). Currently, the majority of these global or continental forest datasets exploit optical data, for instance the Landsat based Hansen Global Forest Change (Hansen, Potapov et al. 2013) or European-wide Copernicus High Resolution Layers (HRL) Forests (Langanke, Büttner et al. 2013) with Sentinel-2 and Landsat 8 as the primary input data source. Recently, the synergy of Synthetic Aperture Radar (SAR) and optical sensors or SAR-only based products are also increasingly addressed by research (Kangas, Astrup et al. 2018, Rüetschi, Schaepman et al. 2018, Hansen, Mitchard et al. 2020, Dostálová, Lang et al. 2021, Udali, Lingua et al. 2021, Waser, Rüetschi et al. 2021). Among the SAR-only products, global forest maps based on ALOS PALSAR L-Band backscatter mosaics (Shimada, Itoh et al. 2014) and TanDEM-X X-Band interferometric data (Martone, Rizzoli et al. 2018) are available.

The main advantages of the SAR sensors when compared to the optical imagery is their almost all-

weather, day-and-night sensing capability providing regular measurements even in areas of frequent cloud coverage or short sun illumination periods. On the other hand, the wavelength dependent saturation of the microwave signal– in case of C-Band, the radar signal saturates at moderate growing stocks (Santoro, Beer et al. 2011) (Quegan, Le Toan et al. 2000) – together with the sensitivity of the signal to the environmental conditions such as moisture (Lucas, Armston et al. 2010) or freeze/thaw events (Ranson and Sun 2000) represent main limitations of SAR data for the forest monitoring. A number of studies suggest that these shortcomings may, to some extent, be overcome by using multi-temporal SAR data (Santoro, Beer et al. 2011, Dostálová, Hollaus et al. 2016, Rüetschi, Schaepman et al. 2018, Hansen, Mitchard et al. 2020).

Launch of the Sentinel-1 constellation in 2014 and 2016 for Sentinel-1 A and B respectively secured a regular global coverage of high-resolution C-Band SAR data over land according to a pre-programmed acquisitions scenario (Torres, Snoeij et al. 2012). Over the majority of the European continent, 4 to 8 acquisitions in the Interferometric Wide swath (IW) mode are provided every 12 days. IW mode provides dual polarisation (vertical polarisation transmitted and received: VV and vertical polarisation transmitted, and horizontal polarization received: VH) data with spatial resolution of 20 m × 5 m. Apart from the high spatial and temporal resolution, VH polarisation is an important asset for the forestry applications as the cross-polarised backscatter shows high sensitivity to changes in vegetation density and structure (Patel, Srivastava et al. 2006, Soudani, Delpierre et al. 2021). The SAR temporal signal over forests is, in general, connected to the structural and phenological changes in forest (Dostalova, Milenkovic et al. 2016, Frison, Fruneau et al. 2018, Rüetschi, Schaepman et al. 2018, Soudani, Delpierre et al. 2021) as well as to the environmental changes such as temperature changes and freeze-thaw events (Ranson and Sun 2000, Monteith and Ulander 2018) or changes in moisture of the vegetation and the underlying soil (Lucas, Armston et al. 2010, Srivastava, O'Neill et al. 2015).

1.2 Objective and research questions

The aim of this thesis is to assess the suitability of the Sentinel-1 IW dataset for the forest mapping over Europe. The objective is to derive a European-wide forest area and forest type (dominant leaf type) map based on the Sentinel-1 data. To do so, a new algorithm based on the multi-temporal Sentinel-1 data was developed and validated over the entire European continent. This introduces the following research questions:

1) Can the multi-temporal dataset help to overcome some of the known limitations caused by the sensitivity of the SAR signal to the environmental conditions and signal saturation?
2) Can Sentinel-1 data be used to distinguish dominant leaf type?
3) Can a single algorithm be used to describe various types of forest across the European

continent?

4) What are the strengths and limitations of the developed algorithm?

1.3 Study outline

This thesis consists of five chapters of which four are based on manuscripts that have been published in peer-reviewed scientific literature (Publications I to III) or are in preparation for submission (Publication IV). Chapter II assesses the suitability of the multi-temporal Sentinel-1 SAR data to map forest/non-forest areas using statistical parameters derived from the time-series and well-known classification methods. Chapter III describes the forest mapping and forest classification algorithm that was developed within the scope of this thesis. This algorithm is based on a temporally smoothed annual backscatter time series and was developed based on the findings presented in Chapter II. Chapter IV presents the European-wide forest map based on the introduced algorithm and validates it using a multitude of reference datasets, highlighting the strengths and weaknesses of the introduced forest mapping and classification method. Chapter V quantifies possible future improvements of the forest map results when including an additional radiometric terrain flattening step within the Sentinel-1 data preprocessing. Finally, the Chapter VI presents the main conclusions and the scientific impact of this thesis.

1.4 Publication summaries

The research questions were addressed in three/four peer-reviewed scientific publications. This section summarises the articles and experiments. The articles are included in full length in chapters 2, 3 and 4.

Publication I: Dostálová, Alena, Markus Hollaus, Milutin Milenković, and Wolfgang Wagner. "Forest area derivation from Sentinel-1 data." ISPRS Annals of the Photogrammetry, Remote Sensing and Spatial Information Sciences 3 (2016): 227.

In this first study, the potential of the newly launched Sentinel-1 SAR backscatter data for forest area derivation was assessed. The case study focused on well-established classification algorithms (Otsu thresholding (Otsu 1979) and K-means clustering (Hartigan and Wong 1979)) over a study area in Lower Austria. For classification purposes, statistical parameters based on multi-temporal dual-polarization Sentinel-1A backscatter data acquired during winter season 2014-2015 were used. The results were validated with a forest mask derived from full-waveform airborne laser scanning data.

Both methods showed good correspondence to the reference data for the forest/non-forest classification with overall accuracies of 91% and 87% for the Otsu thresholding algorithm and K-means clustering respectively. The results also identified the main deficiencies of the selected approach, namely the strong topographic effects in hilly areas, misclassification of urban areas as

forests and underestimation of mixed and coniferous forest stands. Improvements of these limitations of the simple approach motivated the development of the classification algorithm introduced in Publication II.

Publication II: Dostálová, Alena, Wolfgang Wagner, Milutin Milenković, and Markus Hollaus. "Annual seasonality in Sentinel-1 signal for forest mapping and forest type classification." International Journal of Remote Sensing 39, no. 21 (2018): 7738-7760.

Based on the findings summarized in Publication I, a new classification algorithm was developed for forest area mapping and dominant leaf type (forest type) classification. The main motives during the algorithm development were the following:

- The algorithm should exploit the high temporal resolution of the Sentinel-1 data and use the distinct temporal signature of the forested areas to distinguish these from other land cover and vegetation types.
- The algorithm should consider the differences between the temporal signatures of various forest types. The potential to use these differences for forest type classification should be assessed.

The newly developed classification algorithm was based on the annual temporal signatures and two Sentinel-1 based forestry products were derived, namely forest type and tree cover density. The results were validated in three study areas covered by various forest types including broadleaf temperate, boreal and montane forests against the European-wide Copernicus High Resolution Layers (HRL) forest datasets (Langanke, Büttner et al. 2013). In case of forest area estimation and tree cover density, show high correspondence for all three test sites (overall accuracies of 86% to 91% and Pearson correlation coefficient (r) of 0.68 to 0.74 for forest area and tree cover density respectively). In case of the forest type classification, the overall accuracy decreases in the northern test site (85% in Austria compared to 65% in northern Sweden). When compared to the method introduced in Publication I, the newly developed algorithm provide better results in mountainous regions, does not underestimate the area of coniferous and mixed forests and, apart from the forest area, provides also the forest type information.

Publication III: Dostálová, Alena, Mait Lang, Janis Ivanovs, Lars T. Waser, and Wolfgang Wagner. "European Wide Forest Classification Based on Sentinel-1 Data." Remote Sensing 13, no. 3 (2021): 337.

In the third publication, the forest classification algorithm developed within the scope of the two previous publications was applied over Europe. Continental scale forest maps were created and evaluated against the European-wide Copernicus HRL forest datasets (Langanke, Büttner et al. 2013) and national-scale forest maps from twelve countries. The comparison with the Copernicus HRL

datasets revealed high correspondence over the majority of the European continent with overall accuracies of 86.1% and 73.2% for the forest/non-forest and forest type maps, respectively, and a Pearson correlation coefficient of 0.83 for tree cover density map. Detailed analysis of the results revealed the strengths and weaknesses of the algorithm, showing that the approach is well suited for temperate and hemi-boreal forests. However, its ability to detect forested areas or classify forest type decreases in areas with lower forest density such as Mediterranean forests or areas in northern Sweden and Norway. Lower accuracy can also be observed in mountain forests where the approach is further limited by the topographic distortions in SAR signal. However, the evaluation of both datasets against the national forest maps showed that the obtained accuracies of Sentinel-1 forest maps are almost within range of the HRL datasets. Especially the results for Finland (overall accuracy of 88% for forest/non-forest mapping and 71% for forest type classification) or Switzerland (87% for forest/non forest mapping and 82% for forest type classification) show high potential of Sentinel-1 for forest mapping even in challenging environments.

The introduced approach is especially promising due to the facts that these maps can be produced with a high degree of automation and that only a single year of Sentinel-1 data is required which enables frequent updates of the forest maps.

Publication IV: Dostálová, Alena, Claudio Navacchi, Isabella Pfeil, David Small, and Wolfgang Wagner. "Influence of the Radiometric Terrain Flattening on the SAR-based Forest Mapping and Classification."

Terrain induced variations of radar backscatter represent an important limiting factor in the introduced approach. Despite the effort to limit these effects by using backscatter normalisation and aggregation of all orbits acquired within the entire orbital cycle, decrease of accuracy in mountainous regions is still relatively strong. The last study quantifies the influence of the radiometric terrain flattening method (Small 2011) that minimizes the terrain induced variations in SAR imagery. This method requires considerably more processing time than the previously used radiometric correction to the sigma nought (σ^0) values which makes its use in case of methods based on large datasets challenging. In this study, the algorithm introduced in publication II was adapted for the radiometrically terrain flattened gamma (γ_{rtf})backscatter and compared to the results based on the σ^0 backscatter.

The validation over entire Austria revealed an improvement of overall accuracy by 2% and 3% respectively for the forest/non-forest and forest type classification respectively. Large differences can be observed in regions with rough topography, where the overall accuracies improved by 16% and 17% respectively, while the results are comparable in flatlands. These results show, that using the γ_{rtf} instead of the σ^0 in mountainous regions has the potential to improve the forest classification significantly in mountainous regions and further improve the quality of the derived maps.

1.5 European-wide forest maps

The forest maps (Dostalova, Cao et al. 2021) derived within the scope of this thesis are the first continental-scale forest layers based on Sentinel-1 C band SAR backscatter data. They consist of two layers, namely the forest type and tree cover density layers in 10 and 100m resolution respectively. The forest type map delineates the forest area and classifies the dominant leaf type (coniferous or broadleaf) while the tee cover density map shows the percentage of forest canopy cover within the 100 m pixel. The maps were derived for the year 2017.

1.6 Authors contributions

Publication I: Alena Dostálová prepared the Sentinel-1 data, developed the forest area mapping algorithm, computed the Sentinel-1 based forest maps analyzed the validation results and wrote the manuscript. Markus Hollaus suggested the study design, computed reference ALS forest maps performed the forest maps validation and did the proof reading. Milutin Milenkovic prepared the ALS data and did the proof reading. Wolfgang Wagner was the supervisor and did the proofreading.

Publication II: Alena Dostálová suggested the study design, prepared the Sentinel-1 data, developed the classification algorithm, computed the forest maps, performed the validation, analyzed the validation results and wrote the manuscript. Wolfgang Wagner was the supervisor and did the proofreading. Milutin Milenkovic helped with the development forest type classification algorithm and did the proof reading. Markus Hollaus was the project manager, helped with scientific discussions and did the proof reading.

Publication III: Alena Dostálová suggested the study design, computed the forest maps, performed the validation, analyzed the results and wrote the manuscript. Mait Lang prepared the validation data over Estonia and did the proof reading. Janis Ivanovs prepared the validation data over Latvia and did the proof reading. Lars T. Waser prepared the validation data over Switzerland and did the proof reading. Wolfgang Wagner was the supervisor and did the proof reading.

Publication IV: Alena Dostálová computed the forest maps, performed the validation, analysed the results and wrote the manuscript. Claudio Navacchi processed the sigma and gamma Sentinel-1 data and did the proof reading. Isabella Pfeil helped with scientific discussions and did the proof reading. David Small and Wolfgang Wagner were the supervisors, suggested the study design and did the proof reading.

2 Publication I: Forest Area Derivation from Sentinel-1 Data

This section is reformatted from a paper published in the ISPRS Annals of the Photogrammetry:

Dostálová, Alena, Markus Hollaus, Milutin Milenković, and Wolfgang Wagner. "Forest area derivation from Sentinel-1 data." ISPRS Annals of the Photogrammetry, Remote Sensing and Spatial Information Sciences 3 (2016): 227.

https://doi.org/10.5194/isprs-annals-III-7-227-2016

Abstract

The recently launched Sentinel-1A provides the high resolution Synthetic Aperture Radar (SAR) data with very high temporal coverage over large parts of European continent. Short revisit time and dual polarization availability supports its usability for forestry applications. The following study presents an analysis of the potential of the multi-temporal dual-polarization Sentinel-1A data for the forest area derivation using the standard methods based on Otsu thresholding and K-means clustering. Sentinel-1 data collected in winter season 2014-2015 over a test area in eastern Austria were used to derive forest area mask with spatial resolution of 10m and minimum mapping unit of 500m2. The validation with reference forest mask derived from airborne full-waveform laser scanning data revealed overall accuracy of 92% and kappa statistics of 0.81. Even better results can be achieved when using external mask for urban areas, which might be misclassified as forests when using the introduced approach based on SAR data only. The Sentinel-1 data and the described methods are well suited for forest change detection between consecutive years.

2.1 Introduction

Since 1991 radar data are available on a continuous basis from different sensors (e.g. ERS-1, ERS-2, JERS, SIR-C/X-SAR, RADARSAT, SRTM, EnviSAT-ASAR, RADARSAR-II, LIGHTSAR, ALOS-PALSAR, TerraSAR-X). The recently launched Sentinel-1A and the planned Sentinel-1B satellites continue this time series and will provide a Synthetic Aperture Radar (SAR) data base with much higher spatial and

temporal resolution than with previous radar missions. Sentinel-1A, C-Band (central frequency of 5.405 GHz) SAR was launched on 3rd April 2014. Starting in October 2014, regular coverage is available in both VV and VH polarizations for central Europe. The Interferometric Wide Swath mode (IW) offers regular, dual polarization coverage with 20x5m spatial resolution.

The high potential of radar data for forestry applications is known since several decades. The main advantages are the capability for mapping vegetation cover in regions characterized by frequent cloud cover as for example tropical and boreal forests and the provision of time series data with high calibration stability as e.g. achieved with ERS-1 and ERS-2 data. In addition to being almost insensitive to weather conditions, SAR data is a useful data source providing information on the structure and moisture status that is complementary to the information provided by optical remote sensing (Le Toan and Floury 1998).

These strengths were used in a multitude of studies e.g. on forest mapping ((Dontchenko, Johannessen et al. 1999); (Dwyer, Monaco et al. 2000, Quegan, Le Toan et al. 2000) (Sgrenzaroli, De Grandi et al. 2002); (Strozzi, Wegmueller et al. 1998); (Wagner, Luckman et al. 2003)), forest change detection ((Saatchi, Soares et al. 1997, Gimeno, San-Miguel et al. 2002, Hese and Schmullius 2005)) and biomass measurements ((Dobson, Ulaby et al. 1992, Le Toan, Beaudoin et al. 1992, Le Toan and Floury 1998, Wagner, Luckman et al. 2003)). The delineation of forested areas from remote sensing data is a fundamental task in forestry. The area and location of forests is an essential input in studies on forest resources, forest contribution, global carbon cycle, forest ecosystems and on their productivity functions. Furthermore, the changes of the forest areas are in the focus of operational forest management and forest studies of forest change detection due to e.g. fire, storm, diseases or logging activities. Due to the relatively low spatial and temporal resolution of available SAR data their application for operational forest mapping is still limited. The availability of Sentinel-1 data will change this situation significantly.

The data from Sentinel-1 satellite were already demonstrated to be useful for land cover classification as a possibility to complement the cloud-covered areas ((Balzter, Cole et al. 2015)) or to be used for a forest change detection to identify clear-cuts ((Olesk, Voormansik et al. 2015)). Similarly, the dual-polarization data from Radarsat C-Band sensor were already used to complement forest cover maps from ALOS-PALSAR L-Band SAR systems (Mitchell, Tapley et al. 2014). Due to the high temporal coverage of Sentinel-1 data with an acquisition up to every three days in central Europe, the advantage of multi- and hyper-temporal combination of images may be used for forest

classification. The short revisit time also strongly supports the change detection applications.

The objective of this paper is to show first results of delineated forest areas from multi-temporal Sentinel-1 data from an Austrian study site. The results are validated with a reference forest mask derived from airborne full-waveform laser scanning data.

2.2 Study area and data

2.2.1 Study area

The northern part of the federal state Burgenland in Austria was selected as study area (Figure 1). In addition to the flat area around the Lake Neusiedl, this region contains two hilly areas with the highest elevation of 748 m and 484 m a.s.l., respectively. Both hilly regions are almost completely covered with mixed forest (deciduous and coniferous trees) with about 400 km2 each, while there are also several smaller forest areas up to 40 km2 outside the closed forests. The rest of the study area is rather flat, open land or urban area, with elevations ranging from 110 m to 260 m a.s.l., while in the eastern part the lake Neusiedl is located.

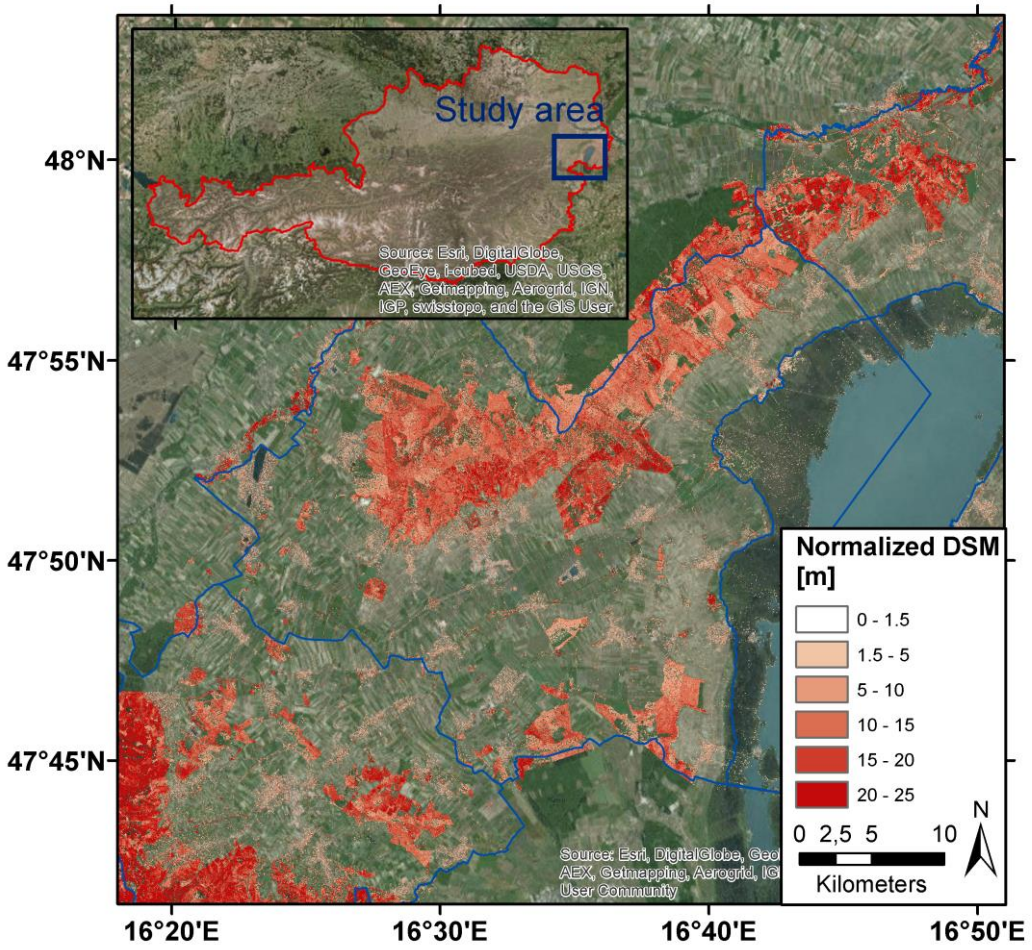

Figure 1: Overview of the study area. The ArcGIS Online basemap orthophoto is overlaid with the normalized DSM, derived from ALS data. The cells where the normalized DSM is smaller than 1.5 m are plotted as transparent.

2.2.2 Data

Sentinel-1A IW Ground Range Detected (GRD) Level-1 product was used in this study. The IW data have spatial resolution of 20m with the pixel spacing of 10m. Over the study area, regular coverage in VV and VH polarization is available since October 2014 with a temporal resolution of 4 days on average.

As the volume scattering at C-Band in forests (representing permanently vegetated areas) and dense agricultural crops (representing seasonally vegetated areas) may cause similar backscatter values over these two classes in summer time acquisitions and thus make the two classes less separable ((Balzter, Cole et al. 2015)), only the winter period (1st December 2014 to 31st March 2015) data were selected. All acquisitions from the specified time frame were used, regardless of the environmental conditions (snow, precipitation, temperature) or differences in orbit and thus in local incidence angles. On average, 30 acquisitions are available for each pixel within the study area.

In addition to Sentinel-1 data, full-waveform airborne laser scanning (ALS) data are available. The ALS data were collected in April 2010 with Riegl LMS-Q560 and LMS-Q680 sensors under the leaf-off and snow-free conditions. The ALS data cover the whole study area with an average point density in the nonoverlapping areas of 4 points/m2 , while recording up to 15 echoes per single laser shoot. The laser footprint of the recorded data was not larger than 60 cm in diameter. The ALS data are used for deriving a reference forest mask used for validating the Sentinel-1 derived forest area.

2.2.3 Reference forest mask

For the generation of the reference forest mask the approach from (Eysn, Hollaus et al. 2012) is applied. This comprehensive approach is based on ALS data by considering the criterions tree height, crown coverage (CC) and the minimum area and width. The criterion of land use is not considered in this approach. Based on the slope adaptive echo ratio map, which describes the transparency for laser beams of the top most surface, it is possible to differentiate between buildings and trees. For the calculation of the CC the approach from (Eysn, Hollaus et al. 2011) is applied, which uses clear geometric definition of the CC and works on a similar way than it is the case for manual assessment of the CC based on aerial orthophotos. This approach uses the area of the convex hull of three neighbouring trees as reference unit and thus overcomes limitations from e.g. pure moving window approaches such as smoothing effects along the forest border or the dependency on the kernel size and shape of the moving window. The entire workflow is implemented in the software package Opals ((Pfeifer, Mandlburger et al. 2014)).

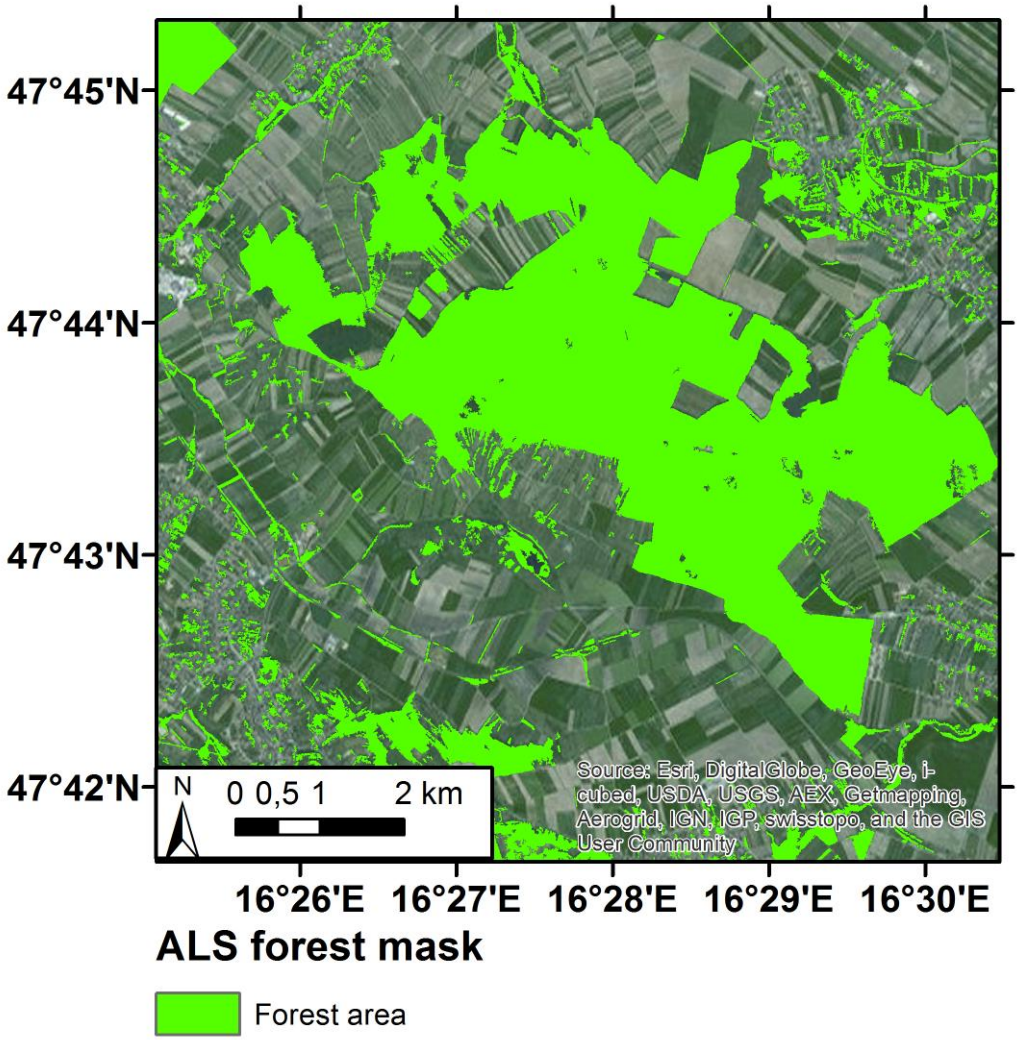

Figure 2: Subset of the derived forest mask with a minimum mapping unit of 500 m², crown coverage ≥30%, minimum height 3m and minimum width of 10 m. In the background an ArcGIS Online basemap orthophoto is shown.

2.3 Methods

The presented SAR forest map is based on statistical parameters derived from Sentinel-1 multi-temporal data-series over single winter period. The methodology is divided into the following steps: Sentinel-1 data pre-processing that includes processing of the level-1 data into the stack of georeferenced and quality checked images; forest area derivation, which includes statistical parameters derivation, their analysis and forest classification and validation using the ALS reference forest map.

2.3.1 Sentinel-1 data pre-processing

The Sentinel-1 data were pre-processed using the Sentinel-1 Toolbox software (version 1.1.1). The processing steps included radiometric calibration to the sigma nought (σ^0)

values, range-Doppler terrain correction using SRTM digital elevation model ((Jarvis, Reuter et al. 2008)) and conversion from linear to decibel scale. The data were checked for corrupt or shifted images and the precision of the georeferencing was tested. Extremely low backscatter values (below -30 dB) at the image edges caused by the thermal noise were masked. Since large number (~30) of measurements was used to retrieve the parameters for classification, no multilooking or spatial filtering to reduce speckle noise was applied.

2.3.2 Forest area derivation

The combination of two polarization bands (VV and VH in this case) offers the possibility to use the backscatter intensities from the C-Band SAR sensor for a classification of various land cover types ((Balzter, Cole et al. 2015)). This is illustrated on Figure 3-a, which presents an RGB composite of the two polarizations and their difference for a single Sentinel-1 acquisition from 25th December 2014 over a 10 by 10 km subset of the region of interest. Forested areas (appearing green on the RGB composite) are typical for their relatively high backscatter intensities in both polarizations (especially in VH) and relatively low difference between the two polarizations when compared to the agricultural cropland. However, speckle noise and relatively strong topographic effects in the single SAR acquisition decreases the precision of a single image based classification. To reduce these limitations, acquisitions from entire winter period (1st December 2014 to 31st March 2015) were combined.

Number of statistical parameters was computed from the backscatter time-series for each pixel (e.g. mean, median, quartiles or standard deviation). Those providing the highest separability of forested and non-forested areas quantified by Bhattacharyya distance (Fukunaga 2013) together with a low sensitivity to terrain variations were selected for the classification. The best results for both polarizations are achieved by the so-called dry parameter computed as the average of all values below first quartile of each pixel. The RGB composite of VH and VV polarization and their difference is presented in Figure 3-b. When compared to Figure 3-a, the speckle noise is reduced and the contrast between forested and non-forested land is enhanced.

For the classification, the dry parameter for VV and VH polarizations and the difference between the two polarizations is used. Two approaches are tested: a thresholding method based on the thresholds derived by the Otsu algorithm ((Otsu 1979)) (Fig. 4-a) and a k-means clustering ((Hartigan and Wong 1979)) (Fig. 4-b). The thresholds and cluster centres for the forest and non-forest classes were specified over the 10 by 10 km training area presented at Figures 2, 3 and 4 and were used for the entire region of interest.

Minimal mapping unit of 500 m2 was applied.

Both algorithms based on the above mentioned parameters tend to falsely classify urban areas as forests. For urban areas mapping, different parameters need to be selected. (Dekker 2003) showed that the measure with the best preformation for the urban areas delineation is the mean SAR intensity. This approach works well in flat areas, however it leads to over classification in hilly areas. Another possibility is to use external ancillary data such as Corine land cover dataset ((Bossard, Feranec et al. 2000)) to mask out the urban areas. Both approaches were evaluated in this study.

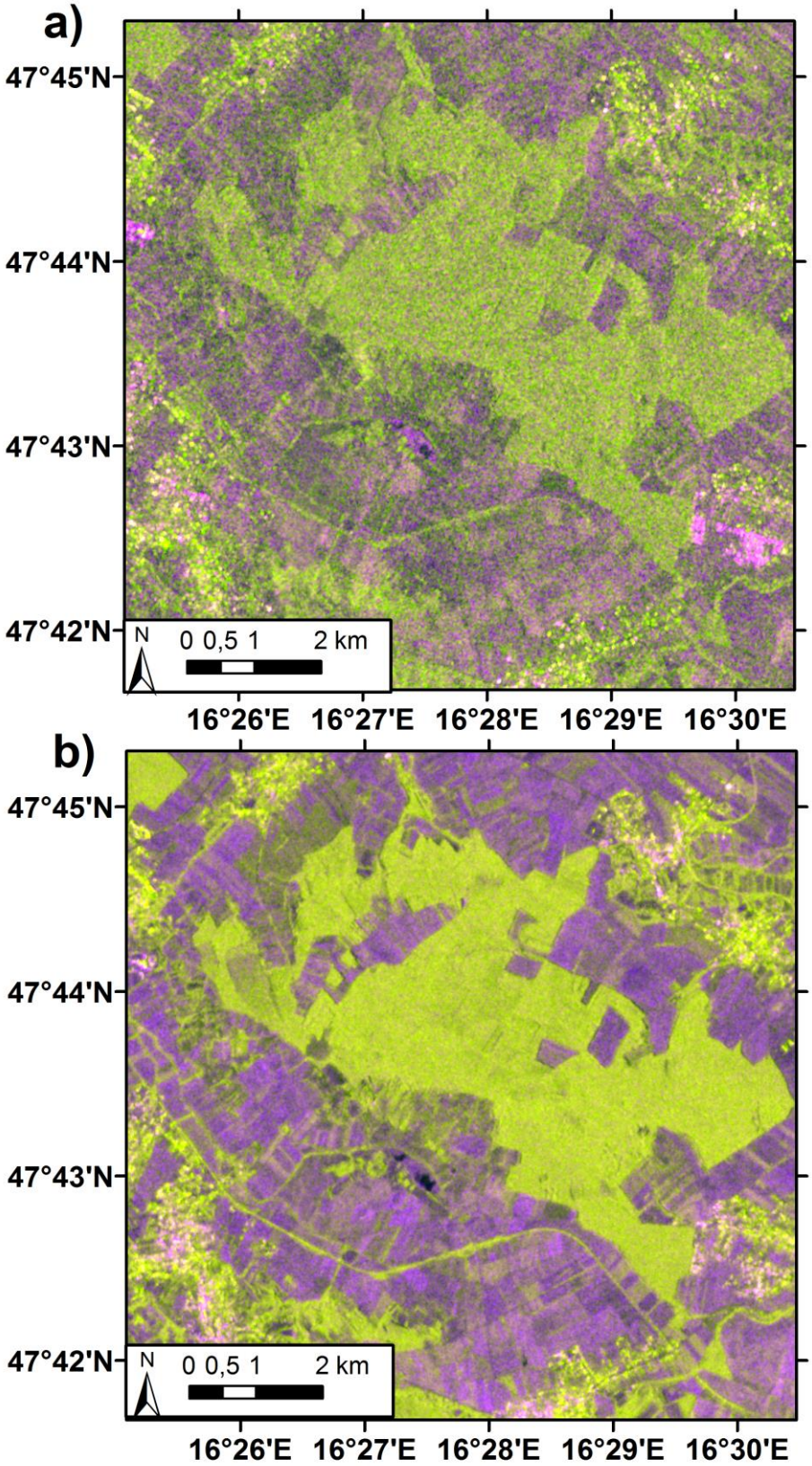

Figure 3: 10 by 10 km training area: a) RGB composite of VV polarization backscatter in red band, VH polarization backscatter in green band and their difference in blue band from 25th December 2014, b) RGB composite (VV, VH and their difference) of the dry parameter over the winter period.

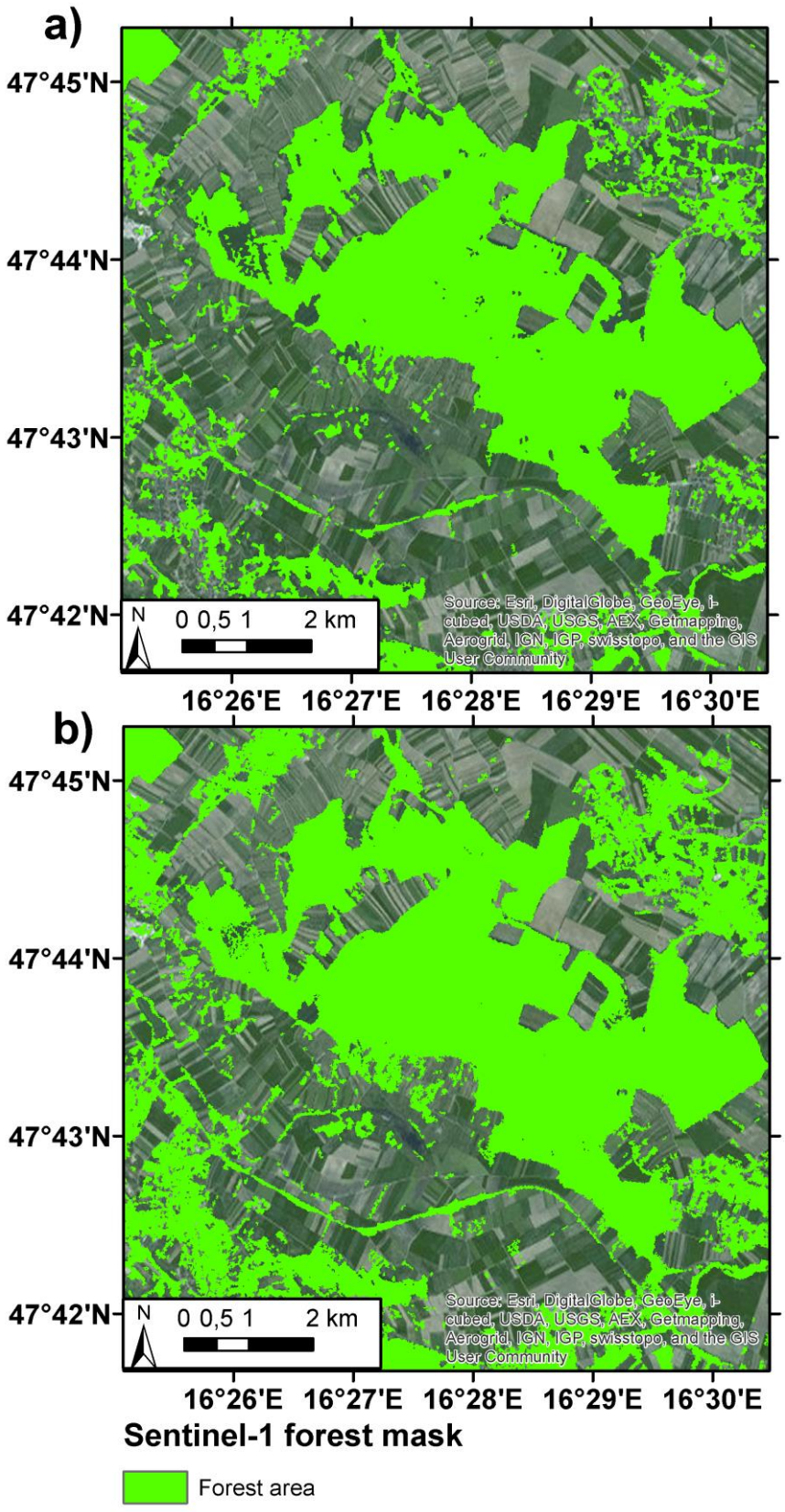

Figure 4: 10 by 10 km raining area: a) result of the thresholding approach classification, b) result of the k-means clustering approach classification

2.3.3 Validation

For the validation of the derived forest masks from the ALS derived forest mask (cp. section 2.2) is used as a reference. The minimum mapping unit for all forests masks is set to 500m2 . The accuracy statistics are summarized in error matrixes, In addition to the overall accuracies, the producer and user accuracies as well as the kappa coefficients ((Congalton and Green 2019)) are calculated for each derived forest mask.

2.4 Results and discussion

The ALS and Sentinel-1 (thresholding approach) forest masks for the entire test area are presented at Figure 5 and their differences are highlighted at Figure 6. The urban areas are masked with the mean SAR backscatter parameter. Spatial resolution of both datasets is 10m and minimal mapping unit is 500m2 . The accuracy statistics for both the thresholding and the k-means approach are summarized in Table 1. The results are listed separately also for the different urban area masks (based on Sentinel-1 data and Corine land cover).

Both methods show overall good correspondence of the derived Sentinel-1 forest mask and the reference ALS forest mask. The kappa values range between 0.77 in case of k-means clustering approach complemented with the urban mask based on mean Sentinel-1 backscatter and 0.83 in case of thresholding approach with Corine land cover urban mask. The generally lower user's accuracy (75 and 78%) and very high producer's accuracy (96%) of forests in case of the k-means clustering approach show that the method tends to overestimate the forest area. The overall accuracy is also lower than in case of the thresholing method. The thresholding method shows overall accuracies over 90% with balanced user's and producer's accuracies for both classes.

The urban mask based on external Corine land cover data performs better than the SAR based urban mask. The mask based on average SAR backscatter does not classify areas with lower building density as urban areas and these are then often falsely classified as forests (Figure 6). Strong topographic effects in some hilly areas might also lead to misclassifications as these are recognized as build up areas when using the simple approach based on average SAR intensity. Further research is needed to develop a better classification approach to distinguish forested and urban areas using Sentinel-1 data.

As the training area included only deciduous forests, the SAR based forest masks tend to underestimate forest area in regions, dominated by mixed and coniferous forests (Figures 5 and 6, South-Western part of the test area). Classification of multiple forest classes

might further improve the result.

Table 1: Accuracy statistics for Sentinel-1 forest masks using ALS forest mask as reference.

Classification method	**Thresholding approach**		**K-means clustering approach**	
Urban mask	**Sentinel-1**	**Corine land cover**	**Sentinel-1**	**Corine land cover**
Produces's accuracy: forest	89%	89%	97%	97%
Producer's accuracy: no forest	92%	94%	81%	85%
User's accuracy: forest	85%	88%	72%	87%
User's accuracy: no forest	94%	94%	98%	98%
Overall accuracy	91%	92%	87%	89%
Kappa statistic	0.80	0.83	0.73	0.78

It should also be noted, that the temporal difference between the ALS and Sentinel-1 forest map is almost 5 years. No manual correction of the forest changes (clear-cuts, forest grow) was applied before the validation. This reduces the achieved accuracies, but also highlights the potential of the Sentinel-1 data to be used for change detection. Figure 7 represents the area where the changes in forest area are visible between the ALS and Sentinel-1 acquisition time (April 2010 and December 2014 to March 2015 respectively).

Generally, the accuracy of the Sentinel-1 forest mask exceeds 90% when compared to the reference ALS mask at the 10m spatial resolution. As the Sentinel-1 forest mask is based on data from a single winter season, yearly forest masks might be derived in future in case of a sufficient temporal coverage. Especially after the launch of Sentinel-1B, even interseasonal change detection might be possible with the presented accuracy. Further research is needed to assess the applicability of the approach for a larger scale and diverse forest types.

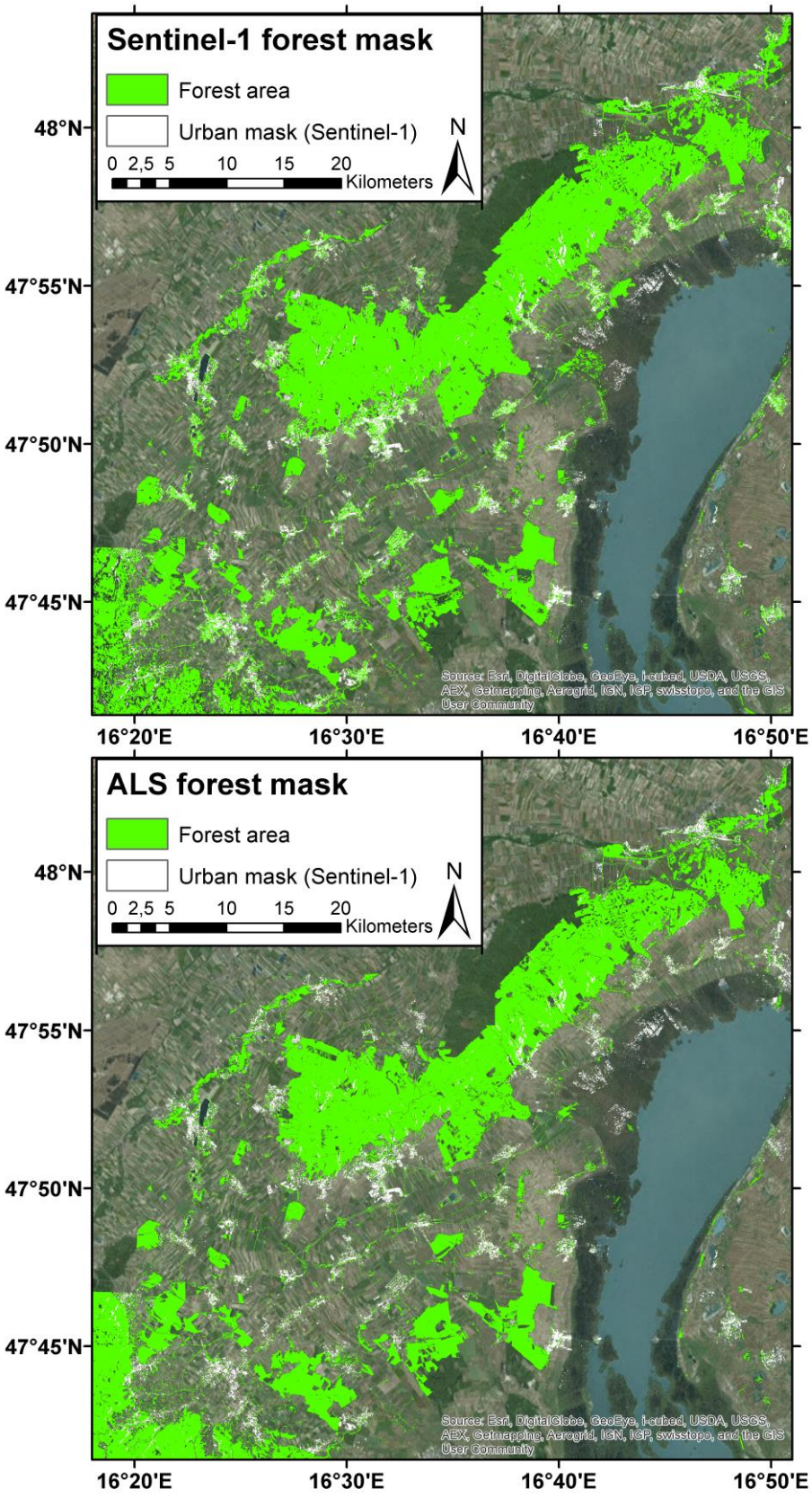

Figure 5The ALS and Sentinel-1 (thresholding approach) forest mask for the entire region of interest overlaid on the ArcGIS Online basemap orthophoto

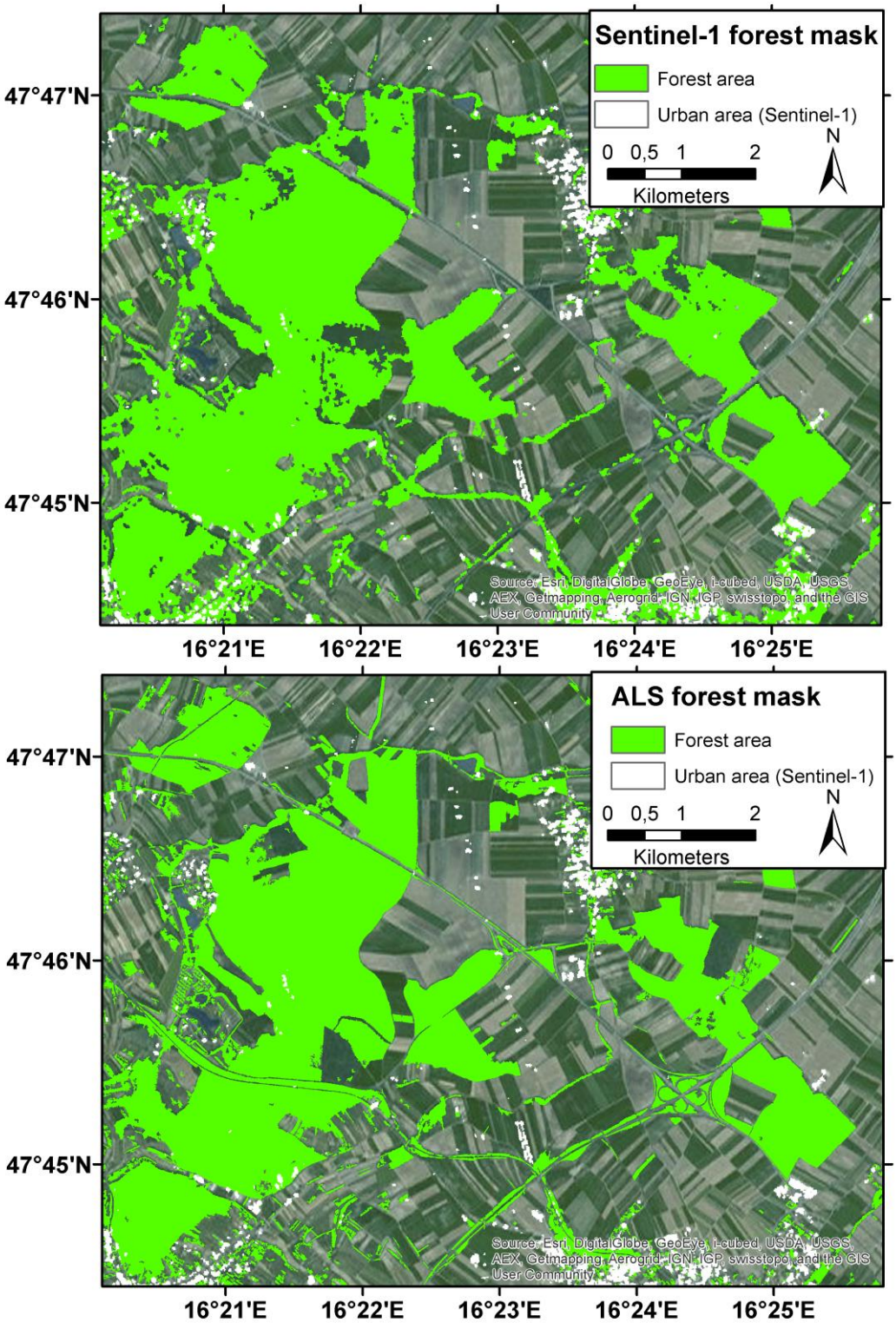

Figure 6: Subset of the ALS and Sentinel-1 based forest mask showing the clear-cut and forest growth changes between April 2010 and winter 2014/2015. The masks are overlaid on the ArcGIS online basemap orthophoto.

2.5 Conclusion

Forest mask was derived over a study area in eastern Austria using a single winter season

Sentinel-1A acquisitions. The resulting 10m resolution mask was validated using the reference ALS forest mask of the same area. Despite the temporal gap of almost 5 years between the ALS and Sentinel-1 data acquisitions, the overall accuracy reached 93% with kappa statistics of 0.83 when using the threshold method and Corine land cover data to mask the problematic urban areas. Without external data for urban masking, the overall accuracy reached 92% with kappa value of 0.81. The forest mask from Sentinel-1 data has high potential for forest change detection mapping. Further research is needed to assess the applicability of the method on larger scale and for various forest types.

Acknowledgements

This work is founded from the European Community's Seventh Framework Programme (FP7/2007–2013) under grant agreement No. 606971, the Advanced_SAR project.

3 Publication II: Annual Seasonality in Sentinel-1 Signal for Forest Mapping and Forest Type Classification

This section is an accepted manuscript version of the following article, accepted for publication in the International Journal of Remote Sensing:
Dostálová, Alena, Wolfgang Wagner, Milutin Milenković, and Markus Hollaus. "Annual seasonality in Sentinel-1 signal for forest mapping and forest type classification." International Journal of Remote Sensing 39, no. 21 (2018): 7738-7760, available at https://doi.org/10.1080/01431161.2018.1479788.

Abstract

The Sentinel-1 satellites provide the formerly unprecedented combination of high spatial and temporal resolution of dual polarization synthetic aperture radar data. The availability of dense time series enables the derivation and analysis of temporally filtered annual backscatter signals. The study concentrates on the use of Sentinel-1 seasonal backscatter signatures for forest area estimation and forest type classification. A classification method based on time series similarity measures is introduced and tested in three test areas covered by various forest types including broadleaf temperate, boreal and montane forests. The results are compared with two European-wide Copernicus high resolution layers, namely forest type and tree cover density (TCD). The correspondence of forest/non-forest maps and TCD is high in all test areas, with overall accuracies for forest/non-forest classification between 86% and 91% and Pearson correlation coefficients for TCD between 0.68 and 0.74. The forest type classification (non-forest, coniferous and broadleaf forest classes) provides best results in temperate forests with an overall accuracy of 85%; in boreal forest, the accuracy decreases to only 65%. Generally, the method provides reliable results for forest area estimation, including regions where methods based on static parameters are often problematic (mountainous areas), and it enables forest type classification in temperate forests.

3.1 Introduction

The high potential of microwave remote sensing instruments for providing information on the structure and moisture status of the vegetation has been recognized for several decades ((Ulaby, Moore et al. 1986)). One of the main motivations for using microwave sensors for the monitoring of vegetation is their low sensitivity to weather conditions, such as cloud cover or rainfall, as well as their independence from the solar illumination of the earth surface. These aspects are important as vegetation represents a dynamic target that changes in time. Many applications, such as agricultural monitoring, phenology measurements or deforestation mapping, require regular image acquisitions of the same region; in areas with frequent cloud coverage or short sun illumination periods, this can often be a limiting factor for optical sensors. Microwave approaches may therefore be a valuable complement to the well-established methods based on the optical remote sensing.

Synthetic aperture radars (SARs) are active microwave sensors with a relatively high spatial resolution of several metres to hundreds of metres. In forestry, a multitude of methods have been developed over the past decades that are based on the information provided by the SAR instruments. Their main applications include above ground biomass estimation ((Le Toan, Beaudoin et al. 1992); (Joshi, Mitchard et al. 2015);(Minh, Le Toan et al. 2016)), forest height retrieval ((Wallington and Woodhouse 2006); (Kugler, Schulze et al. 2014); (Yu, Hyyppä et al. 2015)), forest cover mapping ((Le Toan, Mermoz et al. 2014); (Shimada, Itoh et al. 2014); (Dostálová, Hollaus et al. 2016)) and clear-cut detection ((Motohka, Shimada et al. 2014); (Reiche, Verbesselt et al. 2015); (Barreto, Rosa et al. 2016)). The limitations of these methods are already well described. Methods based on radar backscatter, especially the short wavelength sensors (X- or C-band) are limited by the wavelength dependent saturation ((Imhoff 1993)). Furthermore, the radar backscatter is sensitive to changes in environmental conditions, such as moisture variation in both vegetation and the underlying soil ((Lucas, Armston et al. 2010)) or freeze-thaw events ((Ranson and Sun 2000)). This might lead to the erroneous interpretation of the imagery or to a lower sensitivity to the observed phenomena ((Sharma, Leckie et al. 2005); (Olesk, Voormansik et al. 2015)). A number of studies suggest that the use of multi-temporal measurements might partially overcome these limitations and provide more reliable results. For instance, multi-temporal combination of individual growing stock volume estimates have been demonstrated to improve the retrieval as compared to the single-image case ((Santoro, Beer et al. 2011)). Another possibility is to compute parameters from multiple SAR acquisitions such as averages of

selected images ((Dostálová, Hollaus et al. 2016); (Haarpaintner, Davids et al. 2016)) or measures of temporal change ((Quegan, Le Toan et al. 2000)). These can be used for forest area estimation instead of the single images.

In case of the forest mapping, the main limitation of the multi-temporal approach is the similarity of the derived parameters over forests and some other land cover classes. For instance, non-forest land cover classes covered by woody vegetation, such as vineyards or residential urban areas, have the absolute value of backscatter close to that of forest and are therefore often misclassified ((Dostálová, Hollaus et al. 2016)). Furthermore, stable non-forest targets (e.g. urban areas) and forest regions exhibiting significant variability due to flooding or freeze – thaw effects represent the main error sources in case of the temporal stability approach. Especially montane and boreal forests require the proper selection of the datasets used, as the acquisitions taken under frozen conditions introduce large variations in backscatter values ((Quegan, Le Toan et al. 2000)).

Multi-temporal SAR acquisitions of forested areas have also been studied to better understand the sources of backscatter variations ((Ahern, Leckie et al. 1993); (Pulliainen, Kurvonen et al. 1999); (Proisy, Mougin et al. 2000); (Magagi, Bernier et al. 2002); (Sharma, Leckie et al. 2005); (Santoro, Fransson et al. 2009)). In addition to the changing environmental conditions and noise, the vegetation growth cycle and seasonal changes in forest structure are also expected to influence the SAR response from forested regions. Until recently, however, studies looking at the annual signal variations caused by vegetation growth reported mostly pessimistic results. Backscatter time series over forest stands were reported to be chaotic or only very weak seasonal signals caused by tree phenology were found ((Proisy, Mougin et al. 2000)). These studies were often limited by the low temporal sampling of about 10–15 measurements per year. This is a problem as the long repeat period between the acquisitions does not allow a reliable separation of the short-term backscatter variations caused by changing environmental conditions and the noise from the annual changes caused by the vegetation growth cycle. Despite the limited temporal coverage, some differences between various forest types have been observed. For instance, (Sharma, Leckie et al. 2005)) reported slight increase of backscatter during wintertime in the case of hardwoods while (Ahern, Leckie et al. 1993) showed that there are observable differences between softwoods and deciduous forest types; the deciduous tree species, including tamarack, were reported to have higher backscatter relative to the coniferous species under leaf-off conditions.

The so-far unprecedented temporal and spatial coverage of high resolution C-Band SAR data provided by the Sentinel-1 constellation motivates further analyses of the annual

seasonality in SAR signal. For instance, (Guccione, Lombardi et al. 2016) performed a statistical analysis of the seasonal effects of the Sentinel-1 radar backscattering coefficient for various vegetation classes including deciduous and boreal forests. Significant statistical differences between the seasonal periods (3 months) were reported for both forest types. Furthermore, (Dostalova, Milenkovic et al. 2016) focused on the single-year time series over forested areas and derived a temporally filtered seasonal signal. Differences in the annual backscatter variation were attributed to the forest type (coniferous, deciduous or mixed forest) and forest structure. The results of (Ahern, Leckie et al. 1993) or (Dostalova, Milenkovic et al. 2016) suggest that the differences in the seasonal behaviour of SAR backscatter might be used for forest type classification.

The measurement of the forest area and location is a fundamental task in forestry. It represents an essential input to studies of forest resources, global carbon cycle, forest ecosystems and their productivity functions. Furthermore, changes in the forest area are a major focus of operational forest management and studies of forest change detection. The recent studies of (Dostálová, Hollaus et al. 2016) or (Haarpaintner, Davids et al. 2016) showed that the Sentinel-1 data can be used for forest area mapping in both temperate and boreal forests. The objective of this article is to exploit the potential of the multi-temporal Sentinel-1 dataset for forest area mapping and forest type classification. In contrast to the previous studies, the temporally smoothed backscatter time series (SAR seasonality) are used for the classification instead of the parameters describing the backscatter response or its temporal behaviour. We assume that the use of the time series might limit the error sources in the forest/non-forest classification as the forested regions are expected to have distinct seasonal signal that can be differentiated from other vegetation types and land cover classes. The differences in annual growth cycle between various tree species, especially between the coniferous and broadleaf tree types, may also enable forest classification. The approach for forest mapping and forest type classification based on a full year Sentinel-1A time series is developed and tested in three regions with different climatic conditions and various forest types ranging from temperate to boreal forest. The results are validated against Copernicus high resolution layers (HRL) forest type (FTY) and tree cover density (TCD; (Langanke, Büttner et al. 2013)) products.

3.2 Data

3.2.1 Sentinel-1

The Sentinel-1 constellation comprises two satellites: Sentinel-1A and Sentinel-1B, launched on 3 April 2014 and 25 April 2016, respectively. Each of the satellites has a

repeat orbit cycle of 12 days. Both satellites carry a C-Band SAR sensor that is capable of providing dual polarization observations in several measuring modes. The main mode used for land applications is Interferometric Wide swath (IW) mode, which provides data with the spatial resolution of 20 m × 5 m and, in central Europe, delivers up to four measurements in dual polarization – vertical transmit and vertical receive (VV) and vertical transmit and horizontal receive (VH) – per orbit cycle of a single sensor. In winter, parts of northern Europe are acquired also in Extra Wide swath (EW) mode with a spatial resolution of 100 m × 25 m and horizontal transmit and horizontal receive (HH) and horizontal transmit and horizontal receive (HV) polarizations.

Within this study, all available IW mode Level 1 Ground Range Detected (GRD) data in both polarizations from 2015 are used over the selected test areas. The maximal temporal resolution is four measurements within a single repeat orbit cycle, however, the actual number of measurements is considerably lower, especially in Swedish regions. Figure 7 presents the number of the available IW mode acquisitions from 2015 over Europe. The locations of the test areas are highlighted with blue squares. Table 2 summarizes number of used acquisition for each region.

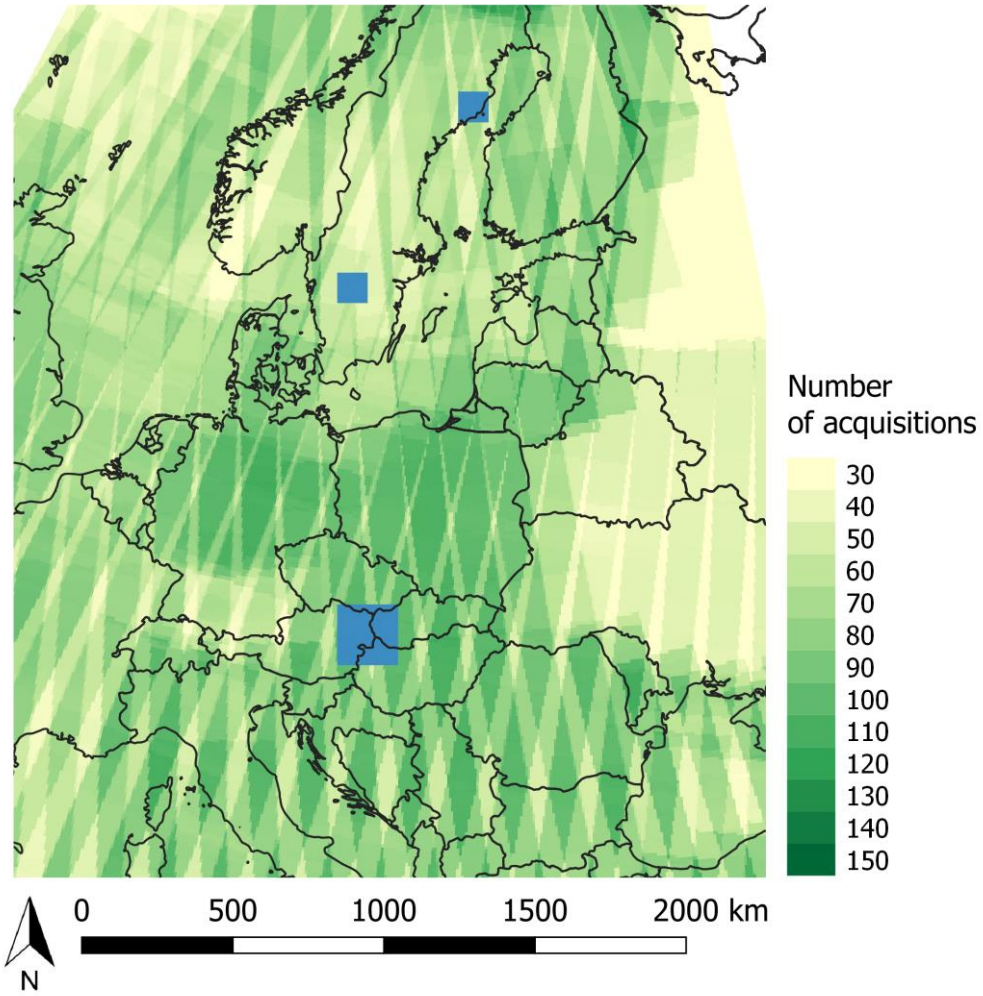

Figure 7: Data coverage of Sentinel-1 A IW dual polarization data in 2015. Blue squares highlight the test areas.

Table 2: Summary of the Sentinel-1 A IW dual polarization data in 2015 over the test areas.

Test area	Size (km)	Number of acquisitions	Coverage per pixel	Maximal temporal gap (days)
Neusiedl Lake	200 × 200	336	56-132	12
Remningstorp	100 × 100	146	44-78	24
Krycklan	100 × 100	209	70-125	60

3.2.2 Copernicus HRL datasets

The main objective of the Copernicus HRLs is the high resolution, homogenous land

cover monitoring in European countries. The products cover 39 member states and affiliated countries to the European Environment Agency (EEA). As a reference, the freely available pan-European Copernicus HRL 20 m FTY and 100 m TCD products were used. These datasets are provided by the EEA Global Monitoring for Environment and Security/Copernicus Initial Operations Land and were derived using semi-automatic classification and computer aided visual refinement based on high resolution satellite imagery that included Indian Remote Sensing-ResourceSat 2 (IRS-RS2), Satellite Pour l'Observation de la Terre (SPOT) and RapidEye acquired in 2011 and 2012.

The TCD dataset represents the degree of TCD of each pixel in percent. No minimum mapping unit (MMU) is applied, only a minimum mapping width (MMW) of 20 m. All detectable trees are included, independent of their use. The shrub land, dwarf pine and green alder in high or mountainous areas and Mediterranean bush land are excluded as well as open areas within forests such as roads or clear cuts in cases where no tree cover can be detected from the 20 m resolution imagery. The FTY product is closely aligned to the forest definition of Food and Agriculture Organization (FAO) meaning that the forests are defined as lands of more than 0.5 ha with a tree canopy cover of more than 10% which are not primarily under agricultural or urban use (FAO 1998). The 20 m × 20 m FTY product is produced from the 20 m TCD product by applying a threshold of TCD of at least 10%, MMU of 0.5 ha and MMW of 20 m. The dominant leaf type of the trees within each pixel is specified, using two classes – broadleaf and coniferous (EEA 2013).

Validation of the Copernicus HRL forest layers was done using manual interpretation of high and very high resolution reference data for 17,297 sample units over Europe. Both layers were validated at a spatial resolution of 100 m using confusion matrix in case of the forest type and coefficient of determination (R^2) of a linear regression in case of the TCD. The R^2 is defined as:

$$R^2 = \frac{\sum_{i=1}^{n}(f_i-\bar{y})^2}{\sum_{i=1}^{n}(y_i-\bar{y})^2} \quad (1)$$

In the equation, n represents number of samples, y the sample value, $\bar{y}$ the average value and f the predicted value using the linear regression. Results for forest type, forest/non-forest classification and TCD (Table 3) vary according to their biogeographical region. Therefore, overall results are listed as well as results for all biogeographical regions that cover at least part of the test areas of this study (Alpine, Boreal, Continental, Pannonian regions). Details about the validation procedure and results can be found in the Copernicus HRL forest validation report (SIRS 2016).

Table 3: Results of the Copernicus HRL 100m forest type and tree cover density validation (SIRS 2016). In the table, I. stands for broadleaf forest class and II. For coniferous forest class.

	TCD	Regrouped forest class		Forest type			
Biogeographical region	**R^2**	**Producers accuracy (%)**	**Users accuracy (%)**	**Producers accuracy (%)**		**Users accuracy (%)**	
				I.	**II.**	**I.**	**II.**
Alpine	0.71	90	83	77	71	50	63
Boreal	0.75	93	89	37	84	17	58
Continental	0.75	92	87	86	67	65	80
Pannonian	0.79	89	88	88	62	69	98
Overall	0.67	89	83	73	75	57	58

3.3 Test areas

Three test areas representing different climatic conditions and biomes were chosen to test the methods as described in the next section. The regions were selected from the test areas of the European Community's Seventh Framework Programme Advanced_SAR project using the overlapping Equi7 Grid ((Bauer-Marschallinger, Sabel et al. 2014)) 100 km × 100 km large tiles. These test areas include areas around Neusiedl Lake in eastern Austria together with four overlapping Equi7 Grid tiles, Remningstorp forest holding in southern Sweden and Krycklan area in northern Sweden, both including single overlapping Equi7 Grid tile.

3.3.1 Neusiedl Lake

The largest test area is centred at 48° N and 17° E and covers four Austrian federal states (Burgenland, Niederösterreich, Steiermark and Wien) as well as part of western Slovakia and Hungary and south-east Czech Republic, covering a total area of 200 km × 200 km. The eastern part of the region is flat and characterized by temperate broadleaf forest while the western part is mountainous with altitudes ranging up to 2000 m asl. In the highest elevations, montane forests can be found. The lowlands are densely populated and dominated by agricultural fields, a large wetland area around the Neusiedl Lake and some vineyards regions around Vienna, Neusiedl Lake and Sopron. The study area includes large cities (e.g. Vienna and Bratislava) as well as numerous small villages. In the lowlands, the forest patches are typically broadleaved, rather small and are composed of oaks, beeches or hornbeams. In areas along the Danube River, poplar trees are also common. Coniferous species in the flat parts of the study area are mostly pine trees. In hilly and mountainous areas, larger mixed or coniferous forests can be found. Broadleaf species are represented by oaks, beeches, maple trees and birches while spruce and pine trees are the most common occurring conifers.

Generally, the Sentinel-1 IW data coverage is very dense in central Europe; the largest temporal gap in 2015 was 12 days within the Austrian test area, meaning that in each orbital cycle at least one acquisition was secured. Typically, two to four observations per orbital cycle were available in 2015.

3.3.2 Remningstorp

The test area in southern Sweden covers an area of 100 km × 100 km and is centred at 58° N and 14° E around the forest holding of Remningstorp. The region is located in the Västra Götland County and is characterized by hemi-boreal forest and flat topography with elevations between 100 and 370 m asl. The area spans between lakes Vänern and Vättern and the dominant land cover types are forest and agricultural land. Moreover, numerous lakes and some wetlands can be found. The prevailing tree species are spruce, pine and birch and stem volumes range typically up to 400 m^3ha^{-1} although in some areas volumes can reach up to 700 m^3ha^{-1} ((Santoro, Fransson et al. 2009)).

A large part of the Scandinavian Peninsula has low coverage of Sentinel-1 A IW mode data during wintertime. This concerns both of the Swedish test areas. In the case of the Remningstorp area, the number of acquisitions in January to March 2015 is strongly limited with longest gap between subsequent acquisitions being between 7 February 2015 and 3 March 2015. From April onwards, regular coverage of at least one measurement per 12 day orbital cycle is available.

3.3.3 Krycklan

The Krycklan test area is located within boreal zone at around 64° N and 20° E in northern Sweden (Västerbotten County) and covers an area of 100 km × 100 km. The area is sparsely populated with only a single large city (Umea) located on the shores of the Gulf of Bothnia. Most of the area is covered by forests, together with some agricultural areas, lakes and wetlands. The topography is undulating with several gorges and elevations ranging between sea level and 400 m asl. The forests are relatively sparse with typical stem volumes around 150 m^3ha^{-1} and maximum values of 400 m^3ha^{-1} ((Santoro, Fransson et al. 2009)). The most common tree species are pine and spruce among conifers and birch among broadleaf trees.

Similar to the Remningstorp region, the coverage of the Sentinel-1 IW mode acquisition during the winter season of 2015 is strongly limited to only a few images between January and May 2015. In the south-west part of the area, there is a gap of two months (11 January 2015 to 12 March 2015) between acquisitions. Due to the limited data

availability during winter, the short vegetation growth period and the relatively high influence of the forest understory layer when compared to the denser forests in the southern regions, the Krycklan area was expected to be the most challenging.

3.4 Method

The algorithm for forest/non-forest, FTY and TCD retrieval is outlined in Figure 8 and consists of the following major blocks:

1) Sentinel-1 level 1 GRD data pre-processing using the SAR Geophysical Retrieval Toolbox (SGRT) software ((Elefante, Wagner et al. 2016))
2) Generation of temporally smoothed backscatter time series (SAR seasonality)
3) Forest/non-forest and FTY classification and TCD derivation

These steps are described in detail in the following sections.

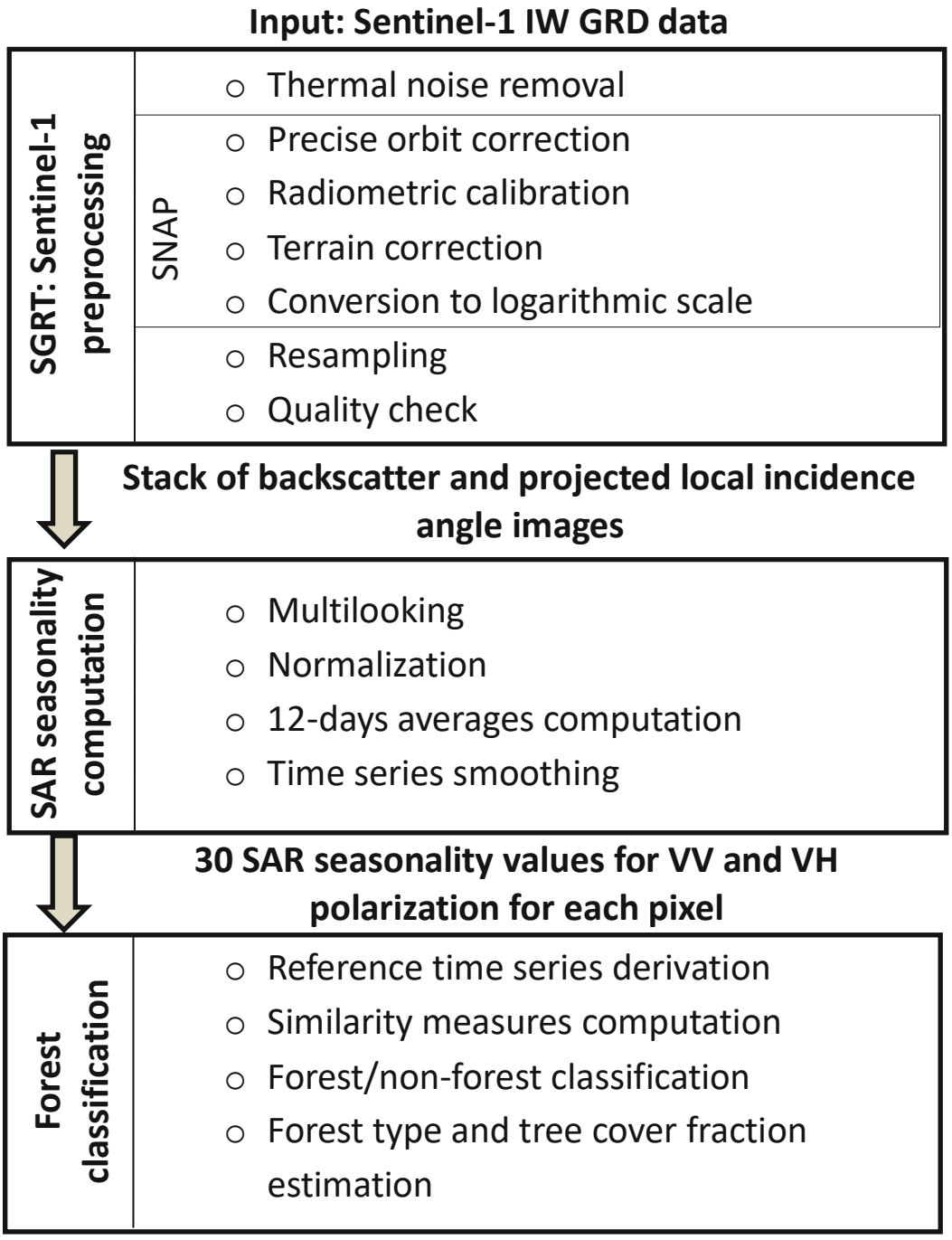

Figure 8: Overview of the algorithm used to classify forest type and compute tree cover density from Sentinel-1 data

3.4.1 Sentinel-1 data pre-processing

The pre-processing block requires Sentinel-1 level 1 GRD data as an input and produces a stack of radiometrically calibrated (sigma nought – σ°) and terrain corrected geocoded images resampled to the Equi7 Grid 100 km × 100 km large tiles with 10 m pixel spacing in geotiff format. This is done using the pre-processing workflow within the SGRT

software. This software was developed at Technische Universität (TU) Wien and aims at the automated processing of large volumes of SAR-based products such as soil moisture, forests, wetlands, open water or flood mapping. It is written in Python and includes also some external software modules, in particular the Sentinel Application Platform (SNAP) software that is used for part of the SAR pre-processing. The SGRT software includes three major blocks – the so-called workflows: pre-processing, parameter estimation and product derivation. Within the pre-processing workflow, following steps are applied:

1) Thermal noise removal
2) Precise orbit correction
3) Radiometric calibration to the σ° values
4) Range-Doppler terrain correction using the Shuttle Radar Topography Mission (SRTM) digital elevation model (DEM) ((Farr, Rosen et al. 2007))
5) Conversion from linear to the logarithmic scale
6) Resampling to the Equi7 Grid
7) Quality check for corrupted or shifted images (semi-automated)

All steps except (7) require no manual interaction. Within the last step, only the shifted images are found automatically, the check for corrupted images (i.e. areas of unnaturally high backscatter values as presented in (Dostálová, Naeimi et al. 2016)) is achieved by a manual check of the image quick looks. The steps (2) to (5) are performed in the SNAP software using the graph processing tool functionality. The output of the pre-processing workflow includes σ° and projected local incidence angle (θ) images. The mask of layover and shadows was created using the SNAP software for the area around Neusiedl Lake.

3.4.2 SAR seasonality

The pre-processed Sentinel-1 σ° time series show variations of up to 10 dB over forests and even higher over agricultural land. This is mainly caused by the varying imaging geometry, changing environmental conditions as well as speckle noise. To quantify the considerably weaker seasonal variation, these short-term influences need to be removed. To do so, (Nguyen, Clauss et al. 2015) introduced a method to derive SAR-based phenology information over rice fields using temporal filtering of Envisat Advanced SAR (ASAR) data. This approach was modified for Sentinel-1 and introduced in (Dostalova, Milenkovic et al. 2016). The method includes the following steps:

8) Multi-looking of 2 by 2 pixels to limit the speckle noise.

9) Backscatter normalization to the reference θ of 40° using the slope (β) parameter and the following equation:

$$\sigma^0(40°) = \sigma^0(\theta) - \beta(\theta - 40°) \quad (2)$$

The β parameter is computed from the linear regression between the $\sigma°$ and θ values for each pixel. This approach is based on the assumption of linear relationship between backscatter and projected local incidence angle within the limited range of available incidence angles of a SAR sensor (29.1° to 46.0° in case of Sentinel-1 and flat terrain) and enables the combination of measurements from different relative orbits and thus acquired with different viewing directions. The approach is, however, limited by the low number of various incidence angles in some areas, where no reliable slope value from Sentinel-1 can be derived. In these areas, slope from the full archive of Envisat ASAR Wide Swath mode data was used instead. Furthermore, the β parameter varies with vegetation growth ((Peters, Lievens et al. 2012)), yet it was assumed to be temporally stable, as the data coverage in 2015 is not sufficient to compute its seasonal variation.

10) Computation of 12 day averages (duration of single orbit cycle) to limit the impact of short-term variations caused by environmental conditions (i.e. precipitation and differences in soil and vegetation moisture content) and noise and to ensure regular temporal steps.

11) Application of a Gaussian temporal filter to further limit the impact of the remaining short-term variations, noise and smooth potential outliers.

As a result, 30 SAR seasonality values were derived at 12 day temporal steps for each 20 m × 20 m pixel and both polarizations (VV and VH). Figure 9 presents an example of the pre-processed $\sigma°$, 12 day averages and SAR seasonality time series over several vegetation types within the Austrian test area. While the pre-processed $\sigma°$ values are dominated by short-term variations and differences between various vegetation types are hard to define, the SAR seasonality time series enables better distinction between vegetation types. The annual variation is very strong over most of the agricultural crops and much more stable over forests or vineyards. Generally, the range between minimal and maximal value is typically between 1.5 and 3.0 dB in case of woody vegetation while in case of agricultural crops, seasonal effects cause as much as 8.0 dB difference between summer and winter conditions. However, the differences are observable not only between woody and herbaceous plants, but also between various types of woody vegetation – in this case between coniferous and broadleaf forest and vineyards. While broadleaf forest

can easily be distinguished from the other two vegetation types due to the backscatter drop in spring and summer, coniferous forest and vineyards show similar seasonal behaviour as well as the same absolute values of backscatter. Minor difference can be observed in autumn. In case of conifers, the backscatter decreases steadily from its maxima in late summer while in case of vineyards, enhanced backscatter can be observed both in summer and in autumn. These differences enable the use of the seasonal signal both for forest/non-forest classification and for distinguishing between the two forest types.

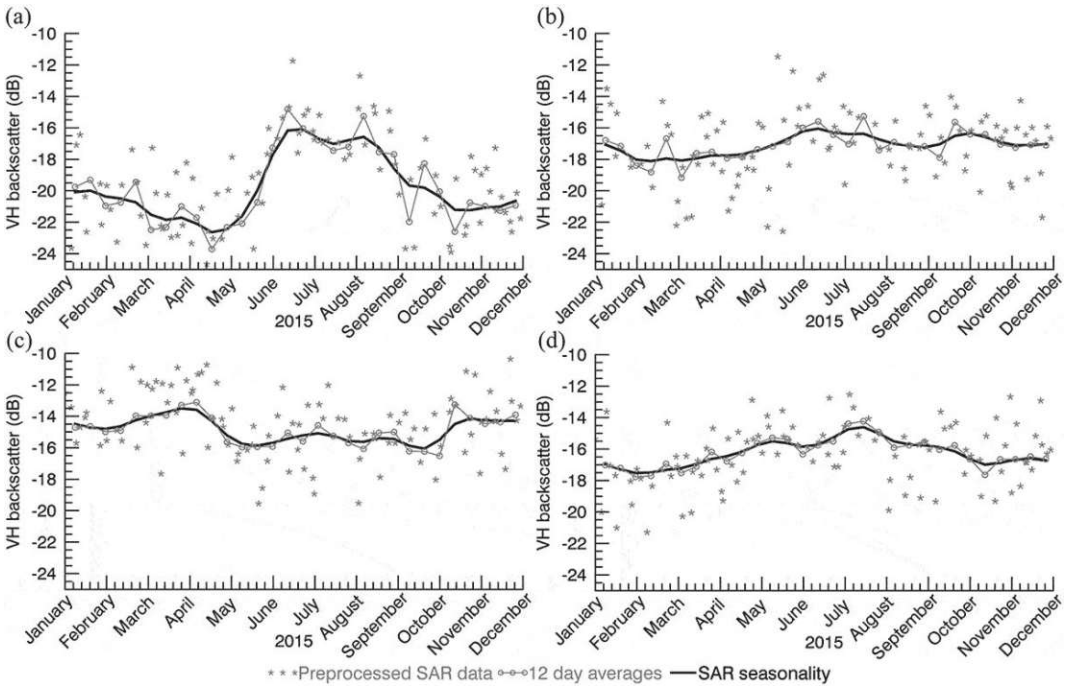

Figure 9: Examples of Sentinel-1 A VH polarization time series in 2015 over various vegetation types: (a) agricultural field, (b) vineyards, (c) broadleaf forest and (d) coniferous forest. Each plot shows pre-processed data, 12 day averages and computed annual signal (SAR seasonality).

3.4.3 Forest classification and TCD computation

The forest/non-forest and forest type classification algorithm is based on the similarity measures – root mean square difference (RMSD) and Pearson correlation coefficient (r) – between the so-called reference time series for different forest types that are selected manually for each test area and respective SAR seasonality time series of each pixel. The FTY and TCD maps are derived using the following main steps:

12) Selection of the reference sites (300 m × 300 m large forested sites that represent the most common forest types within each test area) and the derivation of the reference SAR seasonality time series computed from the average backscatter values over the 300 m × 300 m large sites. For each test area, four reference sites are selected. Alternatively, a reference time series might also be used for any

other vegetation or land cover class that causes classification errors due to its similarity to some of the forest classes (within this study, vineyards class was added in case of the Neusiedl Lake test area).

13) Computation of *r* and RMSD values for each pixel within the test area between the respective SAR seasonality and each reference time series for both polarizations.

14) Image classification based on thresholds for RMSD and *r* values. Each pixel that falls within the thresholds with any of the reference time series is assigned the value 1.

15) Forest type classification based on the lowest value of RMSD in VH polarization. Subsequently, TCD is computed as the fraction of 20 m × 20 m pixels classified as coniferous or broadleaf forests within each 100 m × 100 m area.

16) MMU of 0.5 ha is applied for the forest type map.

Here, we describe the methodology for the Neusiedl Lake area in detail. For this area, the following reference sites (forest classes) are selected: coniferous forest in lowland (managed, row planted, pine forest), coniferous forest in hilly and mountainous regions (mixed forest, dominated by spruce and pine trees, often mixed with some broadleaf trees), broadleaf forest in lowland (dense, high forest, typically dominated by oak trees) and broadleaf forest in mountainous regions (sparse, low trees, often mixed with some conifers). The locations of the selected reference sites are presented in Figure 10 and listed in Table 4 while Figure 11 (a-d) shows the structure of the respective forest classes as recorded in January 2017 under leaf-off conditions. The derived reference SAR seasonality time series are presented in Figure 11 (e and f).

Table 4: Locations of the sites used for computation of the reference SAR seasonality time series.

Point ID	Longitude	Latitude	Forest type	Note
P1	16°17′14.73″	47°46′35.45″	Coniferous	Mountainous terrain
P2	16°08′18.04″	47°46′01.73″	Coniferous	Lowland
P3	16°29′37.45″	47°43′42.93″	Broadleaf	Lowland
P4	15°40′25.65″	47°44′30.94″	Broadleaf	Mountainous terrain

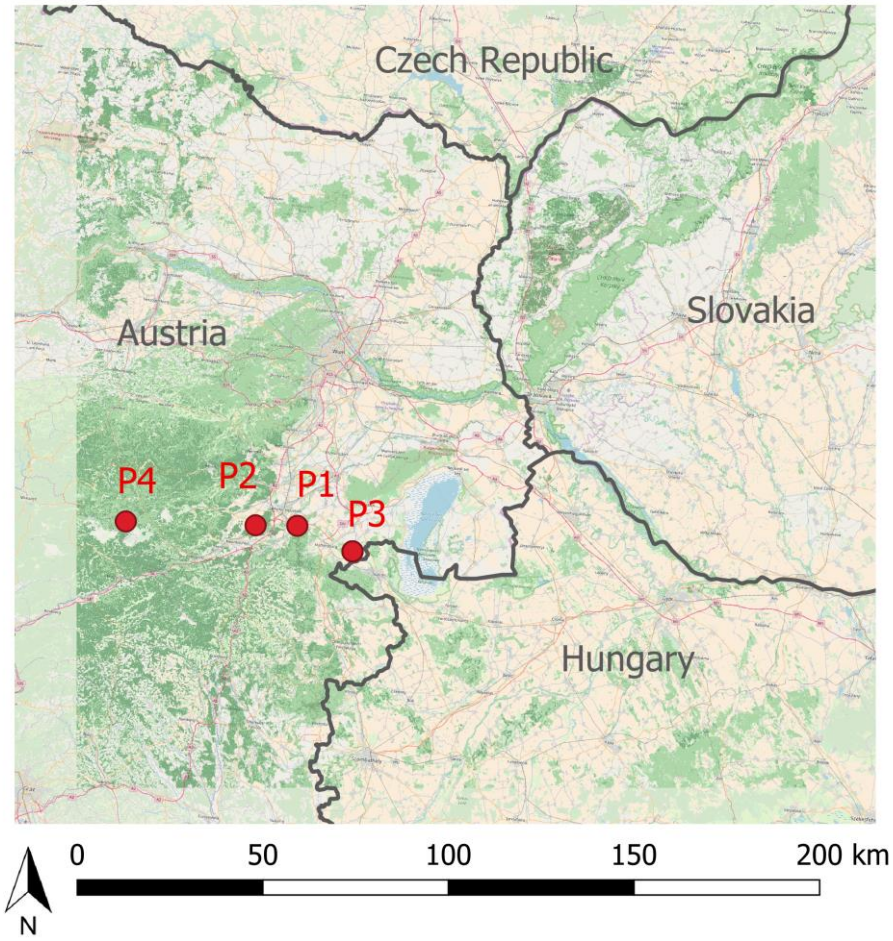

Figure 10: Overview of the Austrian test area and the locations of the sites used for computation of the reference seasonality time series

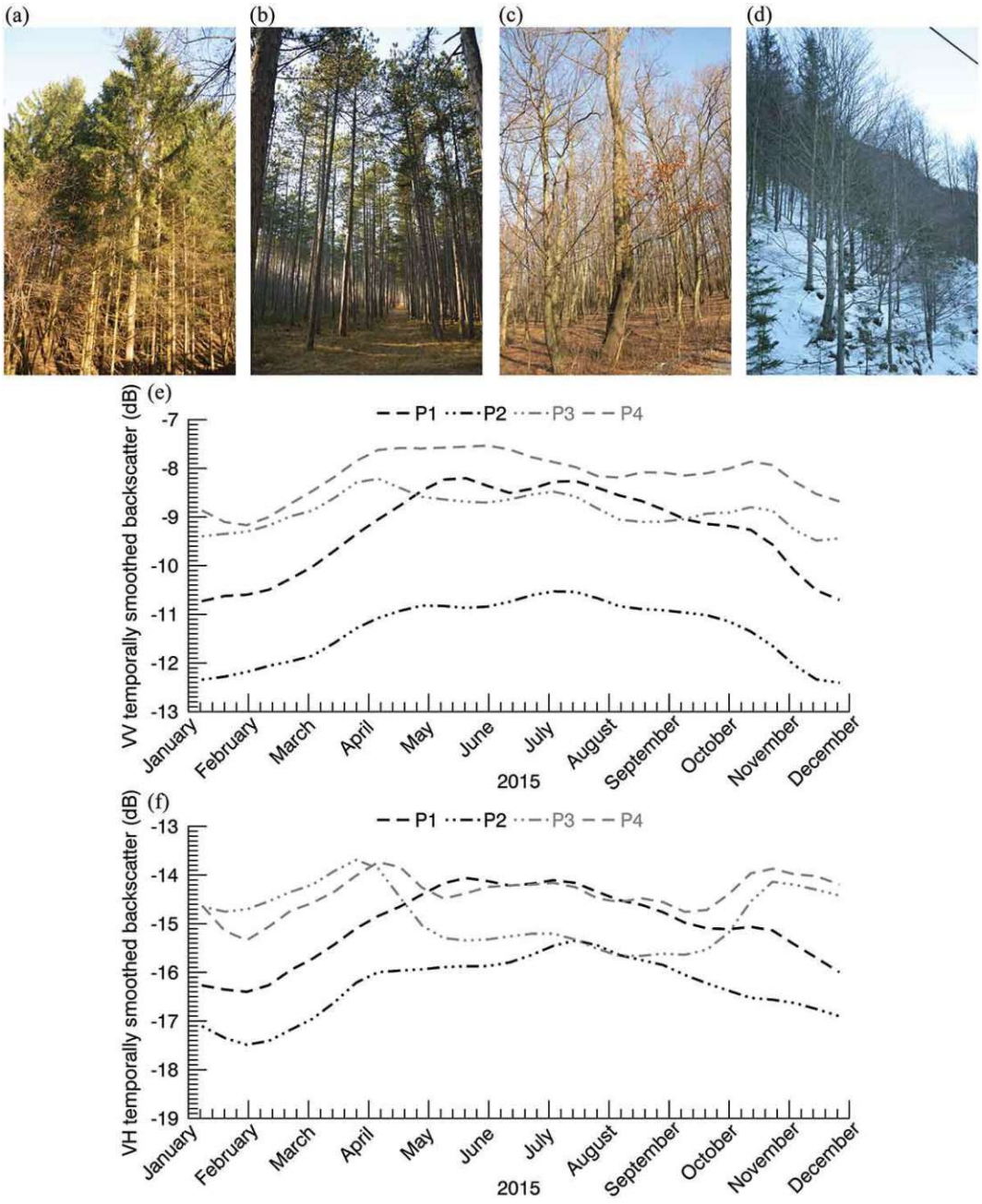

Figure 11: (a)-(d) photographs of the selected forest sites for reference SAR seasonality time series in case of the Austrian area. (a) Reference site P1 (coniferous forest in mountains), (b) reference site P2 (coniferous forest in lowlands), (c) reference site P3 (broadleaf forest in lowlands) and (d) reference site P4 (broadleaf forest in mountains). The images were taken in January 2017 under leaf-off conditions. (e) VV polarization reference seasonality time series for the Austrian test area. (f) VH polarization reference seasonality time series for the Austrian test area.

In the case of both coniferous classes, the minimal values occur in wintertime, after that the backscatter gradually increases towards its maximum between May and August and then decreases again. This behaviour is visible in both VV and VH polarization, and the range between summer and winter values is typically 1.5–3.0 dB. This variation can be caused by many sources, such as the changes in dielectric constant ((Ahern, Leckie et al. 1993)), seasonal needle drop or changes in herbaceous ground vegetation. The two reference areas of the coniferous forests differ in the absolute value of the signal with a

bias of approximately 1.5 dB where the lower values are typical for the planted pine forests in lowland.

The broadleaf woodland shows different temporal behaviour, especially in VH polarization. While in the case of VV polarization, the annual signal is relatively stable with slightly increased values in spring time, the VH polarization shows a significant drop of backscatter in spring and increase in autumn with the magnitudes between 0.5 and 2.0 dB. The higher differences are typically observed in lowlands where the forests are dense. The drop and increase of backscatter is expected to be connected to the seasonal change of the tree foliage, suggesting that the leaves absorb or forward scatter the signal rather than scattering it back ((Ahern, Leckie et al. 1993)). The drop of backscatter signal in summer time aligns with previous findings ((Ahern, Leckie et al. 1993); (Sharma, Leckie et al. 2005); (Dostalova, Milenkovic et al. 2016)), however, evidence also exists for the increase of backscatter during leaf-on conditions ((Ulaby, Moore et al. 1986); (Zoughi, Bredow et al. 1989)). This might be dependent on the tree species, forest structure and density or imaging geometry ((Ahern, Leckie et al. 1993)).

The differences between forests and other vegetation types as well as between forests dominated by coniferous and broadleaf tree species described above enable the forest classification using the similarity measures. These are computed for each pixel within the study area. First, distinction between woody and herbaceous vegetation is made, where each point is assigned the value 1 in cases where the RMSD between any of the reference time series (including vineyards) and the classified pixel is below 1.5 and 2.0 dB for VH and VV polarization, respectively, and the r in VH polarization exceeds 0.4. Otherwise, the pixel is assigned the value 0. These thresholds were specified manually and are the same for all vegetation classes and all study regions. Subsequently, the vegetation type (coniferous forest, broadleaf forest, vineyards) is specified according to the lowest RMSD value in VH polarization. While coniferous and broadleaf forest classes are further handled as forests, the pixels classified as vineyards are added to the non-forest class. Finally, clean-up procedures and product derivation are carried out. For the FTY map, the MMU of 0.5 ha is applied, while the 100 m TCD product is computed from the classified image before the MMU application as a fraction of the 20 m × 20 m large pixels within each 100 m × 100 m area that were classified as forests. The FTY product represents an image with pixel spacing of 20 m and separated classes for non-forests, broadleaf and coniferous forests. The 100 m TCD map gives a portion of each 100 m large pixel that is covered by forests with steps of 4%.

The described methodology applies also for both Swedish test areas with the exception,

that no extra reference time series – such as vineyards class – were used. Furthermore, due to the high topography in Austrian region, the layover and shadow mask derived by SNAP software was used to mask the pixels, where the SAR sensor cannot provide reliable results. This mask was not required in the Swedish test areas.

3.4.4 Validation

The Sentinel-1-based FTY and TCD maps were validated against the reference products from Copernicus HRL using all available pixels. In the case of FTY, confusion matrices and kappa coefficients (κ) ((Congalton and Green 2019)) were computed both for forest/non-forest classification and for FTY classes while for TCD, r, bias and normalized RMSD (NRMSD, the RMSD value was normalized using the range of TCD values and expressed in percent) were derived for each of the test areas.

3.5 Results and discussion

3.5.1 Forest area and forest type classification

The Sentinel-1 and Copernicus HRL FTY maps for all three test areas are presented in Figure 12. Both datasets have a spatial resolution of 20 m and MMU of 0.5 ha. The confusion matrix and κ results for the forest/non-forest and forest type classification are summarized in Table 5. These represent the agreement between the Sentinel-1 and Copernicus HRL FTY maps where the correctness of the forest and non-forest area, as well as the classification into all three classes (non-forest, coniferous and broadleaf forest), is assessed separately.

Table 5: Results of the comparison of the Sentinel-1 and Copernicus HRL forest type maps. In the table, I. stands for non-forest forest class, II. for broadleaf forest class and III. for coniferous forest class.

	Forest/non-forest		**Broadleaf forest/coniferous/non-forest**							
Test area	**κ**	**Overall accuracy (%)**	**κ**	**Overall accuracy (%)**	**Producers accuracy (%)**			**Users accuracy (%)**		
					I.	**II.**	**III.**	**I.**	**II.**	**III.**
Neusiedl Lake	0.79	91	0.69	85	92	69	73	95	77	46
Remningstorp	0.78	89	0.60	77	91	42	67	90	38	72
Krycklan	0.69	86	0.42	65	87	21	69	80	19	69

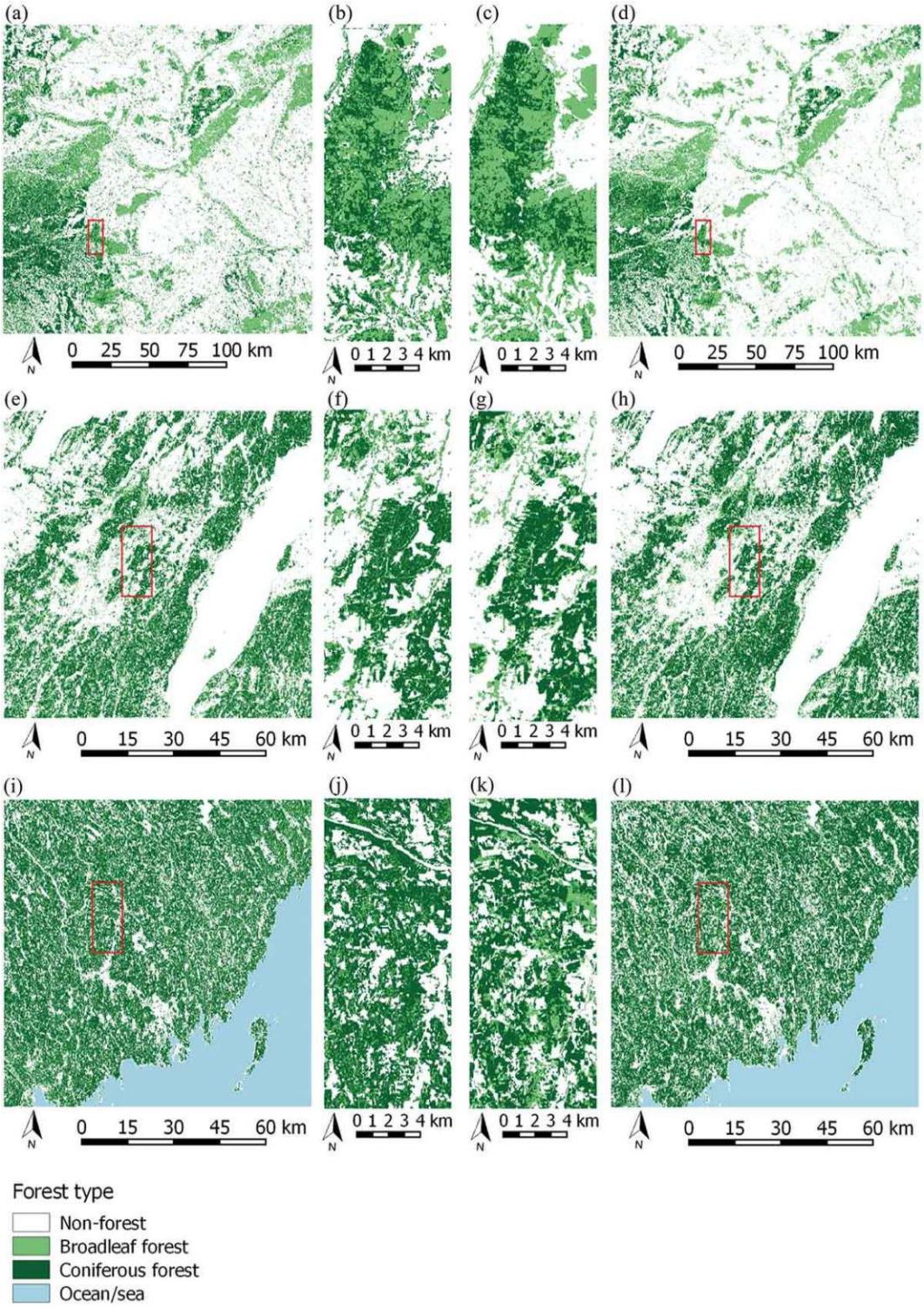

Figure 12: Forest types classification maps. (a) Sentinel-1, Lake Neusiedl, overview, (b) Sentinel-1, Lake Neusiedl, detail, (c) Copernicus HRL, Lake Neusiedl, detail, (d) Copernicus HRL, Lake Neusiedl, overview, (e) Sentinel-1, Remningstorp, overview, (f) Sentinel-1, Remningstorp, detail, (g) Copernicus HRL, Remningstorp, detail, (h) Copernicus HRL, Remningstorp, overview, (i) Sentinel-1, Krycklan, overview, (j) Sentinel-1, Krycklan, detail, (k) Copernicus HRL, Krycklan, detail, (l) Copernicus HRL, Krycklan, overview.

For the forest/non-forest classification, reliable results were achieved in all test areas with overall agreements between 86% and 91% and κ of 0.69–0.79 with the best agreement in the Austrian test area and the worst in Northern Sweden. In case of the Copernicus HRL,

the forest/non-forest classification accuracy increases in Boreal biogeographical region when compared to Alpine, Continental or Pannonian region (Table 3). For this reason, the lower correspondence between the Sentinel-1 and Copernicus HRL forest/non-forest classification is probably due to the decreasing accuracy of the Sentinel-1 based forest map in the hemi-boreal and boreal forests. We assume that the lower accuracy in the northern test areas is due to the decreasing stem volume of the forests and the increasing influence of long freezing periods on the annual backscatter signal as well as due to the lower temporal resolution of Sentinel-1 IW data over the Scandinavian Peninsula. The forest/non-forest classification results are comparable to those presented in previous studies on Sentinel-1 forest area mapping where the overall accuracies ranged between 83% and 92% when compared to forest maps based on optical remote sensing or airborne laser scanning measurements ((Dostálová, Hollaus et al. 2016); (Haarpaintner, Davids et al. 2016)). These studies were carried out in similar regions (temperate forest in Austria and boreal forests in Finland and Iceland). The method introduced in this study has the advantage that the same approach was tested in different forest types from temperate to boreal forest and also proved to be reliable in undulating terrain that was shown to be problematic ((Dostálová, Hollaus et al. 2016)). This was tested in the Austrian test area, where the overall accuracy of 92% and 88% was reached in regions with altitudes below 400 and above 800 m asl, respectively. Furthermore, in the densely populated Austrian region, the need for a separate method for urban area masking was demonstrated in (Dostálová, Hollaus et al. 2016)). The use of the seasonal signal minimizes the misclassification of other land cover classes with the specified forest classes and no additional masks, except the layover and shadow mask in undulating terrain were needed.

The main advantage of this method is, however, its potential to classify forest into predefined classes based on the differences between its seasonal signal – in the case of this study into coniferous and broadleaf forests. The results (Table 5) show high accuracy of the forest type classification (overall accuracy of 85% and κ of 0.69) in the Austrian test area where the best results were achieved in lowlands; the overall accuracy reached 89% for regions with altitudes below 400 m, but decreased to 76% for those between 400 and 800 m and only 67% accuracy is achieved for regions above 800 m. Lower accuracies in higher elevations are most likely due to the following two reasons. First, the SAR signal is generally less reliable in mountainous regions (foreshortening, layover and shadows) and the accuracy of the terrain correction is always dependent on the accuracy of the used DEM. As the 90 m SRTM DEM was used for the terrain correction of 10 m Sentinel-1 IW data, some inaccuracies are to be expected, especially when acquisitions from various imaging geometries are combined. The inaccuracies and the lower spatial

resolution of the used DEM, leading to the fact that the terrain is not described with sufficient detail, result in shifts that might, in sloping terrain, exceed 100 m between various relative orbits, especially when combining acquisitions from the ascending and descending orbit direction ((Dostálová, Naeimi et al. 2016)). The terrain correction accuracy of the Sentinel-1 IW data over mountains was not checked within this study as the quality check aimed to remove only images with systematic shifts and unnatural artefacts in backscatter values. However, the same type of data and processing settings were used as in (Dostálová, Naeimi et al. 2016)), where the accuracy of Sentinel-1 geocoding was assessed over part of the Austrian and Krycklan test areas. Therefore, lower geocoding accuracies in higher elevations are to be expected. Second, the contrast between the annual signal from coniferous and broadleaf forest decreases in higher elevations, when compared to the lowlands. This is due to the fact that the forests in mountainous regions are typically sparser and, often, some conifers might also be found in stands dominated by broadleaf tree species. For these reasons, the typical drop of backscatter in VH polarization during the leaf-on period of the broadleaf tree species (Figure 11) weakens or might not be observable at all.

However, the reliability of the forest type classification decreases strongly in both Swedish test areas. While in southern Sweden, a relatively good correspondence of $\kappa = 0.60$ and an overall accuracy of 77% are observed, in northern Sweden, the FTY classification provides considerably less reliable results ($\kappa = 0.42$ and overall accuracy of 65%). The average stem volumes in this region are below the expected saturation level of C-Band SAR signal (300 m^3ha^{-1} according to (Santoro, Cartus et al. 2013)) and almost no differences between the seasonal signals of coniferous and broadleaf forests can be observed. Furthermore, the validation of the Copernicus HRL FTY dataset (SIRS 2016) shows low accuracies of the forest type dataset in the Boreal region with user and producer accuracy of the broadleaf forest of only 17% and 37%, respectively (Table 3). Low correspondence in the Krycklan test area (Sentinel-1 FTY user and producer accuracy of the broadleaf forest of only 19% and 21%, respectively) can thus be attributed to the low accuracy of the Copernicus HRL dataset as well. For this reason, the validation in this test area requires better reference forest type data that were not available at the time of this study.

3.5.2 Tree cover density

Figure 13 shows the Sentinel-1 based TCD maps together with the Copernicus HRL TCD dataset for all of the test areas while Figure 14 shows the scatterplots of the TCD values. The scatterplots were plotted for 5000 randomly selected pixels per test area and darker

colour represents a higher density of points. Furthermore, *r*, NRMSD and bias values are listed in Table 6 where the statistics are presented in two ways – they are computed for all pixels as well as for the forested areas only, meaning that the points where TCD equals 0 are excluded. This was done to eliminate the influence of the agreement between the forest/non-forest maps and assess the accuracy of the TCD for the forested land only. Nevertheless, for completeness, also the statistics including all available pixels are listed.

The agreement between the Sentinel-1 and Copernicus HRL TCD maps is relatively strong (*r* of 0.68–0.74 and NRMSD between 28% and 30% for the forest pixels only), however, the Sentinel-1-based product tends to overestimate the TCD when compared to the Copernicus dataset. The bias is almost constant for all test areas (17–18%). The overestimation is also evident at the scatterplots in Figure 14, where the highest TCD values in case of Copernicus HRL dataset only rarely exceed 90%, whereas in case of the Sentinel-1 TCD, they often reach 100%. As for the FTY product, the best results are achieved for the Austrian test area, the accuracy decreases slightly in case of southern Sweden and weakest agreement can be found in boreal forest in northern Sweden. Similarly, the accuracy decreases with higher altitudes; in the case of the Austrian area, the numbers listed in Table 6 are representative for areas up to 700 m asl. However, even for elevations between 1500 and 2000 m asl, the *r* and NRMSD equals 0.59 and 31%, respectively. The accuracy of the reference Copernicus HRL FTY is high in all biogeographical regions that are represented within the test areas with R^2 ranging from 0.71 for Alpine region to 0.79 for Pannonian region (Table 3). Decreasing correspondence in northern regions is thus not influenced by the lower quality of Copernicus HRL TCD in these areas as in the case of the FTY product.

Table 6: Results of the comparison of the Sentinel-1 and Copernicus HRL tree cover density maps.

	Using all values			**Excluding TCD = 0% (non-forest points)**		
Test area	**r**	**Bias (%)**	**NRMSD (%)**	**r**	**Bias (%)**	**NRMSD (%)**
Neusiedl Lake	0.87	11	22	0.74	17	28
Remningstorp	0.85	12	24	0.73	17	29
Krycklan	0.74	17	29	0.68	18	30

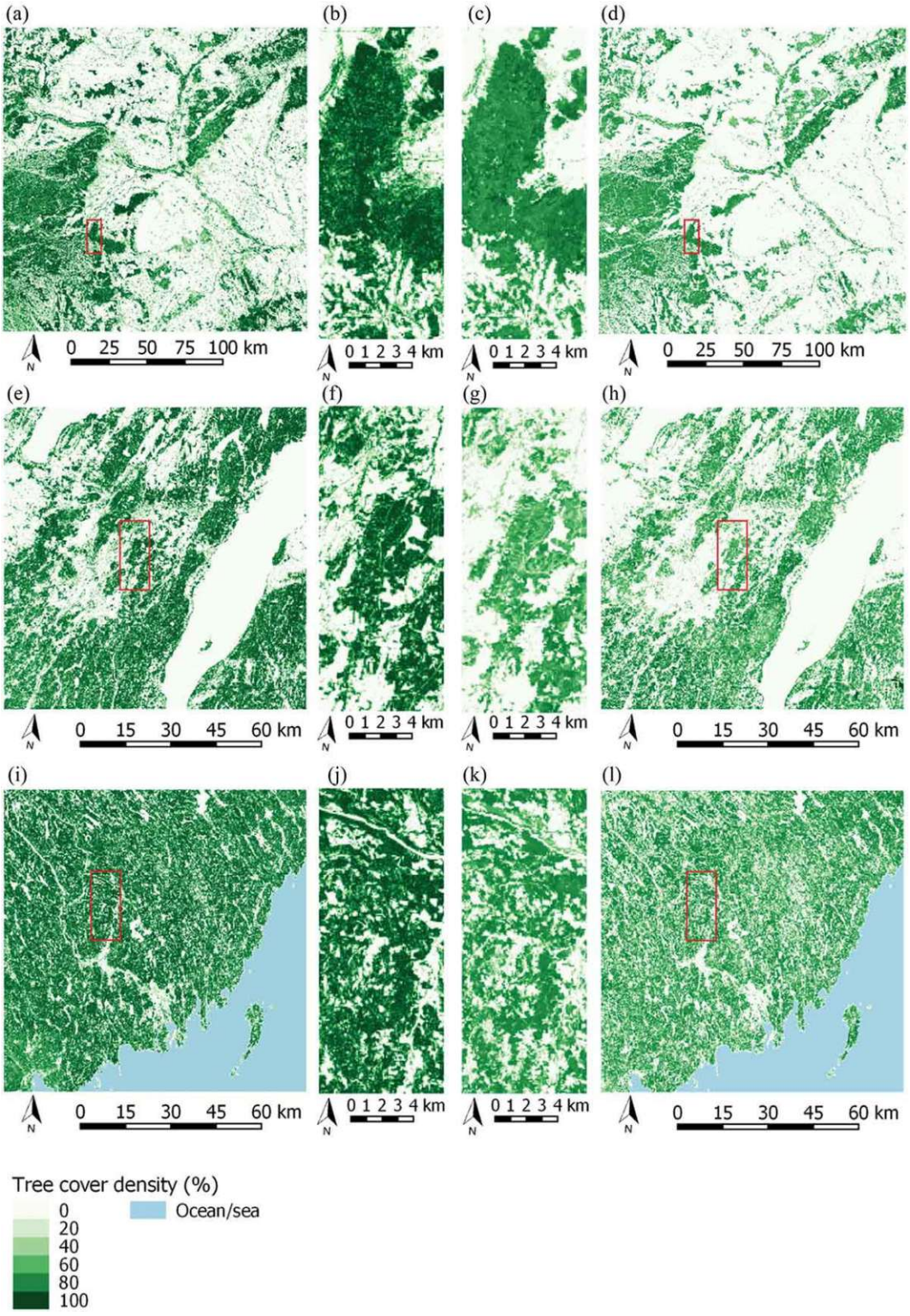

Figure 13: Tree cover density maps. (a) Sentinel-1, Lake Neusiedl, overview, (b) Sentinel-1, Lake Neusiedl, detail, (c) Copernicus HRL, Lake Neusiedl, detail, (d) Copernicus HRL, Lake Neusiedl, overview, (e) Sentinel-1, Remningstorp, overview, (f) Sentinel-1, Remningstorp, detail, (g) Copernicus HRL, Remningstorp, detail, (h) Copernicus HRL, Remningstorp, overview, (i) Sentinel-1, Krycklan, overview, (j) Sentinel-1, Krycklan, detail, (k) Copernicus HRL, Krycklan, detail, (l) Copernicus HRL, Krycklan, overview.

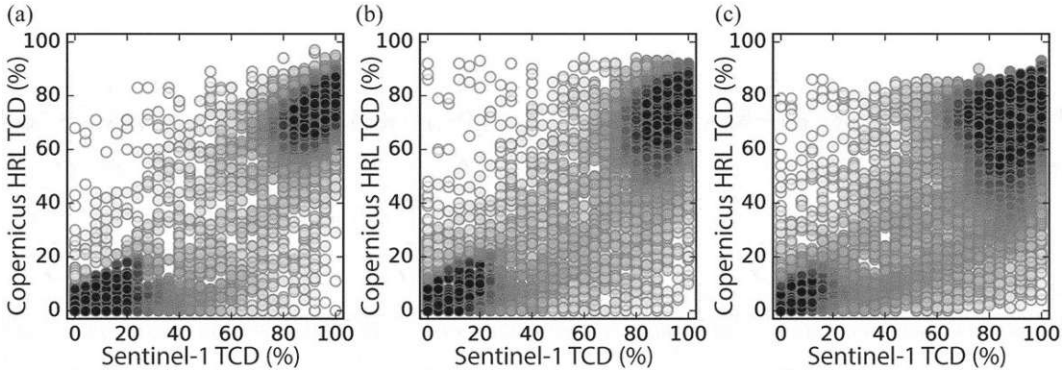

Figure 14: Scatterplots for the randomly selected 5000 points per test area of the Sentinel-1 and Copernicus HRL TCD dataset. Darker colour represents higher point density. (a) Neusiedl Lake test area, (b) Remningstorp test area and (c) Krycklan test area.

3.5.3 Limitations

The main disadvantage of the introduced time series-based approach is the need for storage and processing capabilities to handle big data volumes, especially in case of large regions of interest. Also, the method cannot be automated, as it is dependent on the selection of the reference regions for the forest type classification. Even though the exact location of the reference areas does not influence the results significantly, some knowledge of the area or reliable reference data is required to be able to select the reference time series for each of the forest types represented in the region of interest. Nevertheless, with the appropriate selection of reference time series, the method has significant potential for fine resolution forest mapping and classification over a large variety of regions with no further manual interaction.

3.6 Conclusions

A novel approach using the full year time series of SAR data for forest mapping and classification was introduced in this study. The method takes the advantage of high spatial and temporal resolution of the new Sentinel-1 SAR sensor. The method was tested and validated against Copernicus HRL products in three European test areas. The areas were selected to represent various climatic regions and biomes ranging from broadleaf temperate to boreal forest. The presented results imply that the seasonal signal in Sentinel-1 backscatter provides reliable results for forest/non-forest classification and TCD computation in regions characterized by various climatic conditions, land cover characteristics as well as different forest types. Some areas were found to be more challenging for the method, for example, vineyards that can be confused with specific forest classes. Adding a reference time series for the problematic vegetation types or land cover classes improves the classification results. The agreement between Sentinel-1 and

Copernicus HRL forest/non-forest classification and TCD decreases at higher elevations, however, it still shows relatively high correspondence even in mountainous regions. Generally, the TCD derived from Sentinel-1 tends to overestimate forest density (bias of around 17%) when compared to the Copernicus HRL dataset.

The approach for FTY classification shows promising results in temperate forests but becomes less reliable or even not usable in hemi-boreal or boreal forests, respectively. The applicability of this method is dependent on a sufficient forest density and thus the influence of the leaf growth and fall on the annual backscatter signal, as well as on a sufficient density of the SAR acquisitions. Large parts of the European continent comply with these preconditions and this makes the approach promising also for use over extensive areas. The possibility to classify more detailed forest classes remains an area for further research.

Generally, the results show that the Sentinel-1 C-Band data can be used for forest area mapping in temperate, montane, hemi-boreal and boreal forests as well as for the forest type classification in temperate to hemi-boreal forests. This represents a complementary data source to the maps based on optical remote sensing. Once the reference time series are estimated for the region of interest, the method can be fully automated and yearly maps can be derived and used for forest cover change monitoring.

Funding

This work was supported by the European Community's Seventh Framework Programme (FP7/2007–2013) under grant agreement No. 606971, the Advanced_SAR project.

4 Publication III: European Wide Forest Classifocation Based on Sentinel-1 Data

This section is reformatted from a paper published in Remote Sensing: Dostálová, Alena, Mait Lang, Janis Ivanovs, Lars T. Waser, and Wolfgang Wagner. "European Wide Forest Classification Based on Sentinel-1 Data." Remote Sensing 13, no. 3 (2021): 337.

https://doi.org/10.3390/rs13030337

Abstract

The constellation of two Sentinel-1 satellites provides an unprecedented coverage of Synthetic Aperture Radar (SAR) data at high spatial (20 m) and temporal (2 to 6 days over Europe) resolution. The availability of dense time series enables the analysis of the SAR temporal signatures and exploitation of these signatures for classification purposes. Frequent backscatter observations allow derivation of temporally filtered time series that reinforce the effect of changes in vegetation phenology by limiting the influence of short-term changes related to environmental conditions. Recent studies have already shown the potential of multitemporal Sentinel-1 data for forest mapping, forest type classification (coniferous or broadleaved forest) as well as for derivation of phenological variables at local to national scales. In the present study, we tested the viability of a recently published multi-temporal SAR classification method for continental scale forest mapping by applying it over Europe and evaluating the derived forest type and tree cover density maps against the European-wide Copernicus High Resolution Layers (HRL) forest datasets and national-scale forest maps from twelve countries. The comparison with the Copernicus HRL datasets revealed high correspondence over the majority of the European continent with overall accuracies of 86.1% and 73.2% for the forest/non-forest and forest type maps, respectively, and a Pearson correlation coefficient of 0.83 for tree cover density map. Moreover, the evaluation of both datasets against the national forest maps showed that the obtained accuracies of Sentinel-1 forest maps are almost within range of the HRL datasets. The Sentinel-1 forest/non-forest and forest type maps obtained average overall accuracies of 88.2% and 82.7%, respectively, as compared to 90.0% and 87.2% obtained by the Copernicus HRL datasets. This result is especially promising due

to the facts that these maps can be produced with a high degree of automation and that only a single year of Sentinel-1 data is required as opposed to the Copernicus HRL forest datasets that are updated every three years.

4.1 Introduction

Being vital to many of the Earth's ecosystems, forests play a significant role in the global carbon cycle (Nabuurs, Päivinen et al. 1997, Grace 2004), prevent soil erosion (Pimentel and Kounang 1998) or protect watersheds (Ernst, Gullick et al. 2004, Calder, Hofer et al. 2008). Forests provide a large number of goods including timber, energy or non-wood products. Monitoring of forest resources is an important task from the local to the global scale. Depending on the location, terrestrial based measurements can be costly and are, therefore, not regularly updated or not suitable (e.g., inaccessible areas) (Borre, Paelinckx et al. 2011). Airborne campaigns (e.g., aerial images or Light Detection and Ranging (LiDAR)) based measurements are costly as well, particularly if they are not carried out in the framework of countrywide flying campaigns, and are often not acquired in a repetitive mode. These restrictions often lower the chances of having a frequent monitoring of entire countries. In contrast, besides aerial imagery and LiDAR data, only recently spaceborne remote sensing has been increasingly used for forest monitoring and maintaining forest inventories (Barrett, McRoberts et al. 2016). Nowadays, satellite data combined with field measurements are used in a large number of National Forest Inventories (NFIs) (White, Coops et al. 2016, Kangas, Astrup et al. 2018) and satellite-based forest maps are now available for countries, continents, or the whole world (Hansen, Potapov et al. 2013, Langanke, Büttner et al. 2013, Shimada, Itoh et al. 2014, Lang, Kaha et al. 2018). Currently, these predominantly exploit optical data (Hansen, Potapov et al. 2013, Langanke, Büttner et al. 2013, Lang, Kaha et al. 2018), but research has increasingly addressed the synergetic use of Synthetic Aperture Radar (SAR) and optical sensors or SAR-only products (Dostálová, Wagner et al. 2018, Kangas, Astrup et al. 2018, Rüetschi, Schaepman et al. 2018, Hansen, Mitchard et al. 2020). The main advantage of microwave sensors is their almost all-weather, day-and-night sensing capability providing regular measurements even in areas with frequent cloud coverage or short sun illumination periods. On the other hand, the accuracy of microwave-based products is often limited due to the wavelength dependent saturation of the microwave signal (Imhoff 1993), as well as its sensitivity to the environmental conditions (Ranson and Sun 2000, Lucas, Armston et al. 2010). A number of studies suggest that these shortcomings may, to some extent, be overcome by using multi-temporal SAR data (Santoro, Beer et al. 2011, Dostálová, Wagner et al. 2018, Rüetschi, Schaepman et al.

2018, Hansen, Mitchard et al. 2020).

Dense SAR time series have become available with the launch of Sentinel-1 SAR satellites that acquire dual-polarisation backscatter data in Interferometric Wide Swath mode (IW) over land according to a pre-programmed acquisition scenario (Torres, Snoeij et al. 2012). Over Europe, a new SAR image becomes available every three days on average (but note distinct coverage patterns as, e.g., shown in (Bauer-Marschallinger, Freeman et al. 2019)), which opens up new possibilities in the use of multi-temporal or time-series based methods. The availability of two polarizations, namely the vertical–vertical (VV) and vertical–horizontal (VH) polarisations, is a further asset. In particular, the cross-polarised VH backscatter shows high sensitivity to changes in vegetation density and structure (Patel, Srivastava et al. 2006), and the polarisation ratio VH/VV was found to be sensitive to the vegetation phenology (Frison, Fruneau et al. 2018) or water content (Srivastava, O'Neill et al. 2015). Generally, the temporal signal was shown to be connected to structural and phenological changes in forests (Ahern, Leckie et al. 1993, Dostálová, Wagner et al. 2018, Frison, Fruneau et al. 2018, Rüetschi, Schaepman et al. 2018) as well as to the environmental conditions such as underlying soil and vegetation moisture changes (Lucas, Armston et al. 2010, Srivastava, O'Neill et al. 2015) or temperature changes and freeze–thaw events (Ranson and Sun 2000, Monteith and Ulander 2018).

Recently, a number of studies exploited the short revisit time of Sentinel-1 data and analysed the annual seasonality of backscatter time series over forests (Dostálová, Wagner et al. 2018, Frison, Fruneau et al. 2018, Rodionova 2018, Rüetschi, Schaepman et al. 2018, Dubois, Mueller et al. 2020). For instance, (Dubois, Mueller et al. 2020) described different annual seasonality for coniferous, broadleaf and mixed forest types; while the VH backscatter of the broadleaf forest decreases in spring and summer, coniferous forest showed the highest values during summer months. The same patterns were also described in (Dostálová, Wagner et al. 2018, Rüetschi, Schaepman et al. 2018). All studies connected the decrease in VH backscatter over broadleaf tree species in spring and summer months to the development of foliage; the denser the vegetation canopy, the less signal penetrates the vegetation causing the decrease in the volume scattering and thus lower VH backscatter values. In the case of the coniferous forests, the increase in backscattering coefficient in summer is explained twofold, depending on the canopy cover, i.e., open forest and dense forest. First, the higher water content in needles during the summer months might explain the stronger backscatter observed in this period, and second, the more developed understory layer might increase the vegetation volume scattering component (Dubois, Mueller et al. 2020). The observed differences in

backscatter behaviour were used for forest type mapping, showing overall accuracies of 86% in test areas in Switzerland (Rüetschi, Schaepman et al. 2018), 85% in Austria and 65% to 77% in Sweden (Dostálová, Wagner et al. 2018). Moreover, high temporal resolution of Sentinel-1 data enables also a better forest/non-forest discrimination. For example, a study covering five areas from Alaska to Indonesia (Hansen, Mitchard et al. 2020) revealed that the mean accuracy increases from 77% when using single Sentinel-1 scene to 87% when using mean and standard deviation of VV and VH backscatter computed over one year of acquisitions. Similarly, overall accuracies of 92% were achieved over Austria when using parameters derived from the entire leaf-off season (Dostálová, Hollaus et al. 2016). A different approach was introduced in (Yu, Ni et al. 2020), where only three Sentinel-1 acquisitions were used for forest mapping; these were, however, chosen to capture the conditions before, during and after the freezing period. The method showed an overall accuracy of 93.8% in the test area in North-East China.

So far, all studies on forest area estimation and forest type mapping were limited to relatively small test areas. Of course, one of the most important assets of the Sentinel-1 mission is its favourable coverage, particularly over the European continent. In this study, we tested the applicability over Europe of the method originally proposed in (Dostálová, Wagner et al. 2018) and assessed at a smaller scale up to now. We produced a Europe-wide map of forest type (coniferous or broadleaved) with 10 m spatial resolution and tree cover density with 100 m spatial resolution for 2017. The quality of the maps was assessed by means of comparison with the Copernicus Forest Type and Tree Cover Density (TCD) datasets as well as a variety of NFI datasets and data from universities. This is important for two reasons: firstly, comprehensive validation helps us to better understand the limitations of the proposed algorithm, and secondly, the Europe-wide forest map can be seen as a first test case for prospective worldwide forest mapping efforts using the Seninel-1 SAR data.

4.2 Materials and Methods

4.2.1 Data

4.2.1.1. Sentinel-1 SAR

The Sentinel-1 constellation comprises two satellites: Sentinel-1A and Sentinel-1B. Each satellite carries a SAR C-Band sensor capable of providing dual-polarisation observations. The satellites operate in several acquisition modes. The default mode used for land applications is IW mode with a spatial resolution of 20 m × 5 m and a swath

width of 250 km. The repeat orbit cycle of each satellite is 12 days and over the majority of the European continent; 2 to 4 measurements are acquired per sensor in each orbital cycle. Within this study, all available VV and VH polarisation IW ground range detected (GRD) data from 2017 were used (both ascending and descending orbits), in total almost 46,000 images. The temporal coverage ranges between 110 and 460 acquisitions per pixel.

4.2.1.2. Validation data

Several datasets were used for the accuracy assessment of the Sentinel-1 forest maps. These include the freely available pan-European Copernicus High Resolution Layers (HRL) 20 m Forest Type and 100 m Tree Cover Density (TCD) products (Langanke, Büttner et al. 2013) as well as twelve datasets from national forest inventories or universities.

The Copernicus HRL forest datasets are provided by the European Environment Agency (EEA) Global Monitoring for Environment and Security/Copernicus Initial Operations Land Service and were derived from high resolution satellite imagery from the Indian Remote Sensing-Resource SAT2 (IRS-RS2), Satellite Pour l'Observation de la Terre (SPOT) and RapidEye satellites acquired between 2011 and 2012.

The Copernicus HRL TCD dataset is defined as the vertical projection of tree crowns to a horizontal earth's surface and represents the proportional crown coverage per pixel in percent. Minimum mapping width (MMW) of 20 m is applied, and all detectable trees are included. The forest type product specifies the dominant leaf type for each pixel (broadleaf or coniferous) and is derived from 20 m TCD product by applying a threshold of 10%, minimal mapping unit (MMU) of 0.5 ha and MMW of 20 m (Langanke, Büttner et al. 2013).

The overview of the available national datasets is given in Figure 15 and details are listed in Table 7. Generally, the pre-processing of these datasets included resampling to the Equi7 grid (10 m resolution) (Bauer-Marschallinger, Sabel et al. 2014) in the case of raster datasets and rasterization for the vector dataset. Due to the limited accessibility of the data in some countries, validation over Germany, Latvia and Estonia was performed point-wise using randomly selected points from respective NFIs or forest management inventories data. In cases where the dataset contained more detailed classes such as dominant tree species, the classes were adapted to coniferous (at least 65% of the coniferous tree species), broadleaved (at least 65% of broadleaf tree species) or mixed forest. The mixed forest class was used for forest/non-forest validation only. Details

specific to the national datasets including the source of the data (e.g., in-situ, satellite or aerial imagery) can be found in the **Appendix A**.

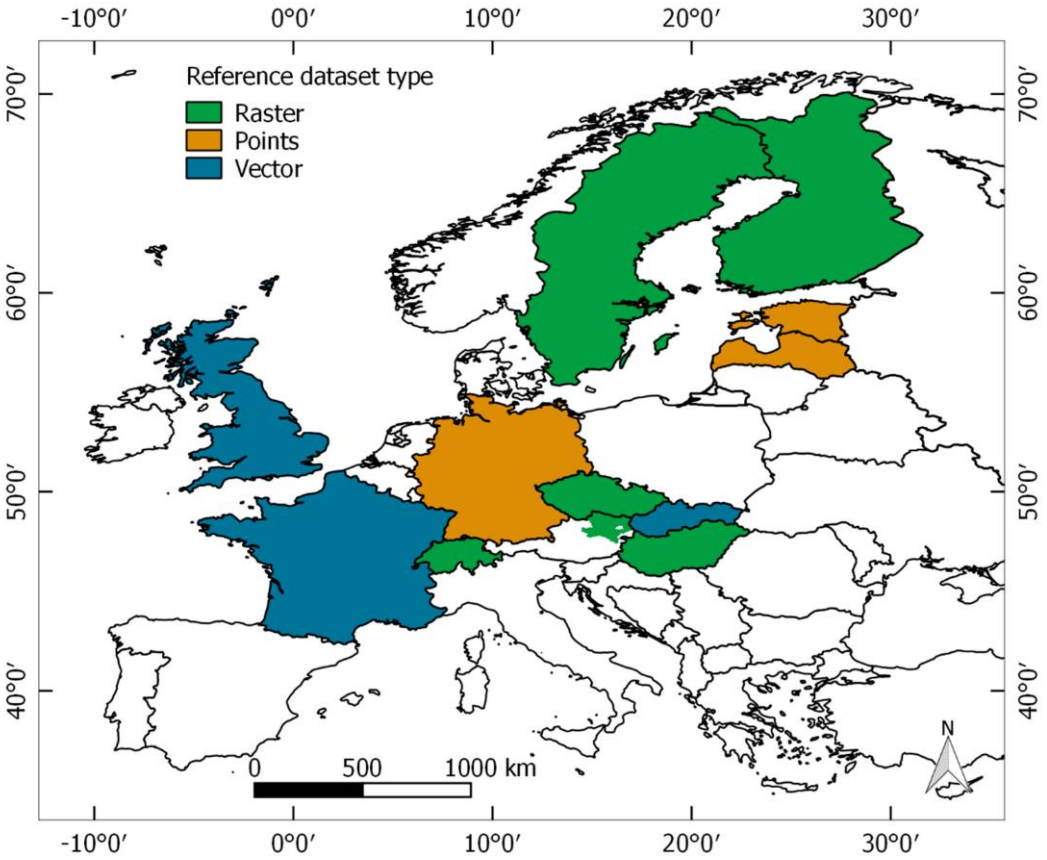

Figure 15: Overview of the national datasets that were used as reference. In the case of Austria, only a forest map of the federal state of Lower Austria was available.

Table 7: Overview of the national datasets that were used as reference.

Country	Dataset provider	Data type	Information content	Spatial resolution	Reference year
Austria	Austrian Research Centre for Forests	Raster	Forest mask	1 m	
Czech Republic	Forest Management Institute	Raster	Dominant tree species within pixel	10 m	2017
England, Scotland, Wales	Forestry Commission	Vector	Forest type	MMU 0.5 ha	2017
Estonia	University of Tartu	Random points	Share of conifers within forest stand	10277 points	2017
France	Institut National de L'Information Geographique et Forestriere	Vector	Forest type	MMU 0.5 ha	2014-2019
Finland	Finnish Environment Institute	Raster	Forest type	20 m	2018
Germany	National Forest Inventory	Points	Forest type	195630 points	2012-2017
Hungary	Nemzeti Földügyi Központ	Raster	Forest type	10 m	2020
Latvia	Latvian State Forest Research Institute Silava	Random points	Forest type	10000 points	2019
Slovakia	Slovakian National Forest Centre	Vector	Dominant tree species within forest stand		2017
Sweden	Swedish University of Agricultural Sciences	Raster	Standing volumes of most common tree species	25 m	2010
Switzerland	National Forest Inventory	Raster	Per-pixel probability of conifers	25 m	2018

4.2.2 Method

The details of the Sentinel-1 forest mapping method are described in (Dostálová, Wagner et al. 2018) and summarized in the following subsection. The process consists of three major blocks: pre-processing, generation of SAR seasonality time series and, finally, the forest type and TCD products construction.

4.2.2.1. Sentinel-1 pre-processing

The pre-processing is done using the SGRT software developed by the Technische Universität (TU) Wien (Elefante, Wagner et al. 2016). The software aims at the automated processing of large volumes of SAR-based products and combines python with some external software modules. In the case of SAR pre-processing, the Sentinel Application Platform (SNAP) is used (SNAP).

The pre-processing steps include thermal noise removal, precise orbit correction, radiometric calibration to the $\sigma 0$ values, orthorectification using the range doppler terrain correction method (Small and Schubert 2008), conversion from linear to logarithmic scale and resampling to the Equi7 Grid. The output comprises a stack of georeferenced $\sigma 0$ and projected local incidence angle (θ) images. In (Dostálová, Wagner et al. 2018), pre-processed images were further multi-looked to 20 m. In this study, this step was omitted, and the SAR seasonality time series and forest type products were derived at a 10 m grid which corresponds to the pixel spacing of the Sentinel-1 GRD IW dataset. In (Dostálová, Wagner et al. 2018), forest maps were created using Sentinel-1 A data from 2015 (Sentinel-1 B was launched in April 2016), while, in the current study, both Sentinel-1 A and B data are used. As a result, approximately twice as many acquisitions are available for each pixel. Moreover, in [16] the maps were validated using Copernicus HRL forest datasets with 20 m and 100 m resolution for forest type and TCD, respectively. In this study, additional higher resolution national datasets are used for quality assessment. Therefore, we decided to omit the additional multi-looking step and derive the forest maps at the highest possible spatial resolution.

4.2.2.2. SAR seasonality time series computation

The SAR seasonality time series are computed from the stack of georeferenced images as temporally smoothed backscatter time series. This is done in order to reinforce the effect of the slowly varying phenological changes of vegetation and limit the noise and short-term variations caused by changing environmental conditions. To enable the combination of images acquired from different relative orbits, the backscatter images are normalized to

common reference angle of 40° using the slope (β) parameter computed separately for each pixel using the linear regression between $\sigma 0$ and θ values. The normalisation equation reads as follows:

$$\sigma^0(40°) = \sigma^0(\theta) - \beta(\theta - 40°) \quad (1)$$

Next, the mean of the normalized backscatter is computed for every 12 days (repeat orbit cycle of Sentinel-1 satellites) and the resulting time-series is again smoothed using a Gaussian temporal filter with standard deviation of 1 (corresponding to 12 days). As a result, 30 SAR seasonality values with 12-day temporal step are derived for each pixel and both polarisations. These temporal signatures show distinct behaviour over various vegetation types. Figure 16 shows an example of the temporal signatures from cross-polarised backscatter for agricultural areas (without separation of crop type, hence the large standard deviation of the signal), coniferous and broadleaf forests.

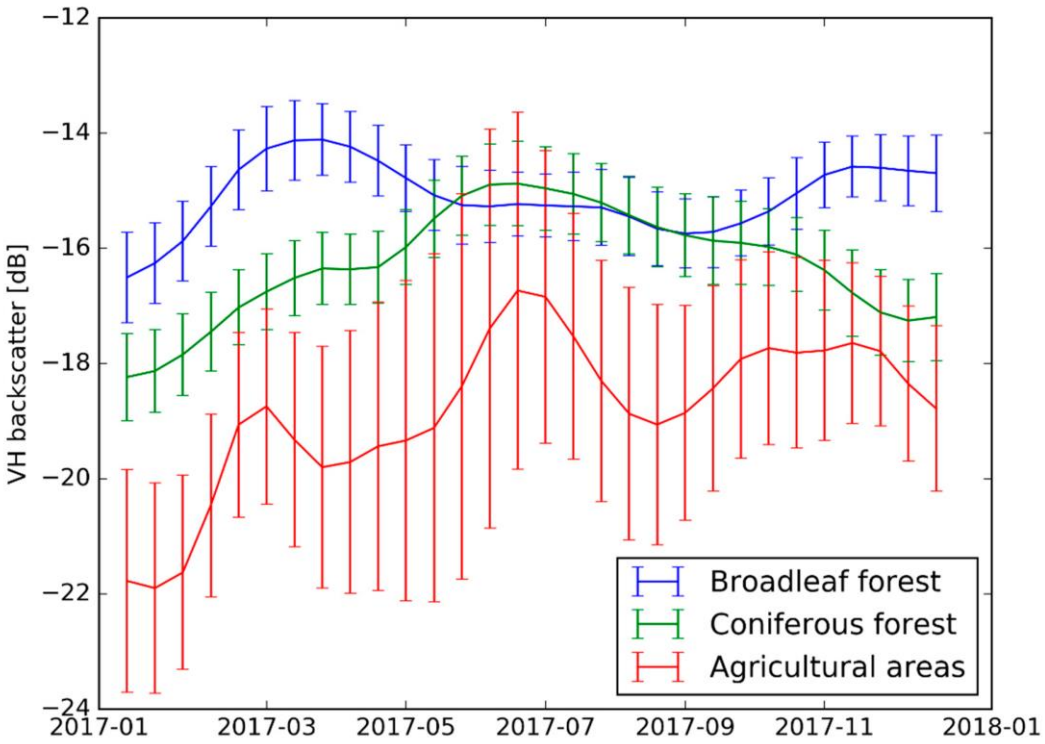

Figure 16: Cross-polarized (VH) backscatter temporal signatures of various vegetation types: agricultural areas (all crop types), broadleaf (dominant tree type—oak) and coniferous (dominant tree type—spruce) forests. The average values (solid line) are computed as averages of 1000 randomly selected pixels for each class in area in central Europe, the error bars represent the standard variation of the backscatter value for each time stamp.

The backscatter normalisation (Equation (1)) is based on the assumption of an indirect linear relationship between backscatter (in decibel scale) and projected local incidence angle within the limited range of available incidence angles of a SAR sensor (29.1° to 46.0° in the case of Sentinel-1 and flat terrain) (Pathe, Wagner et al. 2009, Bauer-Marschallinger, Freeman et al. 2019). In the case of Sentinel-1, this method is, however,

limited by the low number of various incidence angles in some areas, where no reliable slope value from Sentinel-1 can be derived (Bauer-Marschallinger, Freeman et al. 2019). In these areas, fixed value of $\beta = -0.12$ is used instead, which corresponds to the average value computed over the regions, where the Sentinel-1 coverage is sufficient. (Bauer-Marschallinger, Freeman et al. 2019) introduced an alternative approach for the β parameter estimation over the areas of reduced Sentinel-1 coverage. This was, however, developed for lower resolution data (resampled to 500 m) and is not suitable for high resolution (10 m) data. In our study, the effect of varying local incidence angle is further reduced by temporally averaging the data within a single repeat orbit cycle—i.e., combining the measurements from all possible incidence angles into a single value—which is why we consider the simplified slope computation sufficient for this application. Furthermore, the β parameter varies with vegetation growth (Peters, Lievens et al. 2012), yet it was assumed to be temporally stable, as a single year of Sentinel-1 data is not sufficient to compute its seasonal variation.

4.2.2.3. Construction of forest maps

The forest classification algorithm exploits the differences between the temporal signatures of various vegetation types (Figure 16). Signature prototypes are defined for coniferous and broadleaf forest classes. Due to the large variability of forests and their temporal signatures across Europe, the continent was stratified into smaller regions, and, for each region, four signature prototypes were selected and computed. The prototypes are computed as described in the previous chapter using averaged backscatter values over 300 m × 300 m large forested areas (30 × 30 pixels) and are selected to represent both coniferous and broadleaved forest types in each region—typically two prototypes for each class. The regions were selected manually so that they contain areas with similar biomes, forest types and terrain variations using the digital terrain model and the map of habitat suitability of European forest categories (Casalegno, Amatulli et al. 2011). The borders of the regions correspond to the borders of the Equi7 grid tiles. The selection of the signature prototypes location was supported by reference datasets that included Copernicus HRL maps, national forest datasets or orthophotos (if available) as well as average Sentinel-1 backscatter for 2017 to exclude areas with apparent terrain effects or clear cuts. The regions (bold black lines) and reference points (grey dots) are presented in Figure 17. Figure 18 shows an example prototype time series in an area covering central Europe. Note that the difference between the pure stands of a particular tree species might be larger than that between the coniferous and broadleaf forest type, which is why it is essential to select the reference points accordingly in order to be

representative for the most common tree species in each area.

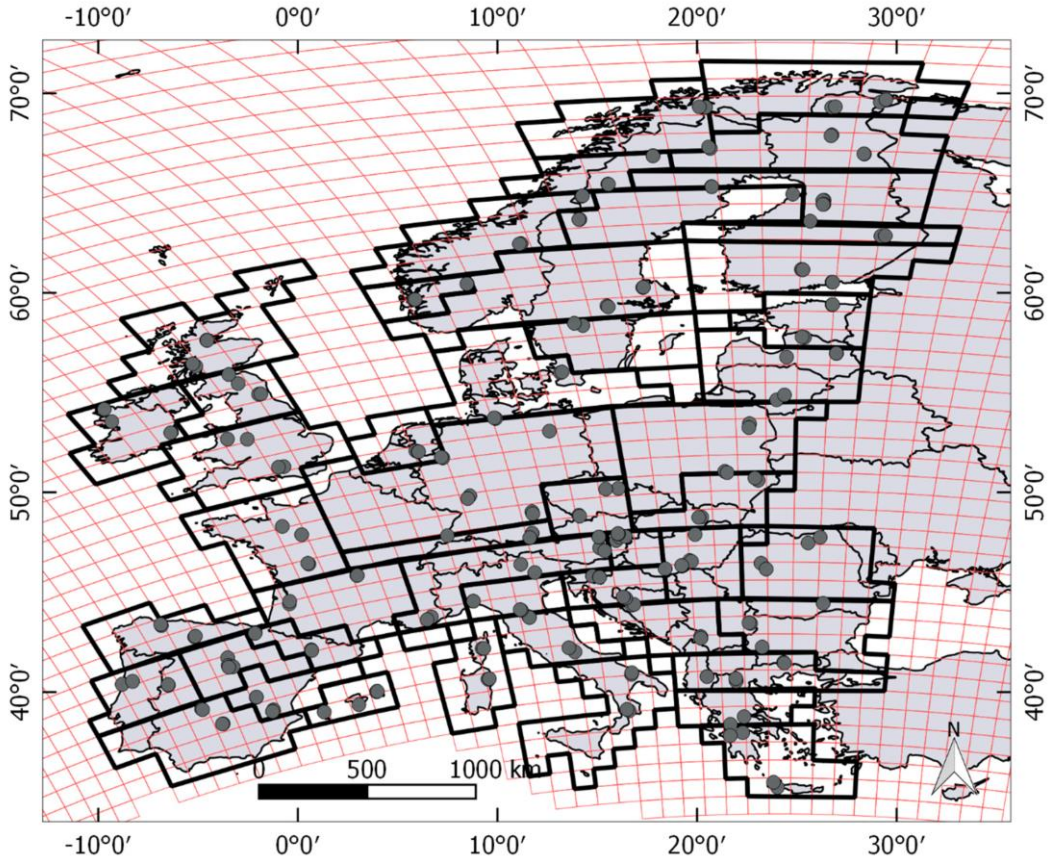

Figure 17: Overview of the regions used for the Sentinel-1 forest maps computation (black lines) and the locations of their respective signature prototypes (grey points) across Europe. Red lines indicate the Equi7 grid tiling.

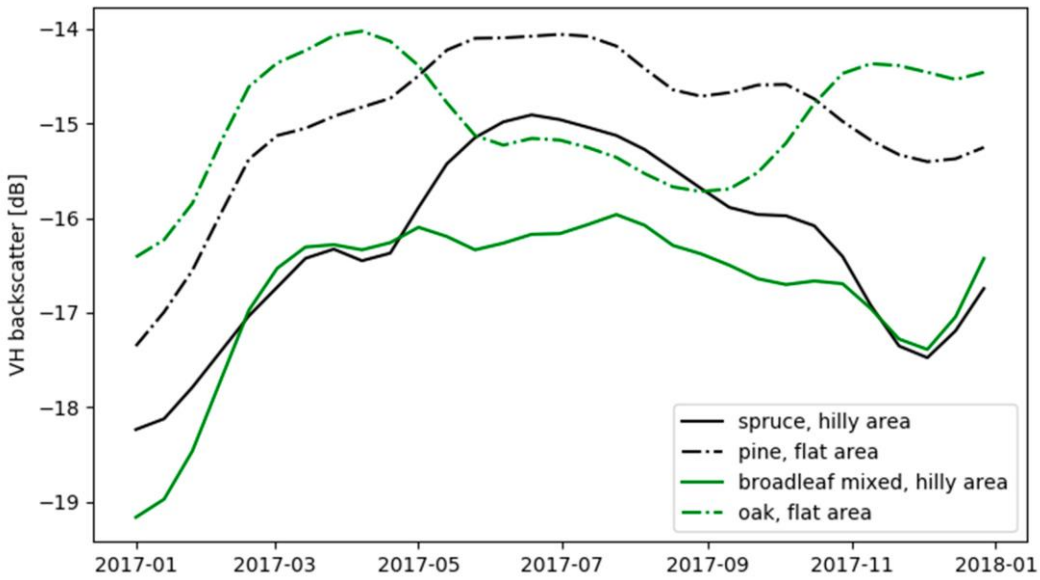

Figure 18: Temporal signature prototypes for the most common tree species in an area in central Europe (located in Czech Republic).

The similarity measures—Root Mean Square Difference (RMSD) and Pearson correlation coefficient (r)—between the prototype signatures and the respective temporal

signature of each image pixel are used for the classification. In the first step, forest/non-forest classification is performed using thresholds that are fixed for entire Europe. Threshold values are 1.5 dB and 2.0 dB for VH and VV polarisation RMSD, respectively, and 0.4 for VH polarisation r. These values were empirically set in (Dostálová, Wagner et al. 2018) as the best fitting for three test sites from Austria to northern Sweden. Each pixel that falls within the thresholds with similarity measures computed for any of the prototype time series is classified as forest; the rest is classified as non-forest. With method, no signature prototypes need to be defined for land cover types other than forests. The forest type (coniferous, broadleaved) is then assigned to each forested pixel according to the lowest RMSD value in VH polarisation. The VH polarisation was selected for the forest type classification due to higher sensitivity of the cross-polarised backscatter to the forest structure (Patel, Srivastava et al. 2006, Dostalova, Milenkovic et al. 2016). For the final forest type product, the MMU of 0.5 ha is applied and the 100 m TCD product is computed as the fraction of the 10 m pixels within each 100 m × 100 m target area that were classified as forests (prior to MMU application).

4.2.2.4. Validation

The accuracy assessment of the Sentinel-1 forest maps was performed in two steps. First, validation metrics between Copernicus HRL datasets and Sentinel-1 forest maps were computed on pan-European level as well as for each 100 km × 100 km Equi7 tile. Second, both Sentinel-1 and Copernicus HRL forest maps were compared to the national forest datasets. The computed validation metrics included overall accuracy (*OA*, Equation (2)), producer's (*PA*), and user's (*UA*) accuracies (Equations (3) and (4), respectively).

$$OA = \frac{T}{N} \tag{2}$$

$$PA_{cl} = \frac{TR_{cl}}{NR_{cl}} \tag{3}$$

$$UA_{cl} = \frac{TC_{cl}}{NC_{cl}} \tag{4}$$

In these equations, T stands for number of correctly classified pixels, N for number of all pixels used for validation, TR_{cl} for number of correctly classified reference pixels of respective class *cl*, NR_{cl} for number of all reference pixels of respective class *cl*, TC_{cl} for number of all correctly classified pixels within respective class *cl* and NC_{cl} for number of all pixels classified into respective class *cl*. The accuracies were computed for forest/non-forest classification as well as for forest type classification (broadleaved or coniferous forest type computed for all pixels classified as forests in both datasets). Furthermore, Pearson correlation coefficient and bias were computed between the TCD products.

The national datasets varied in format and provided information. In the case of raster and rasterised datasets, the statistics were computed for all pixels, while in the case of pointwise comparison, the point information was compared to the corresponding pixel. In the case of national datasets over Estonia and Latvia, only forest type accuracy was computed, as the respective forest inventories do not contain all forested land. Moreover, the forest map of Lower Austria allowed only forest/non-forest validation due to the lack of forest type information.

4.2.2.5. Sensitivity analysis

One of the main challenges of the introduced approach is the susceptibility of the results to the selection of the signature prototypes used for the forest classification. To quantify this effect, we performed a sensitivity test over a single Equi7 grid tile (100 km × 100 km) located in the Czech Republic. A total of 80 sets of reference points were selected for the forest classes with dominant tree types spruce, pine, oak and other deciduous forest. The points were selected using the Czech Forest Management Institute forest map. Forest type and TCD maps were computed for each set of reference points and the results were validated against the Copernicus HRL forest maps. The overview of the test site and the locations of the selected reference points are shown in Figure 19.

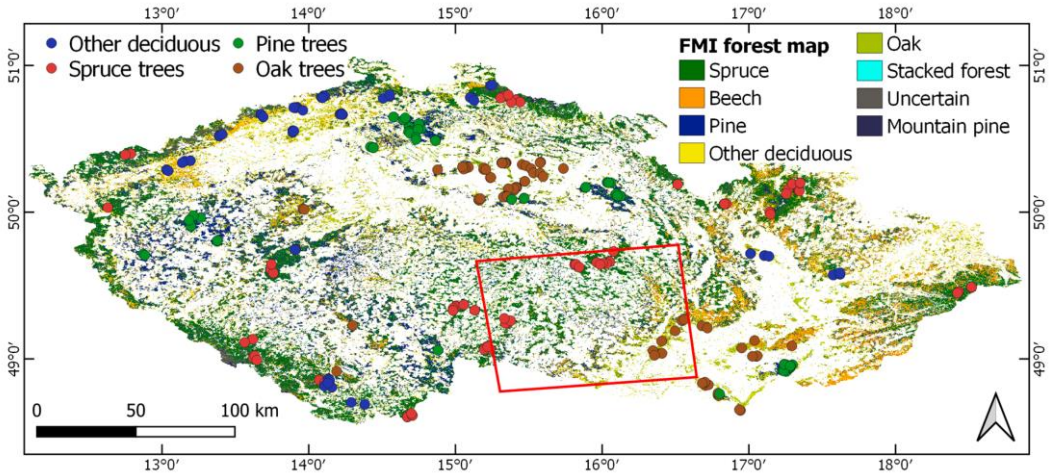

Figure 19: Overview of the performed sensitivity test: red polygon outlines the test site and dots indicate the locations of signature prototypes. The base map is the forest map from the Czech Forest Management Institute (FMI) that was used for the selection of the signature prototypes' location.

4.3 Results

4.3.1 Forest area and forest type

The accuracy of the Sentinel-1 forest type map was assessed both on the European level using the Copernicus HRL forest type products as well as on the national level using the

various national datasets. The forest type maps from Sentinel-1 and Copernicus HRL over the European Continent are shown in Figure 20, while Figure 21 and Figure 22 present the forest type map for Czech Republic and Sicily, respectively. The Figure 20, Figure 21 and Figure 22 also include a difference image highlighting the discrepancies between the two products in red (pixels classified as forest in the Copernicus HRL forest type dataset and as non-forest in the Sentinel-1 forest type dataset), blue (pixels classified as non-forest in the Copernicus HRL forest type dataset and as non-forest in the Sentinel-1 forest type map) and light green (pixels classified as forests in both datasets but assigned different forest types).

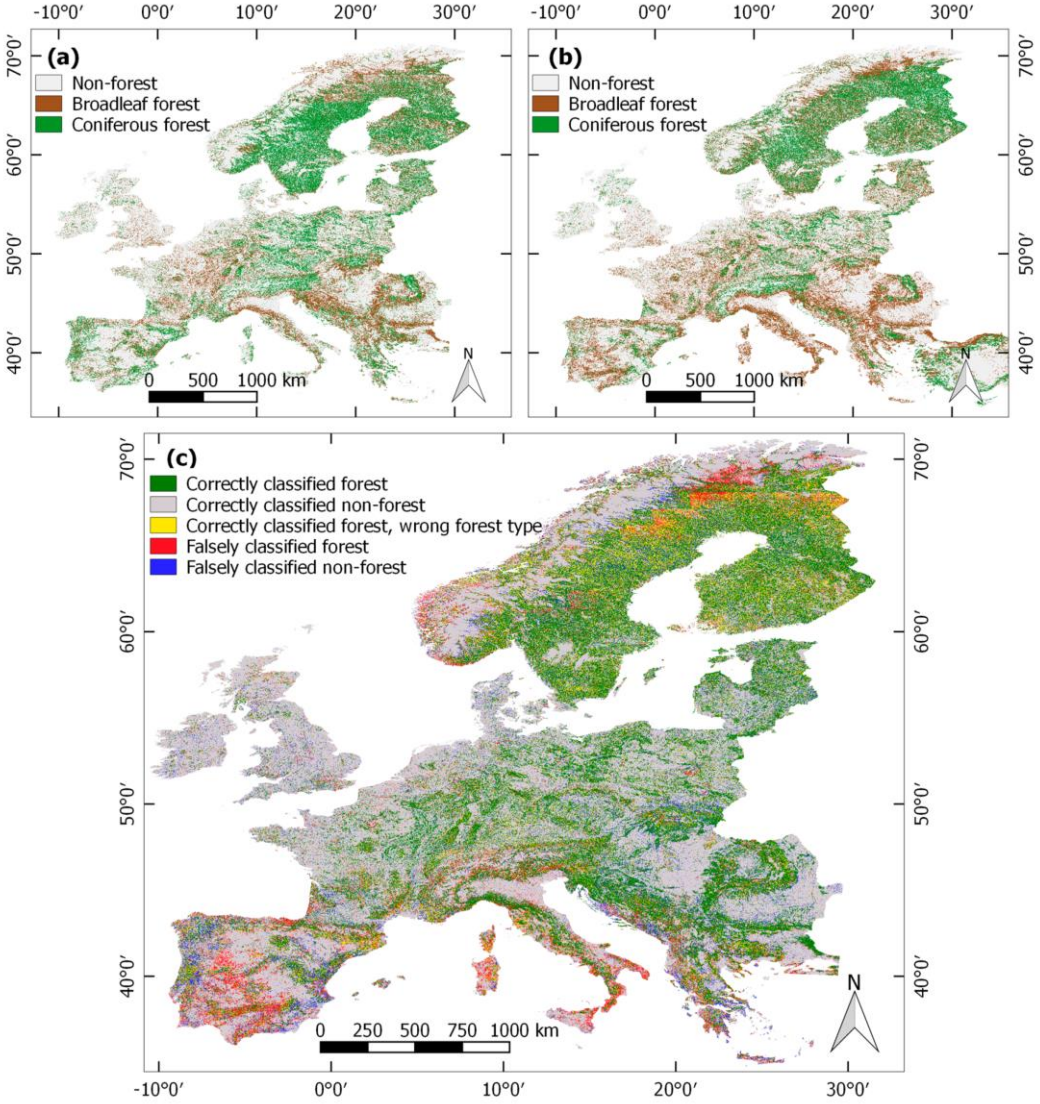

Figure 20: Overview of the forest type maps from (a) Sentinel-1, (b) Copernicus High Resolution Layers and (c) the difference map between the two datasets.

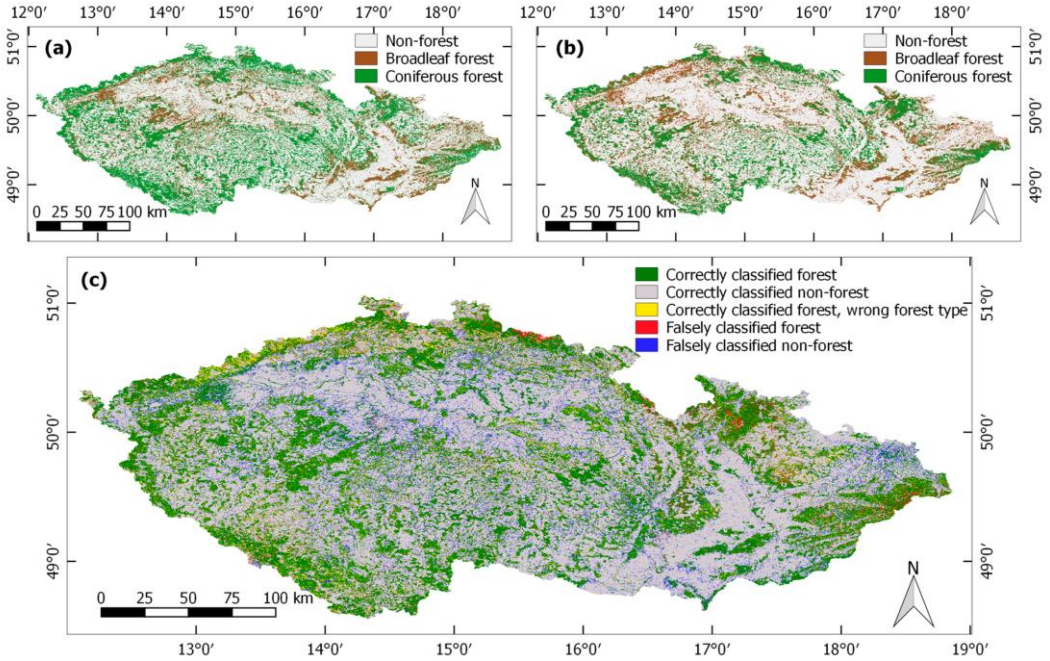

Figure 21: Detailed forest type map of the Czech Republic from (a) Sentinel-1, (b) Copernicus High Resolution Layers and (c) the difference map between the two datasets.

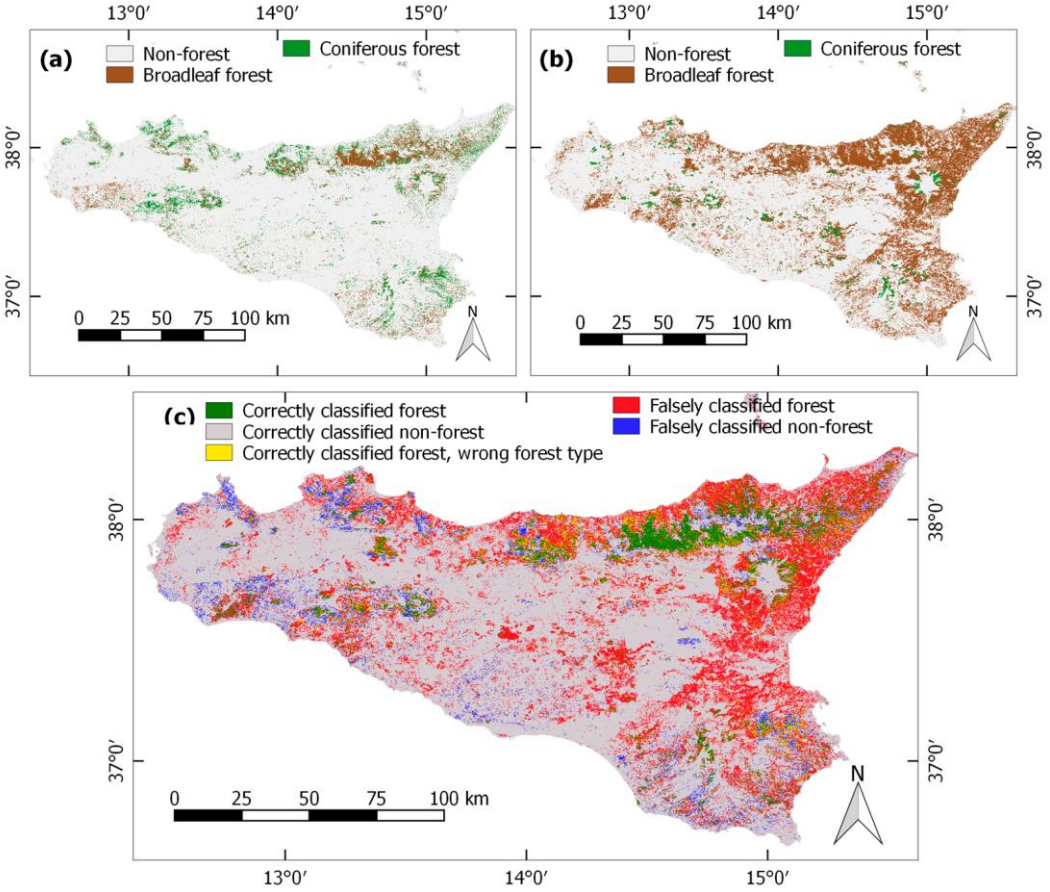

Figure 22: Detailed forest type map over Sicily from (a) Sentinel-1, (b) Copernicus High Resolution Layers and (c) the difference map between the two datasets.

4.3.1.1. Copernicus HRL Dataset

Table 8 shows the accuracies for forest/non-forest and forest type classification computed for the entire study area. The overall accuracy is 86.1% for forest area and 73.2% for forest type, respectively. Since these accuracies strongly vary across the continent, spatial maps showing the overall accuracies for both forest/non-forest classification and forest types are presented in Figure 23. The numbers were specified for each 100 km × 100 km area which represents one Equi7 tile.

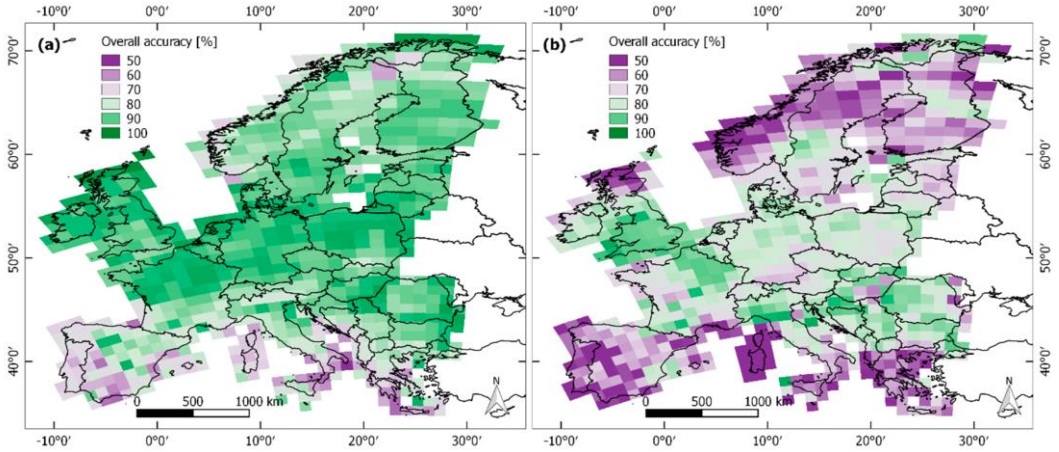

Figure 23: Overall accuracy of the Sentinel-1 (a) forest/non-forest and (b) forest type map computed for each Equi-1 tile. The Copernicus High Resolution Layers forest type dataset was used as a reference, showing the limitations of the presented maps for high latitudes and Mediterranean forests. Lower accuracies can also be observed in mountainous areas.

Table 8: Accuracy of the Sentinel-1 forest/non-forest and forest type map when compared to the Copernicus HRL forest type dataset. The accuracies are summarized for entire Europe.

	Forest/non-forest	Forest type
Overall accuracy	0.86	0.73
Producers accuracy forest/broadleaf	0.83	0.81
Users accuracy forest/broadleaf	0.81	0.68
Producers accuracy non-forest/coniferous	0.88	0.66
Users accuracy non-forest/coniferous	0.89	0.79

Typical results over flatland and hilly areas with the main differences between the Sentinel-1 map and the reference datasets are highlighted in Figure 24. The Sentinel-1 forest type product generally overestimates the forest area in flatlands. In the case of small villages or agricultural areas, some parts are often classified as forests. This is due to large number of trees in gardens or hedgerows between fields or among roads. In addition, vineyards or orchards are common areas of disagreement between the Sentinel-1 forest type map and reference datasets. Vineyards are commonly falsely classified as coniferous forests in Sentinel-1 forest type product while apple orchards are assigned to non-forests class in Sentinel-1 forest type map, but they are often classified as

broadleaved forests in the Copernicus forest type product. Lastly, in areas with large terrain variations, false gaps in forests caused by terrain distortions in SAR data can be observed.

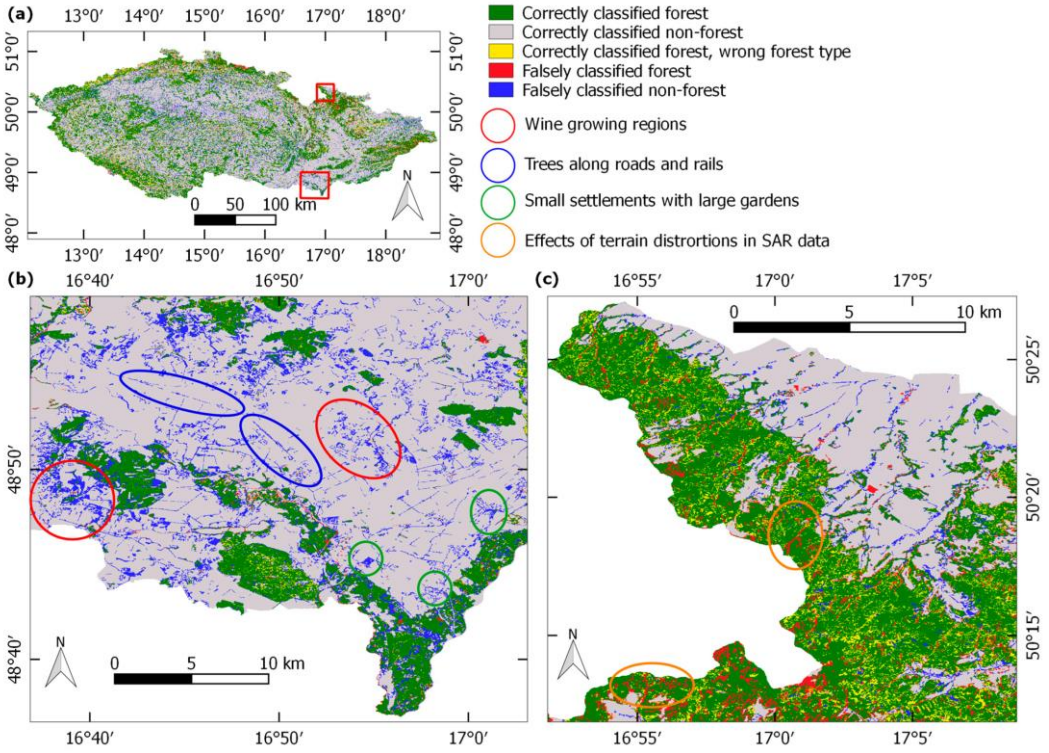

Figure 24: Common reasons of disagreement between the Sentinel-1 and reference Copernicus High Resolution Layers forest maps (Indicated by ellipses). (a) Difference map between the Sentinel-1 and Copernicus forest type map over Czech Republic, (b) detail of the difference map over area in flatland and (c) detail of the difference map over area in mountains.

4.3.1.2. National Datasets

The Copernicus HRL dataset is based on optical satellite imagery, and, according to the validation report, the users' and producers' accuracies vary between 83% and 93% for forest/non forest classification, and between 17% and 98% for forest type, with the lowest accuracies in the boreal and alpine regions. As the highest disagreement between our product and the Copernicus HRL forest type map can be found in these regions, alternative sources of data are needed to better assess the accuracy of both products. For this reason, we compared both maps to different national datasets. Table 9 shows the respective accuracies for forest/non-forest classification and Table 10 for the forest type, respectively. The mountainous regions are well represented in Switzerland and Slovakia, while the boreal regions are covered by datasets from Finland and Sweden.

Table 9: Results of the accuracy assessment using the national datasets for the forest/non-forest classification. The following statistics are listed: overall accuracy (OA), producers' accuracy (PA) and users' accuracy (UA).

	Sentinel 1 vs reference					Copernicus vs reference				
		Forest		Non-forest			Forest		Non-forest	
	OA	PA	UA	PA	UA	OA	PA	UA	PA	UA
Austria	0.91	0.92	0.87	0.90	0.95	0.93	0.93	0.90	0.93	0.95
Czech Republic	0.90	0.94	0.79	0.87	0.97	0.95	0.93	0.91	0.95	0.96
England, Scotland, Wales	0.91	0.74	0.50	0.93	0.97	0.93	0.80	0.56	0.94	0.97
France	0.90	0.83	0.84	0.93	0.92	0.92	0.89	0.87	0.94	0.95
Finland	0.88	0.92	0.88	0.82	0.88	0.87	0.94	0.86	0.77	0.89
Germany	0.93	0.95	0.83	0.92	0.98					
Hungary	0.88	0.88	0.66	0.88	0.97	0.92	0.85	0.79	0.94	0.96
Slovakia	0.82	0.93	0.72	0.75	0.94	0.88	0.93	0.81	0.85	0.95
Sweden	0.82	0.88	0.83	0.73	0.81	0.82	0.88	0.83	0.73	0.81
Switzerland	0.87	0.78	0.76	0.91	0.91	0.88	0.94	0.72	0.86	0.97

Table 10: Results of the accuracy assessment using the national datasets for the forest type classification. The following statistics are listed: overall accuracy (OA), producers' accuracy (PA) and users' accuracy (UA).

	Sentinel 1 vs reference					Copernicus vs reference				
		Broadleaf		Coniferous			Broadleaf		Coniferous	
	OA	PA	UA	PA	UA	OA	PA	UA	PA	UA
Czech Republic	0.84	0.72	0.88	0.93	0.81	0.89	0.95	0.81	0.84	0.96
England, Scotland, Wales	0.74	0.95	0.64	0.56	0.93	0.80	0.95	0.68	0.69	0.95
Estonia	0.87	0.77	0.97	0.97	0.79					
France	0.84	0.87	0.92	0.75	0.62	0.91	0.96	0.93	0.77	0.86
Finland	0.71	0.75	0.14	0.71	0.98	0.88	0.93	0.31	0.88	0.99
Germany	0.91	0.94	0.89	0.87	0.93					
Hungary	0.80	0.81	0.98	0.69	0.15	0.97	0.98	0.99	0.76	0.71
Latvia	0.85	0.68	0.90	0.70	0.90					
Slovakia	0.90	0.93	0.92	0.83	0.86	0.88	0.97	0.87	0.72	0.93
Sweden	0.82	0.45	0.16	0.84	0.96	0.79	0.87	0.21	0.79	0.99
Switzerland	0.82	0.78	0.83	0.85	0.80	0.86	0.83	0.87	0.89	0.86

For forest/non-forest classification, the comparison with most of the national datasets reveals overall accuracies of around 90%. The highest correspondence was obtained for Germany with an accuracy of 93%, and the lowest overall accuracies of 82% were obtained for Slovakia and Sweden. For Switzerland, the most mountainous country in Europe, a high overall accuracy of 87% was obtained. For Finland, that is also predominantly covered by boreal forests, an accuracy of 88% was obtained.

Generally, the correspondence between the Sentinel-1 forest type map and national datasets is slightly lower than between the Copernicus HRL forest type product and national datasets. The highest difference can be observed in the case of the Czech Republic, where the overall accuracies of 95% and 90% were obtained in the case of Copernicus and our product, respectively. On the other hand, in Finland, the Sentinel-1 dataset shows slightly higher overall accuracy than the Copernicus HRL dataset (88% when compared to 87%). In most of the other cases, the difference is around 2%. Except Sweden, the Copernicus HRL dataset shows high accuracies for forest/non-forest mapping, which confirms that it may be used as a reliable reference dataset.

For the forest type classification, the variability between the results for various national datasets is much higher than in the case of the forest/non-forest mapping. For the Sentinel-1 forest type product, remarkably high accuracies can be observed over Germany (91%), Slovakia (90%) or Estonia (87%). On the other hand, problems can be observed in Sweden and Finland, where the overall accuracies are 82% and 71%, respectively, and the users' accuracies for broadleaf forests are very low (16% and 14%, respectively). The same effect can be observed for the Copernicus HRL dataset, where the users' accuracies of broadleaf forests are 21% and 31% for Sweden and Finland, respectively. In addition, England, Scotland and Wales show lower accuracies for both datasets—74% in the case of Sentinel-1 and 80% in the case of the Copernicus forest type product. In both cases, the lower users' accuracies of broadleaf forests and producers' accuracies of coniferous forests indicate that the broadleaf forests tend to be overestimated, while the coniferous tend to be underestimated in both Sentinel-1 and Copernicus HRL forest type maps.

Moreover, the differences between the accuracies of the Copernicus HRL and Sentinel-1 forest type datasets are much higher, reaching up to 17% in the case of Finland and Hungary. In the case of Hungary, this is caused by strong overestimation of coniferous forests in the case of the Sentinel-1 forest type map (users' accuracy of only 15% for coniferous forests and overall accuracy of 80%). On the other hand, in the case of Slovakia and Sweden, Sentinel-1 shows slightly higher overall accuracies than the Copernicus HRL dataset. Generally, overall accuracies in the case of the Sentinel-1 forest type map vary between 71% for Finland and 91% for Germany, while, for Copernicus, they vary between 79% for Sweden and 97% in Hungary.

4.3.2 Tree cover density

The TCD map was validated using the Copernicus TCD dataset only. Both maps, including the difference map as well as the spatial distribution of the *r* value between the

two, are presented at Figure 25 and Figure 26, respectively. The *r* value computed for entire Europe is 0.83 and the bias corresponds to 9.8%, showing that the Sentinel-1 based map overestimates the tree cover density values when compared to the Copernicus product. This is especially visible in the northern part of Europe. While the TCD values in Sweden and Finland often reach 100% for the Sentinel-1 map, they range between 60% and 80% in the case of the Copernicus HRL dataset. Over central Europe, the TCD patterns correspond well and the differences increase towards the south of Europe again.

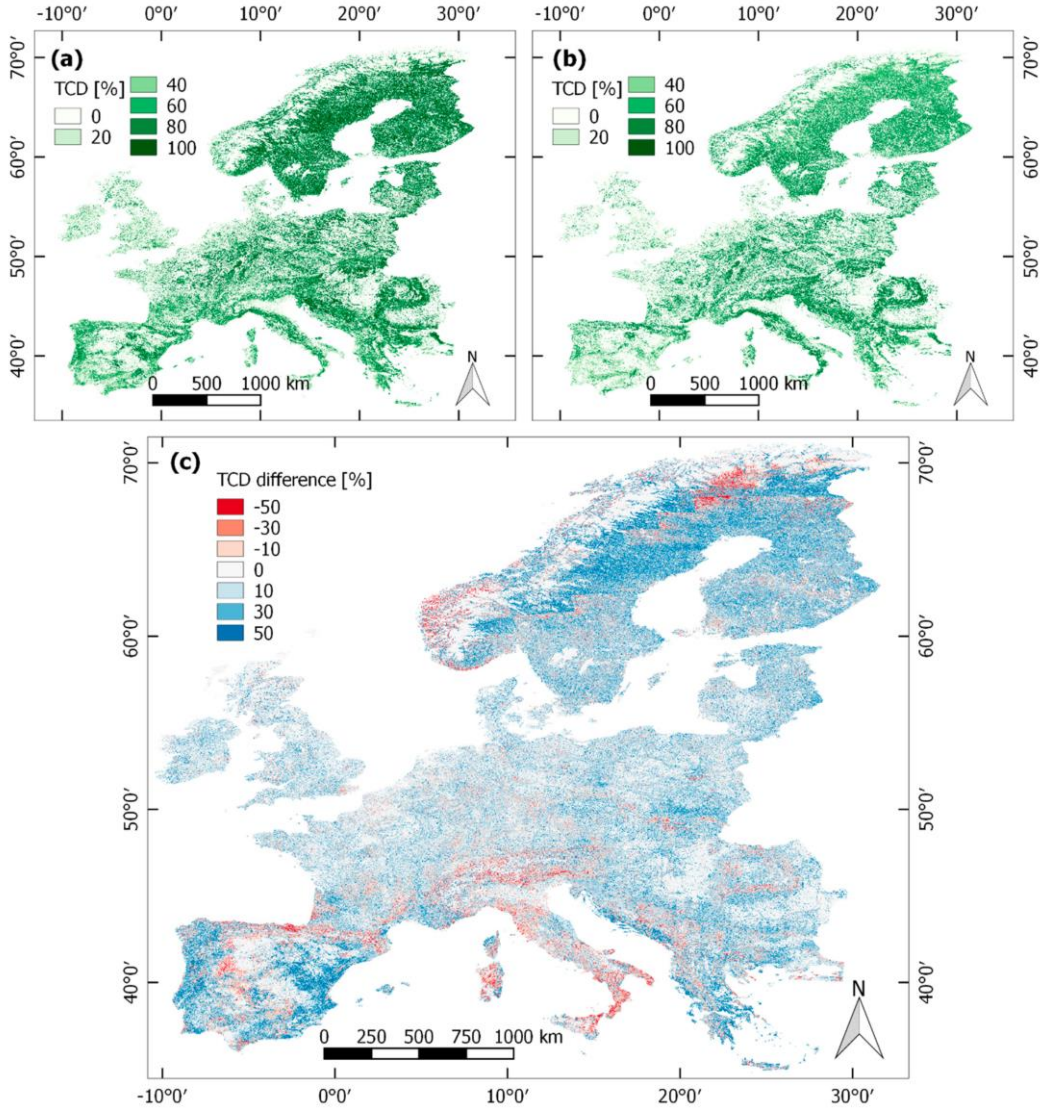

Figure 25: Overview of the tree cover density (TCD) maps from (a) Sentinel-1, (b) Copernicus High Resolution Layers (HRL) and (c) the difference map between the two datasets (Copernicus HRL map was subtracted from Sentinel-1 TCD map).

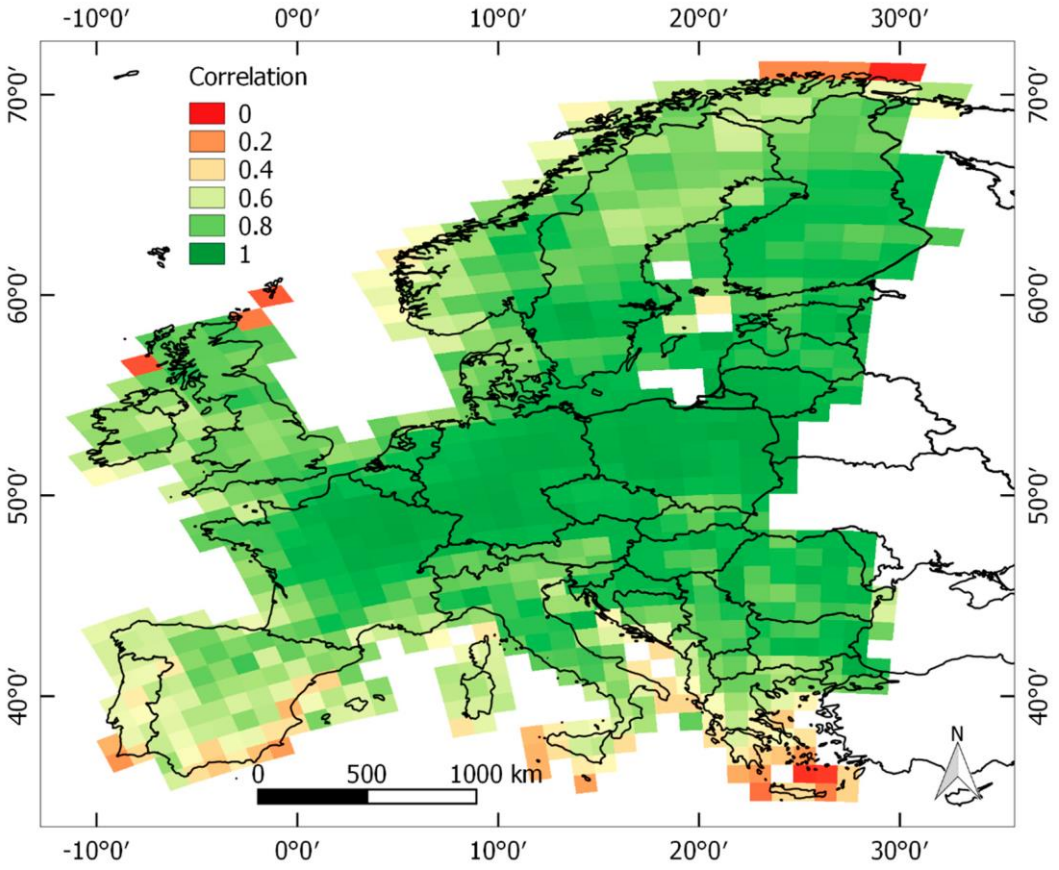

Figure 26: Pearson correlation coefficient between the Copernicus High Resolution Layers and Sentinel-1 tree cover density maps computed separately for each Equi7 tile.

To get a spatial overview, r was also computed for each Equi7 tile (100 km × 100 km area) separately. The spatial distribution (Figure 26) shows strong correspondence with values between 0.85 and 0.95 over large parts of central, eastern, and northern Europe. Lower accuracies (r between 0.65 and 0.85) can be observed over Alpine areas, southern Europe, the United Kingdom, Norway, and part of Sweden. Values below 0.65 are located mainly in southern Italy, southern Spain, Portugal, the islands of Corsica and Sardinia, and coastal areas of Greece, Albania, Croatia, and Norway. These areas typically have uneven topography and steep slopes.

An example of results for the Czech Republic (r = 0.90) and Sicily (r = 0.53) are presented in Figure 27 and Figure 28, respectively. Figure 29 shows boxplot distribution of TCD values for these two regions.

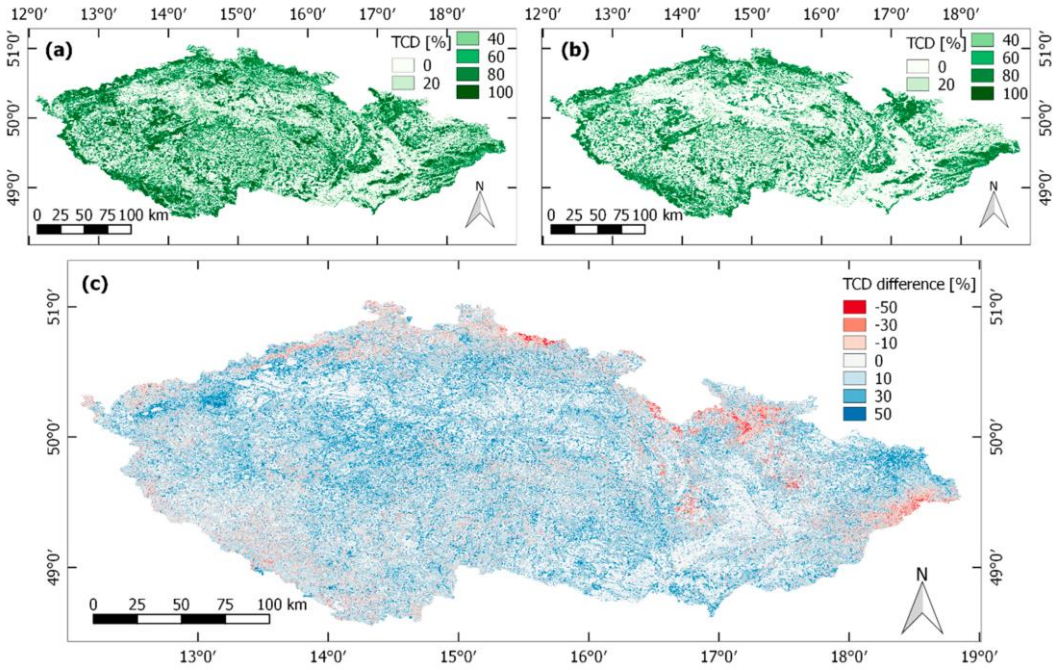

Figure 27: Detailed tree cover density (TCD) maps of the Czech Republic from (a) Sentinel-1, (b) Copernicus High Resolution Layers (HRL) and (c) the difference map between the two datasets (Copernicus HRL map was subtracted from Sentinel-1 TCD map).

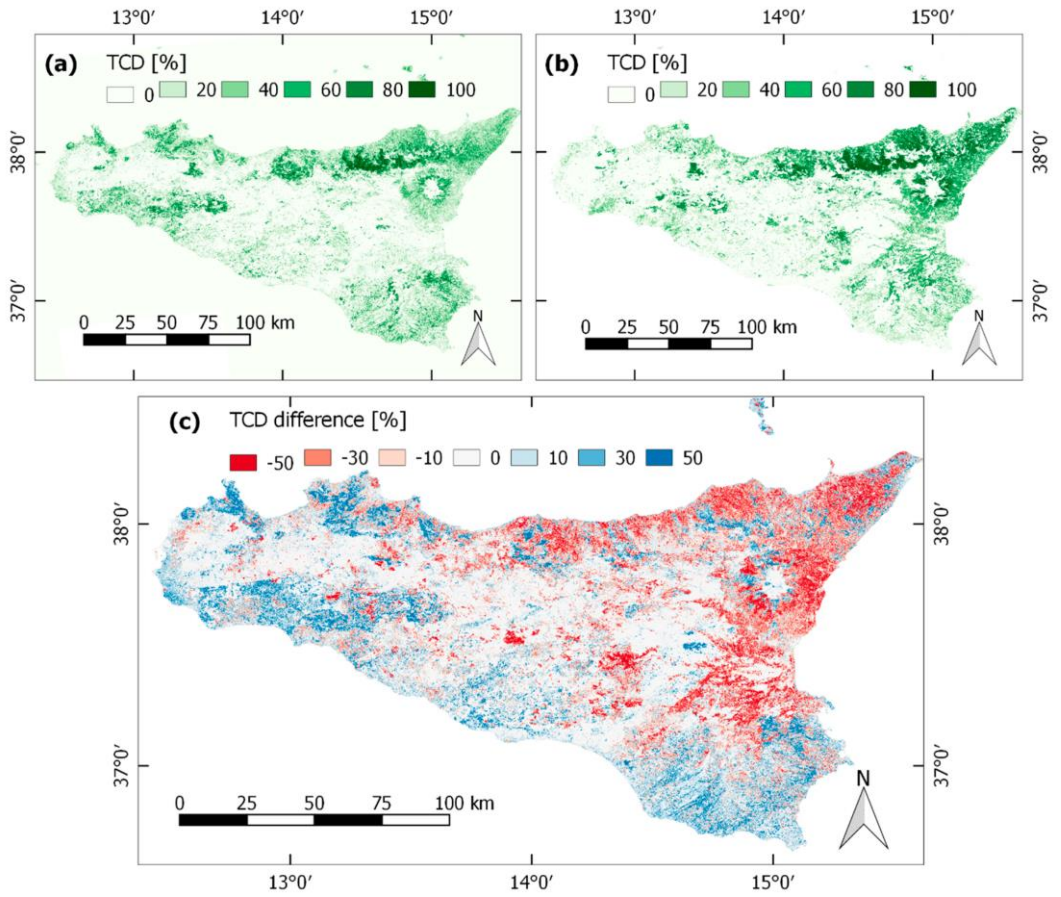

Figure 28: Detailed tree cover density (TCD) maps over Sicily from (a) Sentinel-1, (b) Copernicus High Resolution Layers (HRL) and (c) the difference map between the two datasets (Copernicus HRL map was subtracted from Sentinel-1 TCD map).

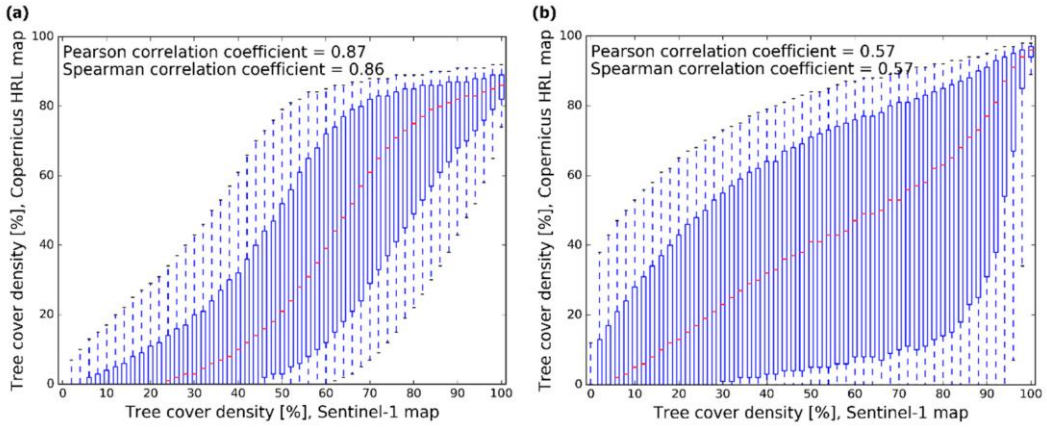

Figure 29: Plots showing the distribution of the tree cover density (TCD) values over (a) Czech Republic and (b) Sicily. Red lines indicate the average TCD value, blue boxes indicate the interquartile range of the TCD values (25th to 75th percentiles), dashed lines indicate the 10th and 90th percentile of the TCD values.

4.3.3 Sensitivity Analysis

Within the sensitivity analysis, 80 forest type and TCD maps were derived for a single Equi7 tile and compared to the Copernicus HRL datasets. The results are presented in Figure 30 with the red line indicating the value of the original set of signature prototypes. In the case of the forest type map, overall accuracies range between 87.4% and 92.0% for forest/non forest, and between 60.3% and 80.6% for forest type classification. The values of the original set of signature prototypes are 90.1% and 77.6% for the forest/non-forest and forest type classification, respectively. In the case of the TCD map, *r* ranges between 0.84 and 0.91, with 0.88 for the original set of signature prototypes.

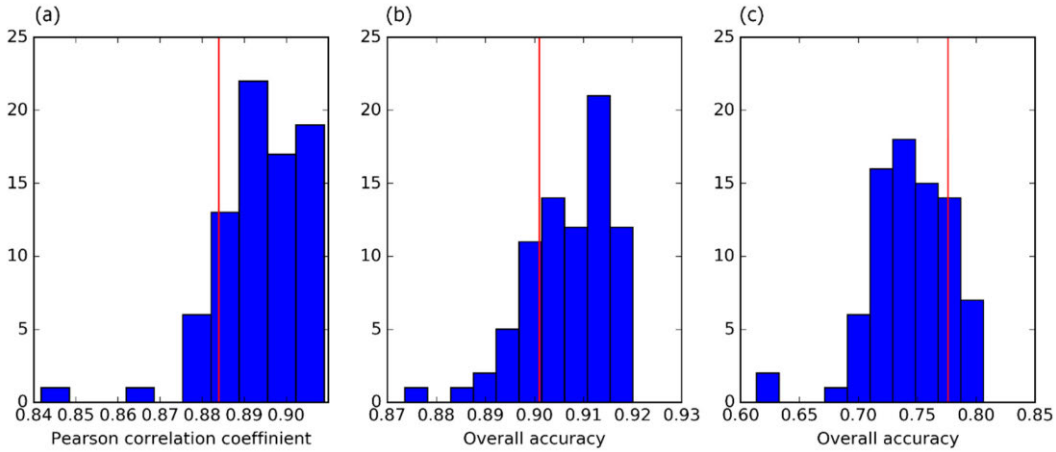

Figure 30: Validation results distribution of the model sensitivity test. Sensitivity of the method to the selection of the location of the signature prototypes was tested using 80 sets of reference points. Validation metrics were computed between the respective Sentinel-1 forest maps and Copernicus High Resolution Layers forest maps. Histograms show (a) Pearson correlation coefficient of the tree cover density maps, (b) overall accuracy of the forest/non-forest classification and (c) overall accuracy of the coniferous/broadleaf forest type classification. Red lines indicate the values computed using the original set of signature prototypes.

4.4 Discussion

4.4.1 Performance of the Sentinel-1 based forest maps

The accuracy assessment revealed that the approach is well suited for temperate and hemi-boreal forests; however, its ability to detect forested areas or classify forest type decreases in areas with lower forest density such as Mediterranean forests or areas in northern Sweden and Norway. Sparser tree coverage in these areas causes lower differences between the temporal signatures of different vegetation types (Figure 31). The high density of temperate forests enables the separation between forest/non-forest as well as forest type classification, while in Mediterranean forests, differentiation between the three classes is often not possible. High omission errors are to be expected, especially in areas with very sparse tree coverage. While in boreal forests, separation between forest and non-forest is feasible, the seasonal drop in temporal signature of broadleaf tree species is no longer visible and it is, therefore, difficult to distinguish between the two forest types (Figure 31). The same applies in high altitudes in montane forests where the approach is further limited by the topographic distortions in SAR signal. A more appropriate approach for terrain correction, such as using the terrain flattened gamma (Small 2011) might improve the results over mountainous areas. Nevertheless, results for Finland (overall accuracy of 88% for forest/non-forest mapping and 71% for forest type classification) or Switzerland (87% for forest/non forest mapping and 82% for forest type classification) show high potential of Sentinel-1 for forest mapping even in these challenging environments.

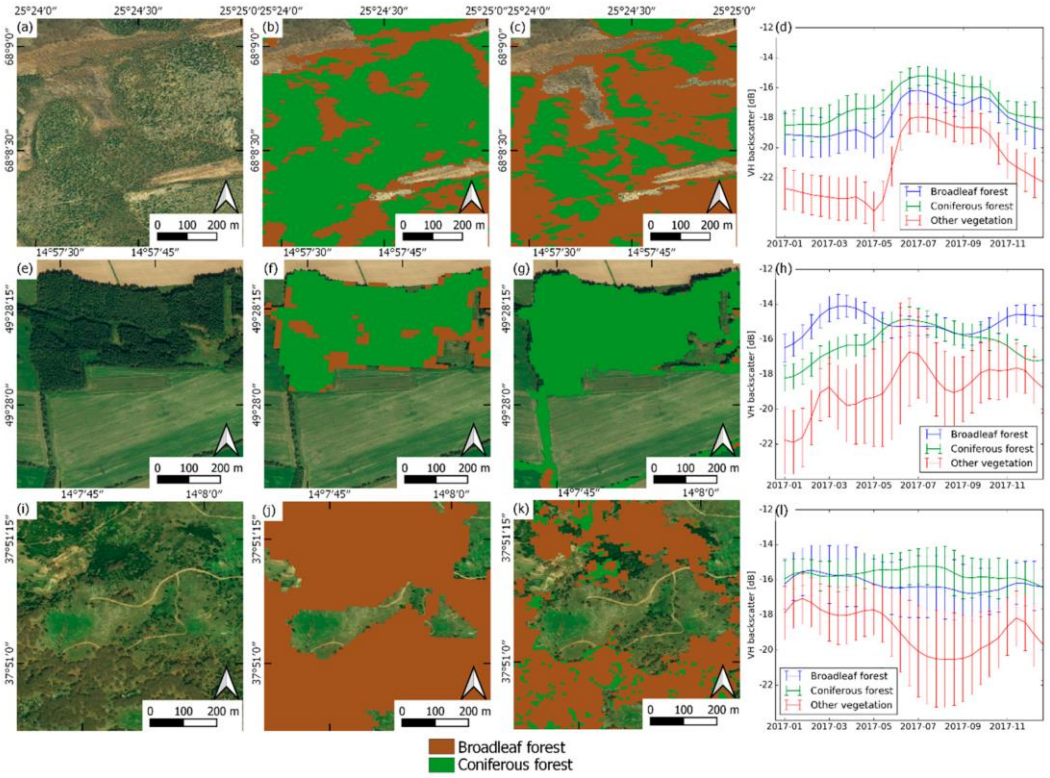

Figure 31: Examples of the forest type maps and cross-polarized backscatter temporal signatures from areas in northern Finland (boreal forest), Czech Republic (temperate forest) and Sicily (Mediterranean forest). The Bing aerial imagery is used as a base map. Temporal signatures are computed from sample of 1000 randomly selected points within a single Equi7 tile for classes coniferous forest, broadleaf forest and other vegetated areas. The solid line indicates the average backscatter value while the error bars indicate its standard deviation for each time stamp. (a) to (d) show subset in northern Finland where (a) shows Bing aerial image (b) Copernicus High Resolution Layers (HRL) forest type map, (c) Sentinel-1 forest type map and (d) temporal signature of the three vegetation classes. (e) to (h) show subset in Czech Republic where (e) shows Bing aerial image (f) Copernicus HRL forest type map, (g) Sentinel-1 forest type map and (h) temporal signature of the three vegetation classes. (i) to (l) show subset in Sicily where (i) shows Bing aerial image, (j) Copernicus HRL forest type map, (k) Sentinel-1 forest type map and (l) temporal signature of the three vegetation classes.

Forest area mapping for relatively small areas based on Sentinel-1 data was recently addressed in several studies. Overall accuracies of 94% were found over study area in North-East China (Yu, Ni et al. 2020), 92% over study area in Lower Austria (Dostálová, Hollaus et al. 2016), and balanced accuracies between 80% and 93% were reported for six sites distributed worldwide (Hansen, Mitchard et al. 2020). Forest type (coniferous/broadleaf) classification using Sentinel-1 was tested in two test sites in Switzerland (Rüetschi, Schaepman et al. 2018) with overall accuracy of 86%. Due to the limited size of the study sites located in Europe, no direct comparison can be made with the presented results. To the best of our knowledge, the only continental or global scale forest/non-forest map based on the SAR backscatter data is derived yearly by the Japan Aerospace Exploration Agency (JAXA) from Advanced Land Observing Satellite (ALOS) Phased Arrayed L-band SAR (PALSAR) data (Shimada, Itoh et al. 2014). Overall accuracy of the global ALOS PALSAR map was estimated at between 85% and

95% depending on the reference data used (Shimada, Itoh et al. 2014). The overall accuracy of the presented Sentinel-1 based map ranges from 86% when compared to Copernicus HRL data to 90% when compared to the national datasets.

4.4.2 Selection of the reference time series

One of the main challenges of the introduced approach is the susceptibility of the results to the choice of the temporal signature prototypes used for the forest classification. The selection of their location represents the only part that cannot be automated and requires not only manual interaction, but also local knowledge of the area or reliable reference data. We aimed to quantify the effect of the reference points selection by running the model repeatedly using different sets of signature prototypes. Our results show that, while the forest/non-forest and TCD accuracy is rather stable (overall accuracy between 87.4% and 92.0%), the forest type accuracy shows higher variation among the different sets of reference points (overall accuracy between 61.3% and 80.6%). Inspection of the Sentinel-1 data revealed that lowest accuracies for the forest type map are related to the selection of the spruce forest reference point located in areas with visible terrain effects. However, within the sensitivity test, the main tree species were known, and a reliable reference dataset was available to support the signature prototypes selection. Accuracy might vary even more strongly in cases where the most common tree species are not captured by the signature prototypes. In the case of the full-European study, it was not feasible to select all reference points accordingly, so that they would represent the most common forest species in the area. In some areas, better selection supported with the knowledge of local conditions might improve the result substantially. However, once the reference points are selected, the approach can rather easily be applied automatically, creating yearly forest maps with no further need of manual interaction, which enables change detection and regular updates of forestry data. As such, it might complement the well-established methods using optical remote sensing data.

4.4.3 Variability of national reference datasets

Relatively high variability of results between the national datasets and both the Sentinel-1 and Copernicus HRL datasets is caused by the large variability of the data sources, formats, resolutions as well as different definitions used for the coniferous and broadleaf classes for the validation. The reference data itself are often, at least partially, based on the remote sensing data and include errors as well. Furthermore, their accuracies were mostly unknown. Temporal gaps between the datasets also add to the uncertainties, especially in the case of the Swedish map, which was created in 2010. Lastly, also the

differences in forest definitions play an important role in the validation results. The Sentinel-1 map applies the MMU of 0.5 ha, but apart from the definition of the minimal area, no further rules are applied to identify the pixel as forest. For this reason, areas with high density of woodland, such as hedgerows or gardening areas, are commonly misclassified as forest. On the other hand, some of the national datasets include the unstocked forest land in the forest class, which leads to further discrepancies between the datasets.

4.4.4 Areas of further research

The radiometric terrain flattening (Small 2011) is expected to increase the applicability of Sentinel-1 in mountainous areas and can, therefore, improve the results over complex terrain. In the present study, this approach was not used due to large demand on processing resources due to the extensive test area. Testing and validating the approach using the terrain flattened gamma backscatter is one of the foreseen further steps. In addition, many areas were still validated using the Copernicus HRL data only, so including more national datasets—also for the tree cover density map—would provide a better overview of the quality of the Sentinel-1 forest products.

4.5 Conclusions

In this study, the first Europe-wide forest maps were introduced based on Sentinel-1 data only. These include a 10 m forest type map and a 100 m tree cover density map. The comprehensive validation included comparison with Copernicus HRL forest datasets and a variety of national datasets. The validation using national datasets showed that the Sentinel-1 forest maps have comparable accuracy with Copernicus HRL forest datasets, with average overall accuracies of 88.2% and 82.7% for Sentinel-1 and 90% and 87.2% for Copernicus HRL for forest/non-forest and forest type maps, respectively. The main advantage of the Sentinel-1 maps is that once the model, including reference points estimation, is established, yearly maps can be derived in a fully automated way. The spatial comparison with the Copernicus HRL dataset showed that the method works best in temperate broadleaf forest biomes, while the accuracy decreases in Mediterranean, boreal and montane forests.

Acknowledgements

We would like to thank people at the head office of the German National Forest Inventory at the Thünen Institute of Forest Ecosystems for providing the forest reference data and

their valuable feedback for the paper draft, and the Austrian Research Centre for Forests, the Forest Management Institute established by the Ministry of Agriculture of the Czech Republic, Institut National de L'Information Geographique et Forestiere in France and Nemzeti Földügyi Központ in Hungary for providing the forest reference data. Moreover, we would like to thank TU Wien for the Open Access Funding.

4.6 Appendix

Details concerning the national reference datasets are listed below.

Austria

The 1 m forest/non-forest mask was provided by Austrian Research Centre for Forests (BFW) for the land of Lower Austria. The mask was resampled to 10 m spatial resolution and to the EQUI7 grid, assigning forest class in cases where 25% of 1 m pixels within the 10 m pixel were classified as forests.

Czech Republic

The forest map was provided by the forest management institute (FMI) that is established by the Ministry of Agriculture of the Czech Republic. The 10 m forest type map was derived from satellite imagery (Sentinel-2), aerial imagery and normalized digital surface model (nDSM). The map classes were adapted as follows:

- Broadleaf type: oak, beech, other broadleaf species;
- Coniferous type: spruce, pine;
- Non-forest: other;
- Masked: uncertain pixels, young trees, wood plantations areas, mountain pine;

England, Scotland, and Wales.

Freely available National Inventory of Woodland and Trees dataset provided by Forestry Commission was used. The map is provided in vector format and covers all forests and woodlands of area over 0.5 ha, minimum width of 20 m and minimum canopy cover of 20%. The map is updated annually using more recent aerial photography, satellite imagery and administrative records of newly planted areas. The revised data for 2017 were used. The classes were specified as follows:

- Broadleaf type: Broadleaved;
- Coniferous type: Coniferous;
- Mixed: mixed, mixed predominantly conifer, mixed predominantly broadleaf;

- Non-forest: Shrub;
- Masked: Coppice, Coppice with standards, young trees, felled, ground prepared for new planting, windblow, failed, assumed woodland, cloud or shadow, uncertain, low density.

Estonia

The share of conifers in the upper layer in percent was provided for 10,277 randomly selected points by University of Tartu. The source of the data is Estonian forest register, reference year 2017. Forests with over 65% of coniferous or broadleaf forest type were attributed to the corresponding class; the rest of the pixels were assigned to the mixed forest class.

France

The forest database data (BD Fôret v2) in vector format was provided by Institut National de L'Information Geographique et Forestiere (IGN). The forest map is derived through interpreting of aerial photographs and contains forest areas of at least 0.5 ha and contains information about the forest type, its density and dominant tree type. The last update of the dataset is dependent on the county and ranges between 2014 and 2019. Forest types were specified as follows:

- Coniferous forest: open coniferous forest, closed coniferous forest;
- Broadleaf forest: open broadleaf forest, closed broadleaf forest, poplar trees;
- Mixed forest: open mixed forest, closed mixed forest;
- Non forest: herbal vegetation;
- Masked: forest without tree cover.

Finland

The freely available Corine Land Cover (CLC) map from the Finnish Environment Institute (SYKE) was used. It provides land cover and land use information, including broadleaf, coniferous and mixed forest classes for the entire country on 20 m × 20 m resolution for the year 2018. It was created by automated interpretation of satellite images from 2016 and 2017 and data integration with existing digital map data.

Germany

The National Forest Inventory (NFI) collects data for cluster plots that are composed of four subplots each. The cluster plots are spread along a base sampling grid of 4 km × 4 km. For some federal states, the sampling is densified. Together, forest relevant

information is collected for 195630 subplots including subplot type information (non-forest, productive or unproductive forest, unstocked forest, short rotation coppice etc.) and forest type information (pure deciduous forest, deciduous forest with admixture of coniferous trees, mixed forest, coniferous forest with admixture of deciduous trees, pure coniferous forest). The full inventory is updated every 10 years with a reduced grid being updated 5 years in between. The last full inventory was conducted in 2012 and that of the reduced grid in 2017. The inventory is updated partially by on-site visits and partially by analysing aerial photography. The NFI subplots were collocated with Sentinel-1 forest type map and the resulting table was provided by the Institute of Forest Ecosystems within the Thünen Institute. For the validation purposes, the classes were defined as follows:

- Non-forest: non-forest;
- Forest: productive forest, unproductive forest, stocked timberland;
- Masked: temporarily unstocked forest, unstocked forest land.

The forest type was validated using the pure deciduous forest and pure coniferous forest classes only.

Hungary

The forest type map of Hungary was rasterized from the National Forest stand Database of Hungary (state of 26th May 2020) and provided by Nemzeti Földügyi Központ (NFK) as a 10 m × 10 m raster containing broadleaved, coniferous, and mixed forest type. The map contains only official planned forest and omits free provision forests.

Latvia

Data from Latvian State Forest Research Institute Silava contain forest inventory data for the Latvian state-owned forests which cover about half of the forest area. A total of 10,000 points were randomly selected from stands with coverage of dominant tree species of at least 80%. These were then compared to the Sentinel-1 based forest type map.

Slovakia

The Slovakian National Forest Centre provides freely available dataset Register jednotiek priestoroveho rozdelenia lesa (JPRL). All forest units are stored in vector format and referenced to a database containing large number of forest description parameters. The database information is updated yearly, version from 2017 was used in this study. The relevant parameters for this study were main tree species, secondary tree species and their proportional representation in percent. All polygons with over 65% of broadleaf species

were classified as broadleaf and those with over 65% of conifers as coniferous. The polygons with lower portion of prevailing tree type were classified as mixed forest. In addition, part of the forest units lacked the tree species information and thus were also classified as mixed forest.

Sweden

The Department of Forest Resource Management of the Swedish University of Agricultural Sciences (SLU) provides freely available SLU Forest Map (Reese, Granqvist-Pahlén et al. 2005). It contains spatial information over most of Sweden's forestland. It combines data from Swedish National Forest Inventory and satellite data from Landsat and SPOT satellites. The map contains information on age, height, species and standing volumes of woodlands and the spatial resolution is 25 m. The last update was published in 2010. For the validation purposes, pixels containing more than 65% of coniferous or broadleaf tree species are assigned as coniferous or broadleaf type, respectively.

Switzerland

The 25 m resolution map was developed in (Waser, Ginzler et al. 2017) provided by the Swiss National Forest Inventory hosted by the Swiss Federal Institute for Forest, Snow and Landscape Research (WSL) and the Federal Office of the Environment (FOEN). The map is based on aerial images from 2012 to 2017 and gives the probability in percent of broadleaf trees. The comparison of the tree type map with independent NFI data revealed high overall accuracies (95% to 99%) and a slight underestimation of broadleaved trees (median of −3.17%) [41]. Pixels with probability above 65% were classified as broadleaf forest, below 35% as coniferous forest and those between the two thresholds as mixed forest.

5 Publication IV: Influence of the Radiometric Terrain Flattening on the SAR-based Forest Mapping and Classification

This section is in review for submission to the Remote Sensing Letters jounal:

Dostálová, Alena, Claudio Navacchi, Isabella Pfeil, David Small, and Wolfgang Wagner. "Influence of the Radiometric Terrain Flattening on the SAR-based Forest Mapping and Classification."

Abstract

Terrain induced variations of radar backscatter represent an important limiting factor of many Synthetic Aperture Radar (SAR) based applications. Radiometric terrain flattening (RTF) is a well established method that minimizes these variations in SAR imagery. To fully understand the implications of SAR RTF, validation of its impact on the derived products is needed. In this study, we quantified the influence of the RTF on a forest mapping and classification algorithm over Austria and compared the classification results for the conventional sigma naught and radiometrically terrain corrected gamma backscatter. The overall accuracy for forest/non-forest mapping and forest type classification improved by 2% and 3% respectively over the whole of Austria with improvements of up to 16% and 17% respectively in regions with strong topography.

5.1 Introduction

Synthetic aperture radar (SAR) is an active microwave imaging system that allows us to remotely map the reflectivity of objects or environments at microwave frequencies with high spatial resolution. Advantages of this remote sensing technique include its penetrability through clouds and independence from the solar illumination of the surface. As such, SAR provides almost all-weather, day and night measuring capability. Currently, SAR imagery is used in a wide spread of applications that make use of the SAR normalized radar cross section (NRSC), which is represented in terms of a backscatter coefficient - an estimate of the backscatter per given reference area. Depending on which reference area convention is chosen for normalisation, one can distinguish between three representations of the backscatter coefficient known as: i) beta naught β^0, ii) sigma naught (σ^0), or iii) gamma naught (γ^0) (Small 2011). The σ^0 and γ^0

coefficients use an ellipsoid for the reference area computation and thus have an important limitation, namely the fact that their radiometric properties are heavily distorted by topographic variations, even in only slightly undulating terrain. The topography-induced variations in SAR backscatter images are typically much larger than changes in backscatter coefficients due to the observed geophysical parameter (Atwood, Small et al. 2012, Villard and Le Toan 2014). As a result, SAR data are often discarded over hilly and mountainous areas.

To overcome this limitation, several methods of the radiometric normalisation of the backscatter coefficient were introduced in the literature. These include methods based on the local incidence angle (LIA) (Ulander 1996, Kellndorfer, Pierce et al. 1998) or the actual ground area visible to the radar which is known as radiometric terrain flattening (RTF) (Small 2011). In recent years, the RTF became widely used, especially in snow or ice melt mapping ((Scharien, Segal et al. 2017, Lund, Forster et al. 2020)) or forest monitoring ((Rüetschi, Schaepman et al. 2018, Akbari and Solberg 2020)). The advantage of the RTF is evident mainly in areas with complex topography (Frey, Santoro et al. 2012, Small, Miranda et al. 2013, Rüetschi, Schaepman et al. 2018, Small, Rohner et al. 2021), yet, to fully understand the benefit of this additional processing step, a validation of derived products with and without this step needs to be performed.

So far, only limited number of studies quantified the influence of the RTF on the end product. Markert et al. (Markert, Markert et al. 2020) evaluated the differences between two automated surface water mapping algorithms using the conventionally calibrated and radiometrically terrain flattened Sentinel-1 data as input for their algorithms. The authors found, that the algorithms using radiometrically terrain flattened data as input yielded higher overall accuracies, these differences were, however, not significant. It should be noted that this analysis was limited to areas below 30 m in height relative to the nearest drainage as represented by the Height Above Nearest Drainage (HAND) index. This means that especially over scenes containing mountainous riverine, the HAND index mask might have masked considerable portions of terrain induced differences between the analysed datasets in case that they lie in high elevations relative to the drainage network. Different approaches of topographic normalisation including no correction (conventional approach), correction based on LIA, correction based on pixel area correction (RTF) and combination of the RTF correction with empirical slope normalisation were analysed in (Atwood, Andersen et al. 2014). The biomass estimations were improved from no correction to LIA based corrections and further to the RTF and combined RTF and empirical slope corrections. This influence was shown to be smaller for estimates based solely on cross-polarisation backscatter than for those based on co-polarized or dual-

polarized data. After adaptation for polarimetric SAR data, the influence of the RTF for the land cover classification was assessed in (Atwood, Small et al. 2012). The largest improvements were observed for the deciduous forest class, and the impact of the RTF step was highlighted by comparing the classification performed separately for regions facing towards and away from the satellite.

Having recognized the high potential of RTF, European Space Agency (ESA) implemented this method in the widely used open-source Sentinel Application Platform (SNAP, (SNAP)) toolbox. Unfortunately, calculating radiometrically terrain corrected (RTC) gamma (γ_{rtf}) backscatter with SNAP requires three to five times more time than calculating σ^0. For this reason, it is essential to assess the potential of this additional processing step on the end product. In this study, we evaluated results of a forest mapping and forest type classification algorithm (Dostálová, Lang et al. 2021) using σ^0 and γ_{rtf} backscatter as an input over Austria. The improvements were quantified in respect to terrain slope and aspect to identify the regions, where this additional step can provide highest improvements.

5.2 SAR Data Pre-processing

For the purpose of this study, Sentinel-1 1 Ground Range Detected (GRD) Interferometric Wide (IW) swath mode acquisitions from year 2017 for the whole of Austria were used. The pre-processing steps for the σ^0 images include precise orbit correction, border noise removal, radiometric correction to the σ^0 values and Range-Doppler terrain correction(Small and Schubert 2008). For γ_{rtf} precise orbit correction, border noise removal, radiometric correction to the β^0 values, radiometric terrain flattening and Range-Doppler terrain correction were applied. A terrain model based on airborne laser scanning (Geoland 2020) with 10 m spatial resolution was used for the radiometric terrain flattening and the Range-Doppler terrain correction steps. The pre-processing was done using the SAR Geophysical Retrieval Toolbox (SGRT, (Naeimi, Elefante et al. 2016)) which invokes several modules from the SNAP toolbox.

5.3 Retrieval Algorithm and Validation

The forest mapping and classification algorithm (Dostálová, Lang et al. 2021) uses either σ^0 or γ_{rtf} backscatter as input, while the rest of the processing steps steps (i.e. SAR seasonality time series computation and construction of the forest maps) remain the same. A brief description of the main steps is provided in the following subsections, details can

be found in (Dostálová, Wagner et al. 2018, Dostálová, Lang et al. 2021).

5.3.1 SAR seasonality time series computation

The forest mapping and classification algorithm(Dostálová, Lang et al. 2021) uses as input one year of Sentinel-1 measurements. Due to the irregular temporal resolution, varying acquisition geometry and changing environmental conditions of the individual acquisitions, SAR seasonality time series with regular time step is derived. First, a normalisation to a common reference angle was applied using the slope (β) parameter. This correction is applied to minimise the effect of the varying sensor-target geometry and the associated changes in incidence angle and enable the combination of the acquisitions taken from various relative orbits (Peters, Lievens et al. 2012). The slope parameter is computed using a linear regression between the backscatter coefficient (in dB) and projected local incidence angle (θ) values. It is computed separately for each image pixel and uses the full time-series of all available Sentinel-1 acquisitions from 2017. The resulting β parameter is stable in time and varies with land cover. The normalisation equation for σ^0 and γ_{rtf} backscatter reads as follows:

$$\sigma^0(40°) = \sigma^0(\theta) - \beta(\theta - 40°) \quad (1)$$

$$\gamma_{rtf}(40°) = \gamma_{rtf}(\theta) - \beta(\theta - 40°) \quad (2)$$

Next, the mean of the normalized backscatter was computed using all available acquisitions covering each 12 day interval, and smoothed using a Gaussian temporal filter with standard deviation of 1 to smooth the signal variation caused by the quickly varying environmental conditions (such as changes in surface and vegetation moisture content or freeze/thaw effects). The resulting time series captures the annual variability of the signal and reflects the seasonal changes of various vegetation types (Dostálová, Wagner et al. 2018, Rüetschi, Schaepman et al. 2018).

5.3.2 Construction of the forest map

The forest classification algorithm(Dostalova, Cao et al. 2021) exploits the differences between the seasonality time series - temporal signatures - of various vegetation types. Signature prototypes are defined for coniferous and broadleaf forest classes as a temporal signature of 300 m × 300 m large region of the given forest class. The model sensitivity to the location of the prototypes is relatively low (Dostálová, Lang et al. 2021). The locations of the signature prototypes over Austria are shown at Figure 32 overlaid on the used DEM. The classification algorithm uses the similarity measures - Root Mean Square Difference (RMSD) and Pearson correlation coefficient r - between the prototype

signatures and the respective temporal signature of each individual pixel. In the first step, forest/non-forest classes are assigned using thresholds (1.5 dB and 2.0 dB for VH and VV polarisation RMSD and 0.4 for VH polarisation *r*). Consequently, the forest type (coniferous, broadleaf) is assigned to each forested pixel according to the lowest RMSD value in VH polarisation. For the final forest type map, minimal mapping units (MMU) of 0.5 ha are applied. The forest type map has 10 m sample interval and three classes: non-forest, coniferous forest and broadleaf forest.

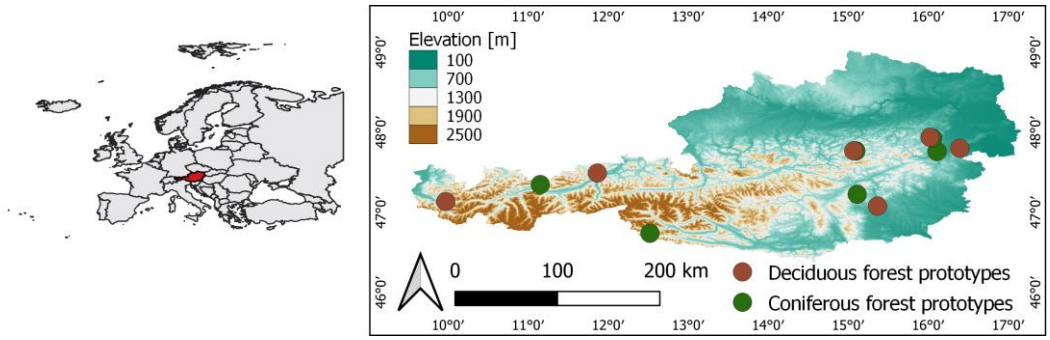

Figure 32: Overview of the study area (Austria) with the locations of the signature prototypes for the forest type classification overlaid on the terrain model of Austria based on airborne laser scanning.

5.3.3 Validation

σ^0 and γ_{rtf} based forest maps were computed for the whole of Austria and compared to reference maps. For the validation of the forest/non forest classification, a 1 m forest/non-forest map based on aerial imagery and ALS data was provided by the Austrian Research Centre for Forests (BFW). For validating the forest type (broadleaf/coniferous class), the Copernicus High Resolution Layers (HRL) Forest Type dataset (year 2015) (Langanke, Büttner et al. 2013) was used. Both reference maps were resampled to the 10 m sample interval, in case of the BFW forest map, 10 m pixel was assigned to forest class in cases where 25% of 1 m pixels within the 10 m pixel were classified as forests. The forest/non-forest accuracies were computed using all pixels. In case of the forest type dataset, pixels that were classified as non-forest in σ^0, γ_{rtf} or HRL forest type dataset were discarded from the classification to ensure, that the errors caused by the forest/non-forest miss-classification would not be transferred to the forest type classification results.

The focus of the validation was put on two aspects. First, the spatial distribution of differences between the σ^0 and γ_{rtf} forest maps was highlighted by computing and plotting the validation statistics for 10 km large tiles as well as for entire Austria. Secondly, the influence of the local terrain aspect and slope on the map's accuracy was assessed by computing the validation statistics separately for various terrain slope and aspect intervals. It should be noted that the accuracy of both reference datasets is

unknown and the differences in forest definitions, temporal gaps as well as differences in spatial resolution between the datasets also add to the uncertainties.

5.4 Impact of the Terrain Flattening

5.4.1 Spatial overview

Spatial overviews of the forest mapping and classification results for γ_{rtf} and σ^0 are shown in Figure 33 and Figure 34 respectively. Each figure shows the reference map (BFW forest mask and Copernicus HRL Forest Type map for forest/non-forest and forest type map respectively) together with the difference images between the reference map the γ_{rtf}- and σ^0-based classification results and the spatial distribution of the difference between the overall accuracy of the γ_{rtf} and σ^0 results.

For forest/non-forest mapping, distinct patterns are apparent in the maps showing the differences in classification and especially the classification accuracy improvements. It is apparent that the largest differences between the Sentinel-1 and reference forest maps are located in mountainous regions (see Figure 32). This is to be expected and was already postulated in previous works ((Dostálová, Wagner et al. 2018, Dostálová, Lang et al. 2021)). Also, the mountainous areas show the largest improvement in quality when substituting γ_{rtf} instead of σ^0 as an input for the classification algorithm - the improvements locally reached as high as 16% in case of the forest/non-forest map. This is mainly due to underclassification of the forest area in mountainous regions, where insufficient correction of the terrain effects hinder the classification algorithm. In the flatland, the overall accuracies of the γ_{rtf} and σ^0 forest/non-forest maps are comparable except few areas located mainly in Southern Austria where the γ_{rtf} based forest map slightly overclassifies forest area and overall accuracy locally decreases causing maximal differences of up to 3%.

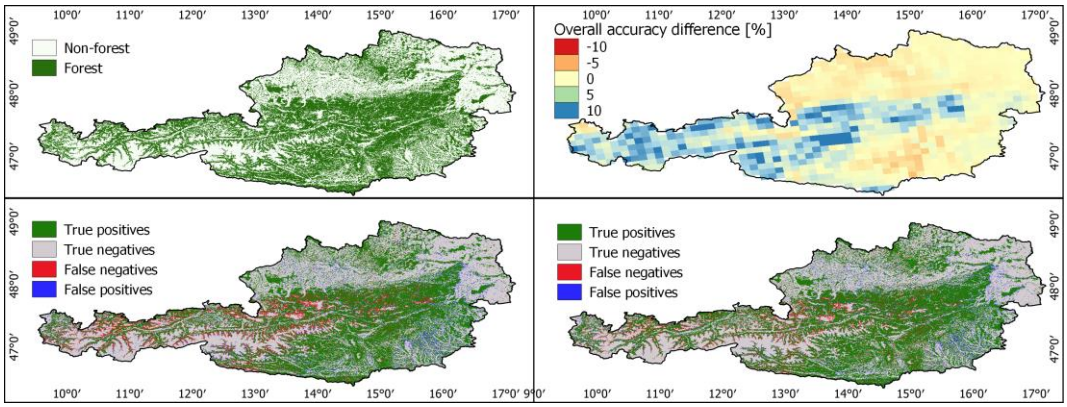

Figure 33: Overview of the results of the forest mapping algorithm. Top, left: Reference forest map from the Austrian Centre for Forests (BFW). Top, right: Difference between the overall accuracy of the σ^0- and γ_{rtf}-forest/non-forest map computed for 10 km large tiles. Bottom, left: Difference map between the σ^0 Sentinel-1 and reference forest/non-forest map. Bottom, right: Difference map between the σ^0 Sentinel-1 and reference forest/non-forest map.

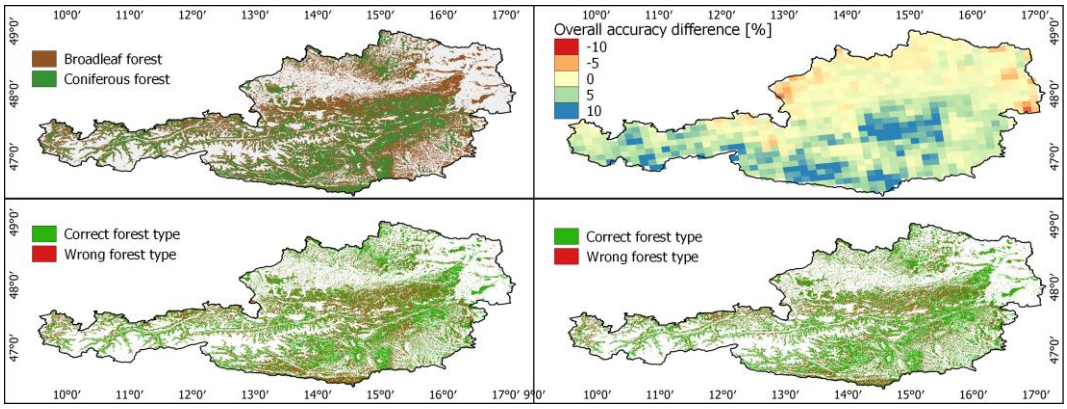

Figure 34: Overview of the results of the forest classification algorithm. Top, left: Reference forest map from Copernicus high resolution layers. Top, right: Difference between the overall accuracy of the σ^0- and γ_{rtf}-forest type map computed for 10 km large tiles. Bottom, left: Difference map between the σ^0 Sentinel-1 and reference forest type map. Bottom, right: Difference map between the σ^0 Sentinel-1 and reference forest type map.

In case of forest type classification, the improvements are also mainly located in mountainous regions, however the pattern followed that of the terrain model less strictly. The greatest improvements of up to 17% were observed in central and Southern Austria where the topography is milder than in Western Austria. However, these are also the areas with largest forest area and a lot of forest type variability. In the flatlands, the differecnes in the overall accuracies of the γ_{rtf} and σ^0 forest type map varied by ±5%.

The overall accuracy as well as user's and producer's accuracies for each class over the whole of Austria are summarised in Table 11. When computed over the entire range of the local terrain slopes, the overall accuracy for forest/non-forest and forest type classification improved 2% and 3% respectively. In case of forest, non-forest and the coniferous forest class, also the user's and producer's accuracies stayed the same or were improved. The only exception was the producer's accuracy of the broadleaf forest class

that decreased by 2%.

Table 11: User's, Producer's and Overall accuracies of the σ^0- and γ_{rtf}-forest/non-forest and forest type maps when compared to the BFW forest mask and Copernicus HRL forest type maps respectively for various local terrain slope ranges.

Slope range [°]		**0-90**		**0-10**		**10-20**		**20-30**		**30-40**		**40-50**		**50-70**	
Metric	**Class**	σ^0	γ_{rtf}	σ^0	γ_{rtf}	σ^0	γ_{rtf}	σ^0	γ_{rtf}	σ^0	γ_{rtf}	σ^0	γ_{rtf}	σ^0	γ_{rtf}
Overall accuracy	Forest/non-forest	0.87	0.89	0.92	0.92	0.89	0.89	0.86	0.88	0.78	0.85	0.73	0.81	0.73	0.78
Overall accuracy	Forest type	0.73	0.77	0.76	0.77	0.76	0.78	0.72	0.77	0.68	0.75	0.66	0.71	0.64	0.68
Producer's accuracy	Forest	0.84	0.87	0.92	0.92	0.90	0.90	0.86	0.88	0.74	0.83	0.63	0.75	0.51	0.61
User's accuracy	Forest	0.89	0.90	0.80	0.80	0.90	0.90	0.94	0.95	0.93	0.96	0.90	0.94	0.78	0.84
Producer's accuracy	Non-forest	0.90	0.91	0.92	0.92	0.86	0.86	0.86	0.88	0.88	0.91	0.89	0.92	0.89	0.91
User's accuracy	Non-forest	0.86	0.88	0.97	0.97	0.86	0.86	0.72	0.76	0.59	0.69	0.60	0.69	0.71	0.76
Producer's accuracy	Broadleaf forest	0.58	0.56	0.62	0.62	0.57	0.57	0.54	0.50	0.59	0.50	0.60	0.51	0.56	0.45
User's accuracy	Broadleaf forest	0.64	0.73	0.84	0.88	0.72	0.78	0.54	0.65	0.46	0.58	0.43	0.49	0.34	0.35
Producer's accuracy	Coniferous forest	0.82	0.88	0.89	0.92	0.88	0.91	0.80	0.88	0.71	0.85	0.69	0.79	0.67	0.75
User's accuracy	Coniferous forest	0.78	0.78	0.72	0.72	0.78	0.79	0.80	0.80	0.81	0.80	0.82	0.81	0.84	0.82

5.4.2 Influence of terrain slope and aspect

Even though the increasing elevation is known to influence the classification accuracy independently of the input data (Dostálová, Lang et al. 2021), left uncompensated, terrain-induced variations in the SAR backscatter deteriorate the classification result in mountainous areas. The influence of the local terrain slope on the overall accuracy of the forest/non-forest and forest type maps is demonstrated in Table 11. In case of the forest type classification, the accuracies based on σ^0 and γ_{rtf} are comparable for slopes up to 20°. With increasing terrain slope, the accuracies of the forest/non-forest map rapidly decrease in case of σ^0, which is mainly caused by the increasing omission error of the forest class. Decrease in accuracies is slower for the γ_{rtf}-based forest/non-forest map. For instance, difference between the overall accuracy of σ^0 and γ_{rtf} forest/non-forest classification for slopes between 40° and 50° reaches 8%. In case of the forest type classification, overall accuracy is higher for all terrain slope ranges, however, in case of the slopes below 20°, this difference is only 1%. Slopes above 70° are not shown due to a small number of available samples.

Due to the changing sensor-target illumination conditions, the algorithm is sensitive to the local terrain aspect. The accuracy remains relatively stable in case of low slopes up to 20° (see Figure 35: left) and is not improved by including the RTF correction. In case of steep slopes between 40° and 50° (see Figure 35: right), the overall accuracy of the σ^0 based forest/non-forest classification varies between 62% and 85% with lowest values for slopes facing the sensor for either ascending or descending orbit pass. This dependency on local terrain aspect is reduced by including the RTF step (the overall accuracies range between 72% and 87%). We conclude that, apart from the effect of applying the proper way of radiometric calibration, also the improved handling of the radar shadows in SNAP toolbox in case of the RTF workflow contributed to the increased accuracy.

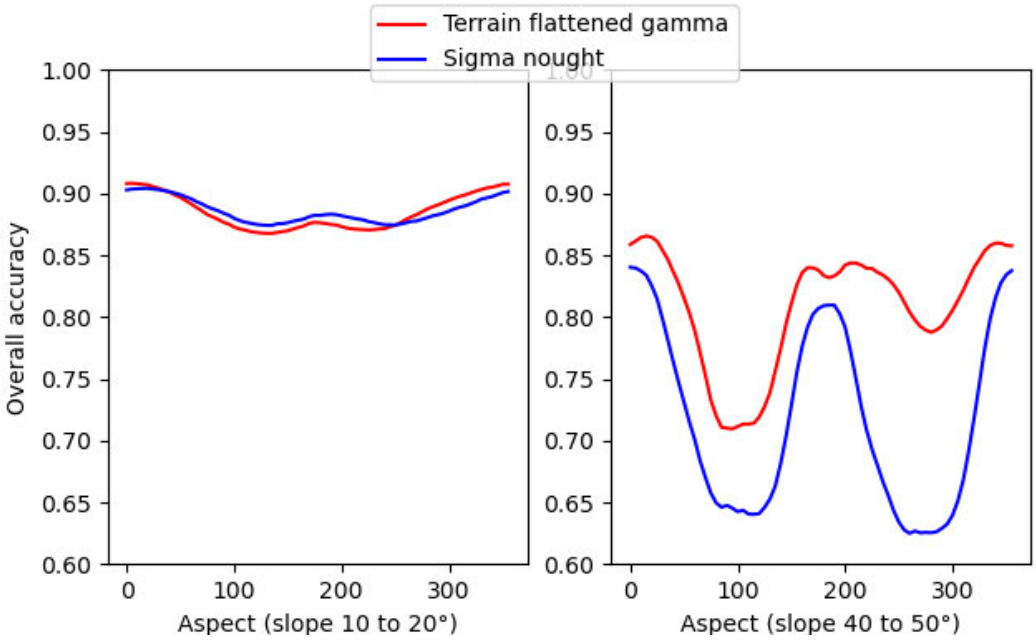

Figure 35: Dependency of overall accuracy of the forest/non-forest classification on the local terrain aspect. Left: local terrain slope range between 10° and 20°, Right: local terrain slope range between 40° and 50°.

5.5 Conclusion

Terrain induced variations in the SAR backscatter have long been a limiting factor to many SAR applications. By replacing conventional ellipsoid-based radiometrically calibrated backscatter coefficients with radiometrically terrain flattened and corrected γ_{rtf} we showed improvements in the data quality over undulated terrain. We quantified the effect of the RTF on the end product accuracy for forest mapping and classification algorithms over Austria. Significant improvements (16% and 17% for forest/non-forest mapping and forest type classification) were observed in highly undulated areas when γ_{rtf} backscatter was used instead of σ^0. In flatlands, the results remained comparable for both backscatter coefficient conventions. These results show, that despite the significantly higher processing demands, including the RTF correction is needed at least for areas with local terrain slopes over 20°.

Acknowledgment

This research was conducted within the Gamma2Cloud (Feasibility of Using Sentinel-1 Terrain-flattened Gamma Naught Backscatter Across EO platforms) project funded by ESA. We also acknowledge funding by the Austrian Research Promotion Agency (FFG) for the Austrian Data Cube project. The authors would like to thank the Austrian Research Centre for Forests for providing the forest reference data.

6 Conclusions and outlook

6.1 Conclusions and scientific impact

The primary objective of this thesis was to derive a continental-wide forest map using the Sentinel-1 SAR backscatter data over Europe. Despite great advances in remote sensing, large-scale forest maps derived in semi-automatic or automatic fashion remain rare and were mainly conducted in individual case studies. In case of microwave remote sensing, many studies showed the high potential of the SAR backscatter for forest mapping or dominant leaf type classification but were mostly limited to specific study areas and rarely validated on larger scale. Up to our best knowledge, the introduced forest maps are the first continental-wide forest area maps from Sentinel-1 and first large-scale forest type maps based on SAR data.

However, as important as the algorithm itself, is also the understanding of its limitations. For this reason, the evaluation of the newly derived maps was an equally important task as the algorithm development itself. Collection of the appropriate reference datasets was one of the crucial tasks within this thesis. Due to the lack of global- or Europe-wide forest type maps with the exception of the Copernicus HRL forest type dataset, multitude of nationally available forest datasets were used as reference data. The communication with the respective national forest inventories or universities also showed me the high interest in the spaceborne remote sensing data as a source of information that can complement the more precise but also much more costly airborne remote sensing or terrestrial and in-situ data collection.

In this regard, the main scientific outcome of this thesis is the knowledge of the potential of the Sentinel-1 to contribute to the forest mapping and classification also on large scale. The evaluation of both the Sentinel-1 and Copernicus HRL datasets against the national forest maps showed that the obtained accuracies of Sentinel-1 forest maps are almost within range of the HRL datasets in temperate and hemi-boreal forests. However, as mountain and boreal forests are both challenging environments for optical remote sensing as well, it might be especially these areas, where the combination of the optical and microwave remote sensing will lead to the highest improvements.

6.2 Outlook and future research

The evaluation of the forest maps presented in Publication III highlighted the areas of future research questions. One of the most important limitations remain to be the

topographic distortions. Nowadays, techniques such as radiometric terrain flattening exist, that improve the quality of the derived SAR products significantly in sloped terrains as it was presented in Publication IV. Similarly, the classification algorithm might be improved in sparse forests in boreal or Mediterranean regions.

Recently, the combination of Sentinel-1 and Sentnel-2 data for tree species classification has also been increasingly addressed by research. Publication II and III showed height potential for the dominant leaf type classification, however, the identification of the optimal features from Sentinel-1 that might help to distinguish tree species is still among the future challenges. Least but not least, the best combination of the forest information derived from the Sentinel-1 data with the other data sources is one of the most important future topics.

Bibliography

Ahern, F. J., D. J. Leckie and J. A. Drieman (1993). "Seasonal changes in relative C-band backscatter of northern forest cover types." IEEE Transactions on Geoscience and Remote Sensing **31**(3): 668-680.

Akbari, V. and S. Solberg (2020). "Clear-cut detection and mapping using Sentinel-1 backscatter coefficient and short-term interferometric coherence time series." IEEE Geoscience and Remote Sensing Letters.

Atwood, D. K., H.-E. Andersen, B. Matthiss and F. Holecz (2014). "Impact of topographic correction on estimation of aboveground boreal biomass using multi-temporal, L-band backscatter." IEEE Journal of Selected Topics in Applied Earth Observations and Remote Sensing **7**(8): 3262-3273.

Atwood, D. K., D. Small and R. Gens (2012). "Improving PolSAR land cover classification with radiometric correction of the coherency matrix." IEEE Journal of Selected Topics in Applied Earth Observations and Remote Sensing **5**(3): 848-856.

Balzter, H., B. Cole, C. Thiel and C. Schmullius (2015). "Mapping CORINE land cover from Sentinel-1A SAR and SRTM digital elevation model data using random forests." Remote Sensing **7**(11): 14876-14898.

Barreto, T. L., R. A. Rosa, C. Wimmer, J. B. Nogueira, J. Almeida and F. A. M. Cappabianco (2016). Deforestation change detection using high-resolution multi-temporal X-Band SAR images and supervised learning classification. 2016 IEEE International Geoscience and Remote Sensing Symposium (IGARSS), IEEE.

Barrett, F., R. E. McRoberts, E. Tomppo, E. Cienciala and L. T. Waser (2016). "A questionnaire-based review of the operational use of remotely sensed data by national forest inventories." Remote Sensing of Environment **174**: 279-289.

Bauer-Marschallinger, B., V. Freeman, S. Cao, C. Paulik, S. Schaufler, T. Stachl, S. Modanesi, C. Massari, L. Ciabatta, L. Brocca and W. Wagner (2019). "Toward Global Soil Moisture Monitoring With Sentinel-1: Harnessing Assets and Overcoming Obstacles." IEEE Transactions on Geoscience and Remote Sensing **57**(1): 520-539.

Bauer-Marschallinger, B., D. Sabel and W. Wagner (2014). "Optimisation of global grids for high-resolution remote sensing data." Computers & Geosciences **72**: 84-93.

Borre, J. V., D. Paelinckx, C. A. Mücher, L. Kooistra, B. Haest, G. De Blust and A. M. Schmidt (2011). "Integrating remote sensing in Natura 2000 habitat monitoring: Prospects on the way forward." Journal for Nature Conservation **19**(2): 116-125.

Bossard, M., J. Feranec and J. Otahel (2000). CORINE land cover technical guide: Addendum 2000, European Environment Agency Copenhagen.

Calder, I., T. Hofer, S. Vermont and P. Warren (2008). "Towards a new understanding of forests and water." UNASYLVA-FAO- **229**: 3.

Casalegno, S., G. Amatulli, A. Bastrup-Birk, T. H. Durrant and A. Pekkarinen (2011). "Modelling and mapping the suitability of European forest formations at 1-km resolution." European Journal of Forest Research **130**(6): 971-981.

Congalton, R. G. and K. Green (2019). Assessing the accuracy of remotely sensed data: principles and practices, CRC press.

Dekker, R. J. (2003). "Texture analysis and classification of ERS SAR images for map updating of urban areas in the Netherlands." IEEE transactions on geoscience and remote sensing **41**(9): 1950-1958.

Dobson, M. C., F. T. Ulaby, T. LeToan, A. Beaudoin, E. S. Kasischke and N. Christensen (1992). "Dependence of radar backscatter on coniferous forest biomass." IEEE Transactions on Geoscience and remote Sensing **30**(2): 412-415.

Dontchenko, V., O. Johannessen, L. Bobylev and S. Bartalev (1999). ERS/SAR data application for Russian boreal forests mapping and monitoring. IEEE 1999 International Geoscience and Remote Sensing Symposium. IGARSS'99 (Cat. No. 99CH36293), IEEE.

Dostalova, A., S. Cao and W. Wagner (2021). European Sentinel-1 Forest Type and Tree Cover Density Maps. TU Data.

Dostálová, A., M. Hollaus, M. Milenković and W. Wagner (2016). "Forest area derivation from sentinel-1 data." ISPRS Annals of the Photogrammetry, Remote Sensing and Spatial Information Sciences **3**: 227.

Dostálová, A., M. Lang, J. Ivanovs, L. T. Waser and W. Wagner (2021). "European Wide Forest Classification Based on Sentinel-1 Data." Remote Sensing **13**(3): 337.

Dostalova, A., M. Milenkovic, M. Hollaus and W. Wagner (2016). Influence of Forest Structure on the Sentinel-1 Backscatter Variation-Analysis with Full-Waveform LiDAR Data'. Living Planet Symposium.

Dostálová, A., V. Naeimi, W. Wagner, S. Elefante, S. Cao and H. Persson (2016). Geocoding uncertainty analysis for the automated processing of Sentinel-1 data using Sentinel-1 Toolbox software. Image and Signal Processing for Remote Sensing XXII, International Society for Optics and Photonics.

Dostálová, A., W. Wagner, M. Milenković and M. Hollaus (2018). "Annual seasonality in Sentinel-1 signal for forest mapping and forest type classification." International Journal of Remote Sensing **39**(21): 7738-7760.

Dubois, C., M. Mueller, C. Pathe, T. Jagdhuber, F. Cremer, C. Thiel and C. Schmullius (2020). "CHARACTERIZATION OF LAND COVER SEASONALITY IN SENTINEL-1 TIME SERIES DATA." ISPRS Annals of Photogrammetry, Remote Sensing & Spatial Information Sciences **5**(3).

Dwyer, E., S. Monaco and P. Pasquali (2000). An operational Forest Mapping Tool using spaceborne SAR Data. ERS ENVISAR Symposium, Göteborg, Sweden.

EEA (2013). Gio Land (Gmes/Copernicus Initial Operations Land) High-Resolution Layers (Hrls)—Summary of Product Specifications. Copenhagen, European Environment Agency.

Elefante, S., W. Wagner, C. Briese, S. Cao and V. Naeimi (2016). High-performance computing for soil

moisture estimation. Proceedings of the 2016 conference on Big Data from Space (BiDS'16), Santa Cruz de Tenerife, Spain.

Ernst, C., R. Gullick and K. Nixon (2004). "Conserving forests to protect water." Opflow **30**(5): 1-7.

Eysn, L., M. Hollaus, K. Schadauer and N. Pfeifer (2012). "Forest delineation based on airborne LIDAR data." Remote Sensing **4**(3): 762-783.

Eysn, L., M. Hollaus, K. Schadauer and A. Roncat (2011). Crown coverage calculation based on ALS data. Proceedings of 11th International Conference on LiDAR Applications for Assessing Forest Ecosystems (Silvilaser 2011).

FAO (1998). FRA 2000 Terms and Definitions. FRA Working Paper 1.

Farr, T. G., P. A. Rosen, E. Caro, R. Crippen, R. Duren, S. Hensley, M. Kobrick, M. Paller, E. Rodriguez and L. Roth (2007). "The shuttle radar topography mission." Reviews of geophysics **45**(2).

Frey, O., M. Santoro, C. L. Werner and U. Wegmuller (2012). "DEM-based SAR pixel-area estimation for enhanced geocoding refinement and radiometric normalization." IEEE Geoscience and Remote Sensing Letters **10**(1): 48-52.

Frison, P.-L., B. Fruneau, S. Kmiha, K. Soudani, E. Dufrêne, T. Le Toan, T. Koleck, L. Villard, E. Mougin and J.-P. Rudant (2018). "Potential of Sentinel-1 data for monitoring temperate mixed forest phenology." Remote Sensing **10**(12): 2049.

Fukunaga, K. (2013). Introduction to statistical pattern recognition, Elsevier.

Geoland. (2020). "Digitalesgeländemodell(dgm) Österreich." Retrieved 30.03, 2021, from https://www.data.gv.at/katalog/dataset/dgm.

Gimeno, M., J. San-Miguel, P. Barbosa and G. Schmuck (2002). Using ERS-SAR images for burnt area mapping in Mediterranean landscapes. Forest fire research and wildland fire safety: Proceedings of IV International Conference on Forest Fire Research 2002 Wildland Fire Safety Summit, Luso, Coimbra, Portugal, 18-23 November 2002, Millpress Science Publishers.

Ginzler, C., B. Price, R. Bösch, C. Fischer, M. L. Hobi, A. Psomas, N. Rehush, Z. Wang and L. T. Waser (2019). Area-wide products. Swiss National Forest Inventory–Methods and models of the fourth assessment, Springer**:** 125-142.

Grace, J. (2004). "Understanding and managing the global carbon cycle." Journal of Ecology **92**(2): 189-202.

Guccione, P., A. Lombardi and R. Giordano (2016). Assessment of seasonal variations of radar backscattering coefficient using Sentinel-1 data. 2016 IEEE International Geoscience and Remote Sensing Symposium (IGARSS), IEEE.

Haarpaintner, J., C. Davids, R. Storvold, K. Johansen, K. Ãrnason, Y. Rauste and T. Mutanen (2016). Boreal forest land cover mapping in Iceland and Finland using Sentinel-1A. Proceedings of the Living Planet Symposium, Prague, Czech Republic.

Hansen, J. N., E. T. Mitchard and S. King (2020). "Assessing Forest/Non-Forest Separability Using

Sentinel-1 C-Band Synthetic Aperture Radar." Remote Sensing **12**(11): 1899.

Hansen, M. C., P. V. Potapov, R. Moore, M. Hancher, S. A. Turubanova, A. Tyukavina, D. Thau, S. V. Stehman, S. J. Goetz, T. R. Loveland, A. Kommareddy, A. Egorov, L. Chini, C. O. Justice and J. R. G. Townshend (2013). "High-Resolution Global Maps of 21st-Century Forest Cover Change." Science **342**(6160): 850-853.

Hartigan, J. A. and M. A. Wong (1979). "Algorithm AS 136: A k-means clustering algorithm." Journal of the royal statistical society. series c (applied statistics) **28**(1): 100-108.

Hese, S. and C. Schmullius (2005). Forest Cover Change in Siberia-Results from the Siberia-II Project. International Conference on Remote Sensing of Environment, Conference Proceedings, St. Petersburg, Russia.

Imhoff, M. L. (1993). Radar backscatter/biomass saturation: Observations and implications for global biomass assessment. Proceedings of IGARSS'93-IEEE International Geoscience and Remote Sensing Symposium, IEEE.

Jarvis, A., H. I. Reuter, A. Nelson and E. Guevara (2008). "Hole-filled SRTM for the globe Version 4." available from the CGIAR-CSI SRTM 90m Database (http://srtm. csi. cgiar. org) **15**: 25-54.

Joshi, N. P., E. T. Mitchard, J. Schumacher, V. K. Johannsen, S. Saatchi and R. Fensholt (2015). "L-band SAR backscatter related to forest cover, height and aboveground biomass at multiple spatial scales across Denmark." Remote Sensing **7**(4): 4442-4472.

Kangas, A., R. Astrup, J. Breidenbach, J. Fridman, T. Gobakken, K. T. Korhonen, M. Maltamo, M. Nilsson, T. Nord-Larsen, E. Næsset and H. Olsson (2018). "Remote sensing and forest inventories in Nordic countries – roadmap for the future." Scandinavian Journal of Forest Research **33**(4): 397-412.

Kellndorfer, J. M., L. E. Pierce, M. C. Dobson and F. T. Ulaby (1998). "Toward consistent regional-to-global-scale vegetation characterization using orbital SAR systems." IEEE Transactions on Geoscience and Remote Sensing **36**(5): 1396-1411.

Kugler, F., D. Schulze, I. Hajnsek, H. Pretzsch and K. P. Papathanassiou (2014). "TanDEM-X Pol-InSAR performance for forest height estimation." IEEE Transactions on Geoscience and Remote Sensing **52**(10): 6404-6422.

Lang, M., M. Kaha, D. Laarmann and A. Sims (2018). "Construction of tree species composition map of Estonia using multispectral satellite images, soil map and a random forest algorithm." Forestry Studies **68**(1): 5-24.

Langanke, T., G. Büttner, H. Dufourmont, D. Iasillo, M. Probeck, M. Rosengren, A. Sousa, P. Strobl and J. Weichselbaum (2013). "GIO land (GMES/Copernicus initial operations land) High Resolution Layers (HRLs)–summary of product specifications." European Environment Agency.

Le Toan, T., A. Beaudoin, J. Riom and D. Guyon (1992). "Relating forest biomass to SAR data." IEEE Transactions on Geoscience and Remote Sensing **30**(2): 403-411.

Le Toan, T. and N. Floury (1998). "On the retrieval of forest biomass from SAR data." EUROPEAN SPACE AGENCY-PUBLICATIONS-ESA SP **441**: 213-214.

Le Toan, T., S. Mermoz, L.-V. Fichet, C. Sannier and A. Bouvet (2014). Comparison of optical and sar data for forest cover mapping: Redd+ may be helped by sar data. 2014 IEEE Geoscience and Remote Sensing Symposium, IEEE.

Lucas, R., J. Armston, R. Fairfax, R. Fensham, A. Accad, J. Carreiras, J. Kelley, P. Bunting, D. Clewley and S. Bray (2010). "An evaluation of the ALOS PALSAR L-band backscatter—Above ground biomass relationship Queensland, Australia: Impacts of surface moisture condition and vegetation structure." IEEE Journal of Selected Topics in Applied Earth Observations and Remote Sensing **3**(4): 576-593.

Lund, J., R. R. Forster, S. B. Rupper, E. J. Deeb, H. Marshall, M. Z. Hashmi and E. Burgess (2020). "Mapping snowmelt progression in the Upper Indus Basin with synthetic aperture radar." Frontiers in Earth Science **7**: 318.

Magagi, R., M. Bernier and M.-C. Bouchard (2002). "Use of ground observations to simulate the seasonal changes in the backscattering coefficient of the subarctic forest." IEEE transactions on Geoscience and Remote Sensing **40**(2): 281-297.

Markert, K. N., A. M. Markert, T. Mayer, C. Nauman, A. Haag, A. Poortinga, B. Bhandari, N. S. Thwal, T. Kunlamai and F. Chishtie (2020). "Comparing sentinel-1 surface water mapping algorithms and radiometric terrain correction processing in southeast asia utilizing google earth engine." Remote Sensing **12**(15): 2469.

Martone, M., P. Rizzoli, C. Wecklich, C. González, J.-L. Bueso-Bello, P. Valdo, D. Schulze, M. Zink, G. Krieger and A. Moreira (2018). "The global forest/non-forest map from TanDEM-X interferometric SAR data." Remote sensing of environment **205**: 352-373.

Minh, D. H. T., T. Le Toan, F. Rocca, S. Tebaldini, L. Villard, M. Réjou-Méchain, O. L. Phillips, T. R. Feldpausch, P. Dubois-Fernandez and K. Scipal (2016). "SAR tomography for the retrieval of forest biomass and height: Cross-validation at two tropical forest sites in French Guiana." Remote sensing of environment **175**: 138-147.

Mitchell, A. L., I. Tapley, A. K. Milne, M. L. Williams, Z.-S. Zhou, E. Lehmann, P. Caccetta, K. Lowell and A. Held (2014). "C-and L-band SAR interoperability: Filling the gaps in continuous forest cover mapping in Tasmania." Remote sensing of environment **155**: 58-68.

Monteith, A. R. and L. M. Ulander (2018). "Temporal survey of P-and L-band polarimetric backscatter in boreal forests." IEEE Journal of Selected Topics in Applied Earth Observations and Remote Sensing **11**(10): 3564-3577.

Motohka, T., M. Shimada, Y. Uryu and B. Setiabudi (2014). "Using time series PALSAR gamma nought mosaics for automatic detection of tropical deforestation: A test study in Riau, Indonesia." Remote Sensing of Environment **155**: 79-88.

Nabuurs, G., R. Päivinen, R. Sikkema and G. Mohren (1997). "The role of European forests in the global carbon cycle—a review." Biomass and bioenergy **13**(6): 345-358.

Naeimi, V., S. Elefante, S. Cao, W. Wagner, A. Dostalova and B. Bauer-Marschallinger (2016). Geophysical parameters retrieval from sentinel-1 SAR data: a case study for high performance

computing at EODC. Proceedings of the 24th High Performance Computing Symposium.

Nguyen, D. B., K. Clauss, S. Cao, V. Naeimi, C. Kuenzer and W. Wagner (2015). "Mapping rice seasonality in the Mekong Delta with multi-year Envisat ASAR WSM data." Remote Sensing **7**(12): 15868-15893.

Olesk, A., K. Voormansik, M. Põhjala and M. Noorma (2015). Forest change detection from Sentinel-1 and ALOS-2 satellite images. 2015 IEEE 5th Asia-Pacific Conference on Synthetic Aperture Radar (APSAR), IEEE.

Otsu, N. (1979). "A threshold selection method from gray-level histograms." IEEE transactions on systems, man, and cybernetics **9**(1): 62-66.

Patel, P., H. S. Srivastava, S. Panigrahy and J. S. Parihar (2006). "Comparative evaluation of the sensitivity of multi-polarized multi-frequency SAR backscatter to plant density." International Journal of Remote Sensing **27**(2): 293-305.

Pathe, C., W. Wagner, D. Sabel, M. Doubkova and J. B. Basara (2009). "Using ENVISAT ASAR global mode data for surface soil moisture retrieval over Oklahoma, USA." IEEE Transactions on Geoscience and Remote Sensing **47**(2): 468-480.

Peters, J., H. Lievens, B. D. Baets and N. Verhoest (2012). "Accounting for seasonality in a soil moisture change detection algorithm for ASAR Wide Swath time series." Hydrology and Earth System Sciences **16**(3): 773-786.

Pfeifer, N., G. Mandlburger, J. Otepka and W. Karel (2014). "OPALS–A framework for Airborne Laser Scanning data analysis." Computers, Environment and Urban Systems **45**: 125-136.

Pimentel, D. and N. Kounang (1998). "Ecology of soil erosion in ecosystems." Ecosystems **1**(5): 416-426.

Proisy, C., E. Mougin, E. Dufrêne and V. Le Dantec (2000). "Monitoring seasonal changes of a mixed temperate forest using ERS SAR observations." IEEE Transactions on Geoscience and Remote Sensing **38**(1): 540-552.

Pulliainen, J. T., L. Kurvonen and M. T. Hallikainen (1999). "Multitemporal behavior of L-and C-band SAR observations of boreal forests." IEEE Transactions on Geoscience and Remote Sensing **37**(2): 927-937.

Quegan, S., T. Le Toan, J. J. Yu, F. Ribbes and N. Floury (2000). "Multitemporal ERS SAR analysis applied to forest mapping." IEEE Transactions on Geoscience and Remote Sensing **38**(2): 741-753.

Ranson, K. J. and G. Sun (2000). "Effects of environmental conditions on boreal forest classification and biomass estimates with SAR." IEEE Transactions on Geoscience and Remote Sensing **38**(3): 1242-1252.

Reese, H., T. Granqvist-Pahlén, M. Egberth, M. Nilsson and H. Olsson (2005). Automated estimation of forest parameters for Sweden using Landsat data and the kNN algorithm. Proceedings, 31st International Symposium on Remote Sensing of Environment.

Reiche, J., J. Verbesselt, D. Hoekman and M. Herold (2015). "Fusing Landsat and SAR time series to detect deforestation in the tropics." Remote Sensing of Environment **156**: 276-293.

Rodionova, N. (2018). "2015–2016 Seasonal Variations of Backscattering from Natural Coverage in the Moscow Region Based on Radar Data from the Sentinel 1A Satellite." Izvestiya, Atmospheric and Oceanic Physics **54**(9): 1272-1281.

Rüetschi, M., M. E. Schaepman and D. Small (2018). "Using multitemporal sentinel-1 c-band backscatter to monitor phenology and classify deciduous and coniferous forests in northern switzerland." Remote Sensing **10**(1): 55.

Saatchi, S. S., J. V. Soares and D. S. Alves (1997). "Mapping deforestation and land use in Amazon rainforest by using SIR-C imagery." Remote Sensing of Environment **59**(2): 191-202.

Santoro, M., C. Beer, O. Cartus, C. Schmullius, A. Shvidenko, I. McCallum, U. Wegmüller and A. Wiesmann (2011). "Retrieval of growing stock volume in boreal forest using hyper-temporal series of Envisat ASAR ScanSAR backscatter measurements." Remote Sensing of Environment **115**(2): 490-507.

Santoro, M., O. Cartus, J. E. Fransson, A. Shvidenko, I. McCallum, R. J. Hall, A. Beaudoin, C. Beer and C. Schmullius (2013). "Estimates of forest growing stock volume for sweden, central siberia, and québec using envisat advanced synthetic aperture radar backscatter data." Remote Sensing **5**(9): 4503-4532.

Santoro, M., J. E. Fransson, L. E. Eriksson, M. Magnusson, L. M. Ulander and H. Olsson (2009). "Signatures of ALOS PALSAR L-band backscatter in Swedish forest." IEEE Transactions on Geoscience and Remote Sensing **47**(12): 4001-4019.

Sgrenzaroli, M., G. De Grandi, H. Eva and F. Achard (2002). "Tropical forest cover monitoring: estimates from the GRFM JERS-1 radar mosaics using wavelet zooming techniques and validation." International Journal of Remote Sensing **23**(7): 1329-1355.

Sharma, R., D. Leckie, D. Hill, B. Crooks, A. Bhogal, P. Arbour and S. D'eon (2005). Hyper-temporal radarsat SAR data of a forested terrain. International Workshop on the Analysis of Multi-Temporal Remote Sensing Images, 2005., IEEE.

Shimada, M., T. Itoh, T. Motooka, M. Watanabe, T. Shiraishi, R. Thapa and R. Lucas (2014). "New global forest/non-forest maps from ALOS PALSAR data (2007–2010)." Remote Sensing of Environment **155**: 13-31.

Scharien, R. K., R. Segal, S. Nasonova, V. Nandan, S. E. Howell and C. Haas (2017). "Winter Sentinel-1 backscatter as a predictor of spring Arctic sea ice melt pond fraction." Geophysical Research Letters **44**(24): 12,262-212,270.

SIRS (2016). Draft HRL Forest 2012 final validation report 1.6, SIRS (Systèmes d'Information à Référence Spatiale).

Small, D. (2011). "Flattening gamma: Radiometric terrain correction for SAR imagery." IEEE Transactions on Geoscience and Remote Sensing **49**(8): 3081-3093.

Small, D., N. Miranda, T. Ewen and T. Jonas (2013). "Reliably flattened radar backscatter for wet snow mapping from wide-swath sensors." ESA-SP(772): online.

Small, D., C. Rohner, N. Miranda, M. Rüetschi and M. E. Schaepman (2021). "Wide-Area Analysis-Ready Radar Backscatter Composites." IEEE Transactions on Geoscience and Remote Sensing.

Small, D. and A. Schubert (2008). "Guide to ASAR geocoding." ESA-ESRIN Technical Note RSL-ASAR-GC-AD **1**: 36.

SNAP. "Sentinel Application Platform." Retrieved 30.03, 2021, from https://step.esa.int/main/toolboxes/snap/.

Soudani, K., N. Delpierre, D. Berveiller, G. Hmimina, G. Vincent, A. Morfin and É. Dufrêne (2021). "Potential of C-band Synthetic Aperture Radar Sentinel-1 time-series for the monitoring of phenological cycles in a deciduous forest." International Journal of Applied Earth Observation and Geoinformation **104**: 102505.

Srivastava, P. K., P. O'Neill, M. Cosh, R. Lang and A. Joseph (2015). Evaluation of radar vegetation indices for vegetation water content estimation using data from a ground-based SMAP simulator. 2015 IEEE International Geoscience and Remote Sensing Symposium (IGARSS), IEEE.

Strozzi, T., U. Wegmueller, J. Askne, P. Dammert, A. Beaudoin, J. Martinez and M. Hallikainen (1998). "European forest mapping with SAR interferometry." EUROPEAN SPACE AGENCY-PUBLICATIONS-ESA SP **441**: 269-276.

Torres, R., P. Snoeij, D. Geudtner, D. Bibby, M. Davidson, E. Attema, P. Potin, B. Rommen, N. Floury, M. Brown, I. N. Traver, P. Deghaye, B. Duesmann, B. Rosich, N. Miranda, C. Bruno, M. L'Abbate, R. Croci, A. Pietropaolo, M. Huchler and F. Rostan (2012). "GMES Sentinel-1 mission." Remote Sensing of Environment **120**: 9-24.

Udali, A., E. Lingua and H. J. Persson (2021). "Assessing Forest Type and Tree Species Classification Using Sentinel-1 C-Band SAR Data in Southern Sweden." Remote Sensing **13**(16): 3237.

Ulaby, F. T., R. K. Moore and A. K. Fung (1986). "Microwave remote sensing: Active and passive. Volume 3-From theory to applications."

Ulander, L. M. (1996). "Radiometric slope correction of synthetic-aperture radar images." IEEE Transactions on Geoscience and Remote Sensing **34**(5): 1115-1122.

Vidal, C., I. Alberdi, L. Hernández and J. Redmond (2016). "National forest inventories." Springer Science+ Business Media. doi **10**: 978-973.

Villard, L. and T. Le Toan (2014). "Relating P-Band SAR Intensity to Biomass for Tropical Dense Forests in Hilly Terrain: $\gamma^ 0$ or $ t^ 0$?" IEEE Journal of Selected Topics in Applied Earth Observations and Remote Sensing **8**(1): 214-223.

Wagner, W., A. Luckman, J. Vietmeier, K. Tansey, H. Balzter, C. Schmullius, M. Davidson, D. Gaveau, M. Gluck and T. Le Toan (2003). "Large-scale mapping of boreal forest in SIBERIA using ERS tandem coherence and JERS backscatter data." Remote Sensing of Environment **85**(2): 125-144.

Wallington, E. D. and I. H. Woodhouse (2006). "Forest height retrieval from commercial X-band SAR products." IEEE Transactions on Geoscience and remote sensing **44**(4): 863-870.

Waser, L. T., C. Ginzler and N. Rehush (2017). "Wall-to-wall tree type mapping from countrywide

airborne remote sensing surveys." Remote Sensing **9**(8): 766.

Waser, L. T., M. Rüetschi, A. Psomas, D. Small and N. Rehush (2021). "Mapping dominant leaf type based on combined Sentinel-1/-2 data–Challenges for mountainous countries." ISPRS Journal of Photogrammetry and Remote Sensing **180**: 209-226.

White, J. C., N. C. Coops, M. A. Wulder, M. Vastaranta, T. Hilker and P. Tompalski (2016). "Remote Sensing Technologies for Enhancing Forest Inventories: A Review." Canadian Journal of Remote Sensing **42**(5): 619-641.

Yu, H., W. Ni, Z. Zhang, G. Sun and Z. Zhang (2020). "Regional Forest Mapping over Mountainous Areas in Northeast China Using Newly Identified Critical Temporal Features of Sentinel-1 Backscattering." Remote Sensing **12**(9): 1485.

Yu, X., J. Hyyppä, M. Karjalainen, K. Nurminen, K. Karila, M. Vastaranta, V. Kankare, H. Kaartinen, M. Holopainen and E. Honkavaara (2015). "Comparison of laser and stereo optical, SAR and InSAR point clouds from air-and space-borne sources in the retrieval of forest inventory attributes." Remote Sensing **7**(12): 15933-15954.

Zoughi, R., J. Bredow, S. Osman and R. K. Moore (1989). "Fine resolution signatures of coniferous and deciduous trees at C band." Remote Sensing **10**(1): 147-169.